December 2015

Ecosystem response to recent climate change in alpine environments

Patrick Shawn Sawyer
University of Nevada, Las Vegas

ECOSYSTEM RESPONSE TO RECENT CLIMATE CHANGE IN ALPINE ENVIRONMENTS

by

Patrick Shawn Sawyer

Bachelor of Science in Chemical Engineering
California State University, Long Beach
1989

Master of Science in Environmental Science
University of Nevada, Las Vegas
2007

A dissertation submitted in partial fulfillment
of the requirements for the degree of

Doctor of Philosophy -- Environmental Science

School of Environmental and Public Affairs
Greenspun College of Urban Affairs
The Graduate College

University of Nevada, Las Vegas
December 2015

UNLV | GRADUATE COLLEGE

Dissertation Approval

The Graduate College
The University of Nevada, Las Vegas

October 16, 2015

This dissertation prepared by

Patrick Sawyer

entitled

Ecosystem Response to Recent Climate Change in Alpine Environments

is approved in partial fulfillment of the requirements for the degree of

Doctor of Philosophy – Environmental Science
School of Environmental and Public Affairs

Haroon Stephen, Ph.D.
Examination Committee Chair

Kathryn Hausbeck Korgan, Ph.D.
Graduate College Interim Dean

Krystyna Stave, Ph.D.
Examination Committee Member

Helen Neill, Ed.D.
Examination Committee Member

David Kreamer, Ph.D.
Graduate College Faculty Representative

Abstract

Recent variations in meteorological conditions indicate the earth's climate is changing in ways that can impact delicate ecological balances in sensitive regions. These impacts threaten the essential services provided by such ecosystems. Determining how climate changes are affecting the biosphere is essential to adapt and mitigate harmful consequences. In order to mitigate the negative effects of climate change and adapt to shifting ecological resource constraints, it is imperative to locate such changes and determine vulnerability of ecological resources to changing environmental conditions.

Identifying climate driven ecological changes faces numerous challenges given the reliance on vegetation indices as the primary measure of vegetative surface cover. It is essential that gaps in the understanding and reliability of these indices be addressed. In this research, the problem of determining climate driven ecological change is addressed using remote sensing techniques to find trends in an ecologically sensitive region over the last 30 years. Relation between climate and vegetation trends is studied and a methodology that does not rely upon a single measure for determining vegetative changes is developed. The comprehension of the scenario when both the red and near-infrared bands shift in the same direction is developed and related to compositional changes. The performance of vegetation indices and transforms is determined using survey data. The non-parametric Mann-Kendall (MK) trend test is used to establish the presence of trends. The research study is conducted in the alpine ecosystem.

New insights into climate driven changes were gained using a novel study design that incorporated several vegetation indices, tasseled cap transforms and spectral mixture

analysis. Surface reflectance throughout the watershed has declined in all six Landsat bands over the last three decades. At the same time, temperatures have demonstrated a statistically significant rise. Vegetative composition changes throughout the study area were identified including widespread declines in needle leaf shrubs. Composition changes are related to red-shift translations as a result of variations in the vegetative structural density. An elevational relationship was found in sparsely vegetated areas with declining vegetation in the lower half of the watershed and vegetative increases in the upper half of the watershed

Correlation of surface reflectance red-shift trends to actual changes in vegetative surface cover was tested against long-term field survey data. Red-shift stretch and downward translation demonstrated close agreement with predicted vegetation increases while red-shift compression and upward translation was not as effective a predictor of vegetative declines. Vegetation indices and tasseled cap brightness and greenness transforms performed remarkably well in predicting vegetation trends. Moreover, a poor performance of the tasseled cap wetness index in predicting vegetation trends is revealed. An additional important finding of this research is the close correlation between the USGS CDR surface reflectance dataset and older dark object subtraction methods for calculating surface reflectance.

It is essential to understand the impact of climate change on the environment in order to deal with potentially severe and rapid consequences brought about by reduced ecosystem productivity. This research provides a useful insight about ecological impacts of climate change using remote sensing.

Acknowledgments

I wish to thank my committee members, Dr. Krystyana Stave, Dr. Helen Neill, and Dr. David Kreamer for their support and guidance during my research program. Their insights and recommendations provided invaluable assistance to me on numerous occasions. I would especially like to thank my committee chair and research advisor Dr. Haroon Stephen for his excellent mentorship as I progressed in this field. Dr. Stephen provided essential knowledge not available in classrooms or from independent studies that allowed me to overcome seemingly insurmountable obstacles at critical points in my research. I would also like to express my sincere gratitude to Dr. David Charlet from the College of Southern Nevada for his assistance with the identification the vegetative species collected during my field surveys.

Completion of this research would not have been possible without the support and assistance of many of my friends, family, and colleagues. Most importantly, I wish to thank my wife Nancy and daughter Abigail for their sacrifice of time and attention that they surrendered in order for me to focus on this work. Their love and support throughout this process enabled me to continue on even during those most difficult times when the completion of this work seemed so far away.

Table of Contents

List of Tables

List of Figures

Chapter 1: Introduction

1.0 Background

Understanding the effect that changing environmental parameters have on fragile ecosystems is essential to our ability to adapt to the potential reduction in ecosystem productivity. Alpine ecosystems are especially vulnerable since these regions exist at the boundaries of climate zones such as the higher and lower latitudes and at high elevations. Biomes that populate habitats in these zones are highly susceptible to changes in environmental conditions (Lindner et al., 2010). Thus, these areas are ideal laboratories to study the impact of changing climatic variables on local species assemblages. In particular, the steep elevation gradients in these regions could provide several ecotones within a small area for climate change impact analysis.

Although several range-limited species will be negatively impacted by climate change, others will see new opportunities as their range limits expand upslope. Many low elevation species will be able to migrate into formerly hostile territory. However, this new migration can have a negative impact on existing populations. Since each species has its own unique life history trait, the dynamics of species interactions will determine what future ecosystem assemblages look like.

This manuscript describes a study conducted to determine what impacts climate change has had on the ecosystem. Identifying the impacts that have already taken place provides solid evidence of risks to the biosphere from warming temperatures. The focus of this study is on what has already happened and how those impacts are determined, not

the forcing factors that are driving altered climatic conditions. This research is conducted in an alpine ecosystem.

2.0 Literature Review

Isolated alpine ecosystems are composed of complex interdependent assemblages that are vulnerable to climate change impacts such as introduction of new predator species and loss of critical assemblage components. Habitat density plays an essential role in determining the local response to climate change. Once the critical population for a specific resource falls below sustainment levels, a chain reaction can occur that fundamentally alters the composition and functioning of the local grouping. Altered environmental parameters such as warmer temperatures or reduced moisture availability can leave individual species in a weakened state, allowing for rapid infestation of predator or competitor species. While natural selection can lead to the development of tolerance traits that enhance the survivability of individual species, this process will most likely take much longer than the changes to the habitat which are driving species extinction (Walther, 2010). Recent literature suggests that the greatest rates of change will take place where local assemblages are complex and highly interdependent.

Changing the environmental parameters of an ecosystem can induce migration, thus, altering species distribution patterns and range limits. Previous studies have examined the climate-induced shift in range limits of species habitat. Kelly and Goulden, (2008) found that the average elevation of the dominant plant species rose by about 65 meters over a 30 year period in the Santa Rosa Mountains of Southern California. This

study area was similar to many in the southwestern United States with arid to semi-arid regions dominated by desert scrub in the lower reaches, transitioning to pinyon-juniper woodlands at higher elevations, followed by chaparral shrubland and conifer forest approaching the summit.

This study found that instead of migration of new species into new territory, most of the observed changes were related to a shift in dominance within local assemblages (Kelly and Goulden, 2008). This is an important finding in that significant compositional changes were observed even though overall range limits were stable. Regional studies that focus on range shifts may miss important changes at the local community level.

Climate change impacts can be determined from observations of altered surface characteristics and processes. Root et al., (2003) identify four characteristic responses to climate change including species density change with range shifts both upslope and in latitude, altered phenology including timing of flowering and migration patterns, morphological change such as species physical and behavioral traits, and altered genetic frequencies (Root et al., 2003). Since these changes alter the vegetative composition and quantity, they affect several other ecosystem components such as fauna and soil microbes. Thus, vegetative surface cover changes serve as an ideal surrogate for the ecosystem as a whole. These climate driven changes are expected to have their most pronounced and observable effects in areas experiencing the highest rate of temperature change (Root et al., 2003). Due to the changes in surface characteristics, remote sensing is a valuable tool to study climate change impacts.

Climate change impacts on vulnerable alpine ecosystems threaten the essential services these regions provide. Altered environmental parameters lead to shifts in species distribution and abundance that can transform the landscape in significant ways. These changes can be observed by analyzing trends in the spectral reflectance of earth's surface. The determination of climate driven alteration of the surface cover is possible through the use of various vegetative indices, spectral unmixing techniques, and spectral band transforms. Analysis of the existing multi-decade data set of surface reflectance is urgently needed to find those changes that have already occurred as well as to elicit clues as to what the future holds for critical habitats and ecosystems.

Measuring changes in surface characteristics brought about by changing environmental parameters is possible through the analysis of remote sensing imagery. The Landsat instruments have proven especially useful in determining vegetative change given their high reliability, orbital frequency, global coverage and over 40 year time span of continuous measurements. The Landsat instruments record surface reflectance in the visible, near infrared and short wave infrared spectral regions. Each of these spectral regions provides unique information that can be used to determine vegetative quantity and vigor. By examining multiple images over the same location through time, patterns in vegetation become apparent that can be attributed to climate driven change.

The use of vegetation indices to elicit vegetation change has seen widespread application. Vegetation indices are designed to take advantage of the large difference in reflectance between the visible and near-infrared (NIR) bands. This difference produces a

characteristic spectral fingerprint for vegetation with low visible reflectance due to absorption by plant constituents such as chlorophyll and high reflectance from the NIR energy reflecting off the internal and surface structures of the plants. This difference is referred to as the red-edge or red-shift. In this study, the term red-shift is chosen for consistency.

The mathematical relationship of ratio based vegetation indices are designed to clearly delineate changes over time when the visible and NIR bands are moving in opposite directions. However, if the visible and NIR bands are trending in the same direction, the index may not provide an accurate measure of what is taking place. There is no current agreement on the interpretation of red-shifts moving in the same direction. Thus, there is a gap in the ability of common ratio based vegetative indices to produce meaningful information when the red and NIR bands are trending in the same direction. Thus, terms positive red-shift translation and negative red-shift translation that refer to cases where the red and NIR bands trend upward and downward, respectively, need careful attention in relation to changes in the vegetative surface characteristics.

3.0 Rationale

Trends in vegetation indices over time are an established method for determining ecosystem health and variation. Numerous vegetation indices have been developed over the last 30 years. These indices have strengths and limitations, and thus should not be relied upon alone for determining climate driven changes (Higginbottom and Symeonakis, 2014). One of the biggest challenges encountered when using vegetation

indices is the interpretation of their relationship to the physical properties of vegetative surface cover. This is especially true in areas of low green surface cover where the understanding of vegetation indices remains unclear (Jin and Eklundh, 2014). This gap in understanding of vegetation indices can be better explained by red-shift response to changes in vegetative surface conditions. In addition, the application of vegetation indices to ecological trend studies has suffered from a scarcity of validation studies comparing index performance against actual field survey data (Steyer et al., 2013).

These findings identify critical gaps in the use of vegetation indices that must be addressed to ensure the reliability and accuracy of climate driven vegetation studies. There is a need for an analytical methodology that incorporates multiple indices to accurately identify vegetative changes. The gap in understanding the meaning of vegetation indices when the red and NIR are trending in the same direction must be validated through testing against surface vegetation plots that have accurate long-term surface cover and composition data. Also, the lack of data validating the performance of these measures needs to be addressed by comparing numerous long-term field survey sites with the prediction efficiency of vegetation indices and tasseled cap transforms.

4.0 Objectives

This research seeks to determine vegetative responses to recent climate change that allow us to hypothesize how those changes will progress under various predicted climate regimes. Specific objectives of this research are

1. Study and evaluation of recent climate change impacts on the ecosystem;

2. Design an analytical methodology that uses remote sensing to determine changes in vegetative surface cover of the ecosystem;
3. Study of red-shift translation in relation to vegetation quantity and composition change; and
4. Measure the performance of vegetative indices and transforms against data from vegetative survey plots.

A brief approach to achieve these objectives is described as follows. Determination of how recent climate change has affected the study area ecosystem is accomplished by finding changes in the vegetative surface cover and comparing those changes to trends in environmental variables including temperature and precipitation. Surface cover changes are identified through the analysis of Landsat imagery collected over the last 30 years. Landsat surface reflectance data is obtained from the EarthExplorer web site operated by the USGS (http://earthexplorer.usgs.gov/).

Temperature and precipitation data for the study area over that same time period is obtained from the University of Oregon's Parameter-elevation Regressions on Independent Slopes Model (PRISM) web site. The PRISM data set is generated by using linear regression adjusted for elevation. The climate parameter calculated by the model is weighted by several factors including distance and topographic facet from the measurement station, (source: http://www.prism.oregonstate.edu/).

Actual field station data is preferred over modeled data such as PRISM. Modeled data carries the risk of relying on weather station data that is too sparse to accurately

capture climate forcing factors such as those caused by variations in terrain or elevation effects (Daly, 2006). However, in remote areas where few meteorological stations exist, data derived from these models is essential. The PRISM model has been evaluated to determine its limitations in climate studies and although not perfect, PRISM offers the best solution for determining climate data in remote areas with significant terrain variation such as alpine watersheds (Daly, 2006).

The methodology developed for this study includes examination of variations in the spectral responses of both soils and vegetation that are used to find changes in physiological processes being altered by changing environmental parameters. These vegetation indices and transforms serve as the surrogate measure of ecosystem vegetation response to recent climate change. The current gap in being able to interpret vegetative changes when red-shift translations are taking place is addressed by development and testing of the red-shift translation hypothesis. Study sites are evaluated using both standard red-shift theory of vegetative increase when there is red-shift stretch and vegetative declines when there is red-shift compression and a new theory of vegetative increases with composition change when there is red-shift downward translation and vegetative declines with composition change when there is red-shift upward translation.

The performance of vegetation indices and tasseled cap transforms is determined by comparing their predictions against actual field plot survey data. Understanding the accuracy of all four red-shift theories as well as vegetation indices and tasseled cap transformations is essential to provide confidence of their use in ecological studies. This

research evaluates the performance of various vegetation indices derived from Landsat surface reflectance data for their ability to determine climate driven ecological changes and determines limitations and inconsistencies with these methods.

5.0 Data and Study Design

This section provides a general description of data and study area applicable to all chapters of the manuscript. In this study, trends in the six Landsat spectral reflectance bands as well as trends in three common vegetation indices and three tasseled cap transforms are used to determine changes in surface vegetation. Using multiple ratio based indices and transforms based on linear band combinations provides redundancy and increases confidence levels in conclusions made from their analysis. In addition to vegetative indices and transforms, spectral mixture analysis is employed at thirty sample sites throughout the study area to determine recent climate induced compositional changes. This study design addresses the gap of reliance on individual measures to identify climate driven ecological changes.

In order to achieve these goals, a study site is selected that has seen minimal human impact and is representative of an ecologically sensitive area containing numerous ecotones. This allows for the analysis of shifting patterns in vegetative surface cover and to link those changes to altered climatic regimes. The study area chosen for this research is the Big Pine Creek watershed located in California's Eastern Sierra's. This watershed is home to the southern-most glacier in the United States, the Palisade. The study area is typical of many alpine environments with a significant elevation gradient, rising from

1200 meters above mean sea level (MSL) at the Owens River to over 3600 meters MSL at the base of the Palisade.

The study area has been relatively stable and unaffected by recent natural and anthropogenic factors. Although warming temperatures increase the risk of fire frequency and intensity in addition to increasing the risk of pest infestation, the Big Pine Creek watershed has remained relatively unscathed. Human impacts are minimal as the majority of the watershed is inside of a protected national forest. While geological impacts to the study area have not been evident in the last few decades, the area is at heightened risk to such events as warming temperatures.

Liu et al., (2013) have found faster rates of rock glacier movement in the southern Sierra Nevada are compared to that further north (Liu et al., 2013). Warming temperatures will not only increase these glacier movements they will also lead to reduced permafrost cover that can have both positive and negative impacts on the area's ecology. As the soil near the summit warms and becomes more amenable to vegetation establishment, the risk of landslides that can devastate large sections of the watershed will also increase.

The persistence of the snowpack is another physical attribute of the study area that affects vegetation response to climate change. Warming temperatures will reduce the number of days the ground is covered which will therefore allow new vegetative establishment. Snowpack levels in the eastern sierras have seen significant declines in the last few years. Belmecheri et al, (2015) have found that the Sierra Nevada snowpack is

currently experiencing its lowest record in the last 500 years with April 1st 2015 levels at only 5 percent of their 50 year historical average. Their data indicates this recent significant decline began in 2010 while data for the previous three decades were within the normal range of variation (Belmecheri et al, 2015).

Moisture availability plays an essential role in the functioning of a healthy ecosystem. The risks to vegetative species from declining moisture levels include not only higher risk of fire, but also from increased susceptibility to pest infestation. Although the Big Pine Creek watershed has not shown evidence of significant pest infestation to date, white pine beetle infestation is reported in surrounding areas of the Inyo national forest, (California Pest Control Council, 2013).

Many of the vegetative species which populate this watershed exist at the limits of their environmental tolerance. This makes them very susceptible to slight changes in temperature and precipitation. This also makes the study area an ideal laboratory for examining ecosystem response to climate change since the effects from the small variations in climate that have already taken place over the last few decades will first be observed in these areas. This study area is also accessible which allows for determination of current surface cover characteristics and for the in situ collection of surface cover samples used to establish baseline spectral data.

6.0 Contributions

This research addresses several gaps identified in the rationale section. New insights into climate driven changes were gained using vegetation indices. Moreover, an

analytical methodology of multiple indices and spectral mixture analysis is produced that accurately identifies vegetative changes. Furthermore, a new understanding of vegetation cover and composition is developed by studying red-shift translation. Finally, the performance of three vegetation indices and three tasseled cap transforms were compared using field survey data.

The scholarly contributions provided by this research include four journal publications and two conference presentations. Two additional research papers have recently been submitted to peer reviewed journals for publication. The first study in this research program examining the spectral response to rising temperatures at 30 sites in the Big Pine Creek watershed found reductions in surface reflectance coincident with the statistically significant increases in temperature across the entire watershed. These initial findings were presented at the River Basins Management VII conference at New Forest, England in May 2013. These results were later published in the Wessex Institute of Technology (WIT) journal WIT Transactions on Ecology (Sawyer and Stephen, 2013).

Another contribution of this research was the discovery that vegetation indices are unable to find trends in vegetative response when the visible and NIR are trending in the same direction. This finding was achieved by exploring the trends in vegetation indices and tasseled cap transformations for the 30 sites examined in the initial study. These results were published in the journal Advances in Space Research (Sawyer and Stephen, 2014).

The next contribution derived from this research is the finding of excellent agreement between the newly published USGS surface reflectance data set and surface reflectance determined using the manual dark object subtraction (DOS) method. This finding eliminates the need to revisit previous ecological studies using the new USGS data set. The findings from this study were presented at the International Conference on Advances in Bio-Informatics, Bio-Technology, and Environmental Engineering held at Westminster University in London, England in June 2014. They were later published in the International Journal of Earthquake Engineering (Sawyer and Stephen, 2014).

The next contribution of this research was the identification of increases in vegetation taking place in developed stands with moderate to severe declines occurring in vegetative cover in sparsely vegetated sites. A significant bifurcation in the response at sparsely vegetated sites was identified with the lower portions of the watershed experiencing significant vegetative declines while the upper elevations were seeing increases in vegetation. Dividing the sites based on vegetative density enabled the determination of changes taking place at the fringes of vegetative assemblages and within established sites. These results were published in the journal Earth Sciences (Sawyer and Stephen, 2014).

An additional contribution of this research is a complete spectral data set containing full visible through NIR spectra from 116 samples. The spectra include numerous examples of common vegetation including broad leaf tree species such as aspen and birch, narrow leaf examples of willow, and several needle leaf pines and firs.

Numerous shrub samples including sages, junipers and manzanitas are included. Spectra of numerous non-photosynthetic vegetation samples (litter) are provided as well as soil and rock types found throughout the watershed. These data were developed into a paper that has been submitted for publication.

Throughout the course of this research, numerous changes to the surface cover vegetation of the study area over the last three decades were identified. Existing theory on red-shift stretch and compression were also determined to not necessarily reflect simple cases of increases or decreases in vegetative cover, but may in fact represent composition change. Key findings from the vegetation indices validation analysis include red-shift stretch and red-shift downward translation trends corresponded to actual increases in vegetative cover in over 90% of the sites.

For the vegetative indices and tasseled cap transformations, there is an overall agreement between the indices and actual field data. However, a striking finding from this study was the poor level of agreement between tasseled cap wetness and actual field survey data. This was unexpected since recent studies have identified tasseled cap wetness as one of the most accurate indicators of vegetative change (Czerwinski et al., 2014). Red-shift stretch and red-shift compression demonstrated the highest level of agreement with actual field data. A paper containing all of the findings form this study has been submitted to a journal for publication.

7.0 Dissertation Outline

This research examines the impacts of recent climate change on fragile alpine ecosystem vegetation through the use of remote sensing imagery. This dissertation is written in a manuscript style where chapters 2 through 6 are papers published or submitted for publication with conclusions presented in Chapter 7. These Chapters investigate several research questions.

In Chapter 2, a time series examination of historical Landsat data is used to find changes in the observed surface reflectance over time based on the predominant land cover classes present within the watershed. Given the importance of determining the impact of higher temperatures on the planet's ecosystems, the effect rising temperatures have on the spectral reflectance properties of vegetation is determined. It is hypothesized that higher temperatures result in higher surface reflectance values in dry regions where the increased temperatures increase evapotranspiration resulting in reduced vegetation. However, in areas where moisture is abundant, higher temperatures are hypothesized to result in lower surface reflectance values brought about by increased vegetative cover generated from increased rates of photosynthesis. The information provided by the reflectance data for each spectral region is used to determine how changes in temperature affect the study area vegetation.

In Chapter 3, a comparison of the surface reflectance generated from a traditional dark object subtraction methodology versus the USGS Climate Data Record data set is provided. This research question investigates the effect different analytical methods have

on the determination of surface reflectance from remote sensing imagery. This is accomplished by comparing the surface reflectance data generated by the USGS with the surface reflectance generated using a simple Dark Object Subtraction (DOS) atmospheric correction based on the Cosine Theta (COST) algorithm developed by Chavez, 1996. The two data sets are compared using simple linear regression. Correlation coefficients are determined for each data set for each of the six reflective bands of the Landsat 5 TM sensor. The data are used in several ways including a simple comparison of all data sets and how those comparisons have trended over time, how the data sets compare based on land class, how the data sets compare based on elevation, and how the data sets compare based on vegetative density to determine which parameters show significant disagreement. It is hypothesized that the surface reflectance determined using older dark object subtraction methods show substantial deviation from the USGS published data set, requiring researchers to revisit previous studies using the new data set.

In Chapter 4, a second time series study examines trends in the spectral response based on elevation. These studies correlate spectral reflectance trends to variations in environmental parameters including temperature and precipitation, taking into account land cover classification, elevation, and vegetative density. It is hypothesized that warming temperatures will drive upslope migration of species leading to composition changes as cold climate species are pushed into a summit trap, reducing their habitable space while increasing the space available for warm weather species to expand into. It is also theorized that higher temperatures will drive increased photosynthesis in water rich

densely vegetated areas while reducing cover in dry sparsely vegetated areas. In order to ensure a representative sample of all the communities present within the watershed, three sample sites representing dense vegetation (ground cover > 50%), medium vegetation (ground cover 10% to 50%) and sparse vegetation (ground cover < 10%) are selected for every 100 meters of elevation gradient within the watershed from 1200 meters MSL to 3600 meters MSL (75 total sample sites; 25 dense, 25 medium, and 25 sparse).

Using the information derived from the previous studies leads to the principal research question of this work; how has recent climate change impacted the Big Pine Creek watershed. It is hypothesized that higher temperatures in alpine watersheds will drive numerous physiological changes including increased vegetative growth in water rich areas and declines in vegetative cover in water poor areas. The physical constraints of alpine regions will promote species turnover as cold weather species are pushed into the summit trap while warm weather species expand into newly habitable zones. To address this question a site survey is conducted at 30 sample sites throughout the watershed. Field collected spectral signatures from the primary endmembers of each site are also provided. Chapter 5 presents the results of the field survey data collection performed in July 2014 and includes spectra of the predominant surface cover vegetation, litter, and soil.

In Chapter 6, trends in vegetative response to recent climate are presented. In this study, thirty sites are investigated for trends in surface reflectance, vegetation indices, and tasseled cap transformations as well as analysis using spectral mixture analysis

(SMA) on each site and performing a trend analysis on the results of the SMA. This analysis of the sample sites identifies specific changes to the vegetative composition taking place.

The study in Chapter 6 also examines the performance of red-shift theory, vegetation indices and tasseled cap transforms against actual field survey data from fifty permanent sites located at several locations in the western United States. Vegetation indices have long been used to elicit information regarding vegetative health and quantity from satellite imagery. However, few studies exist regarding their use in determining trends in vegetative surface cover. Existing theory of vegetative increases under red-shift stretch and vegetative declines under red-shift compression are expanded upon to include the hypothesis of increasing vegetation with composition change under red-shift downward translation and vegetative decline with composition change under red-shift upward translation.

The theory that the information derived from trend studies of vegetation indices and transforms will closely follow the information derived from the long term vegetation plot surveys is investigated. Fifty long term vegetation transects are examined to determine trends in surface cover and composition data. These data are then compared to red-shift theories, vegetation indices, and tasseled cap transform data generated from satellite imagery over those same fifty sites.

Finally, in Chapter 7, a discussion of the findings from each of the studies performed in this research program is presented along with conclusions and

recommendations. Appendix A includes the publisher copyright agreements from the three manuscripts included as chapters in this document as well as the acceptance rate letter for a conference paper that is a part of this manuscript.

Chapter 2: The Big Pine Creek Watershed and Climate Change: A Trend Analysis of Landsat Surface Reflectance Data and PRISM Datasets over the last three decades

Contribution of Authors and Co-Authors

This manuscript was co-authored by Patrick Sawyer and Haroon Stephen. Patrick Sawyer was the first author who conceived and implemented the study design, collected and analyzed the data, wrote the manuscript and presented the findings to the River Basins Management VII conference in New Forest UK in May 2013. Haroon Stephen was the second author who assisted with the study design and provided feedback on statistical analyses and drafts of the manuscript.

Manuscript Information Page

This manuscript has been published in the peer-reviewed Elsevier Ltd. journal Advances in Space Research, Volume 54, pages 37-48, 2014. Copyright information can be found in Appendix A or at the Elsevier web site; (https://www.elsevier.com/about/company-information/policies/copyright).

This manuscript presents the research performed and findings achieved relating to the use of remote sensing in ecological studies. The purpose of this work is determination of ecosystem changes as evidenced by changes in the surface reflectance properties of the study area over the last three decades. This work supports objective number one to study and evaluate recent climate change impacts on the ecosystem.

Abstract

Recent variations in normal meteorological conditions indicate the earth's climate is changing in ways that may impact delicate ecological balances in sensitive regions. Determining how those changes are affecting the biosphere is essential if we are going to be able to adapt to those changes and to potentially mitigate their harmful consequences. This paper presents a time series study of an alpine ecosystem in the Big Pine Creek watershed in California's Eastern Sierra Nevada Mountain's. Raw Landsat data covering the years 1984 through 2011 is converted to observed surface reflectance and analyzed for trends that would indicate a change in the ecosystem. We found that over the time period of the study, observed surface reflectance shows a general decline across the spectrum while our analysis of environmental data demonstrates statistically significant increases in temperatures. While declining reflectance in the visible and short wave bands are indicators of increased surface cover, the fact that the IR band also shows declines is consistent with a decline in tree density. This study provides a useful insight into the ecological response of the Big Pine Creek watershed to recent climate change. These findings suggest that alpine ecosystems are particularly sensitive to increasing temperatures. If these results are replicated in other alpine watersheds it will demonstrate that the biosphere is already showing the effects of a warmer environment.

1.0 Introduction

A significant portion of fresh water supplies are tied to glacial and alpine ecosystems that are vulnerable to variations in the earth's climate (Barnett et al., 2005).

Since these regions exist at the boundaries of climate zones such as the higher and lower latitudes and at high elevations where several ecotones may occur in a small geographic area, they will absorb the first impact of climate change. Biomes that populate these habitats are highly susceptible to changes in environmental conditions (Lindner et al., 2010). Higher temperature levels will alter the nutrient and energy transfers that drive biological processes such as photosynthesis. As the environmental characteristics of individual ecosystems change, the physiological processes dependent on those environmental parameters also change, resulting in variations in the spectral response of both soils and vegetation.

Spaceborne instruments, that can effectively monitor the biosphere, have become essential tools to enhance our ability to adapt to future environmental conditions brought about by complex processes such as climate change and population growth (Chung et al., 2010). Spectral characteristics measured with remote sensing instruments such as the Landsat 5 Thematic Mapper (TM) enable us to analyze ecological properties of vegetation. Vegetation has characteristic spectral responses such as low red reflectance due to chlorophyll absorption and high near infrared (NIR) reflectance due to the reflectance of the internal structures of the canopy (Wessman, 1992). Changes in surface reflectance can thus be correlated with variation in vegetative cover and plant health. Since the constituents of the plants vary over their phenological cycle, it is also possible to identify the various stages of the cycle such as spring flowering and fall senescence.

Soil also demonstrates unique spectral characteristics depending on properties such as its moisture, organic matter content and texture (Jackson et al., 1986). Lower soil moisture content, a possible indicator of water stress in vegetation, would cause higher surface reflectance in the mid-wave infrared (MWIR) region that can be detected using Landsat data (Musick and Pelletier, 1988). Higher temperatures combined with lower humidity levels will increase evapotranspiration resulting in less soil and vegetation moisture which will place additional burden on ecosystem vegetation. These effects are heightened in regions experiencing historic droughts such as the southwestern United States (Adams et al., 2009). Jackson et al. (1986) found that plant water stress will decrease the NIR response while increasing the reflectance in the red region of the spectrum. In addition to altering the spectral reflectance properties of the vegetation, plant stress can alter the geometry of the plant through processes such as drooping or wilting, resulting in a higher soil fraction component of the response signal (Jackson et al., 1986). Todd and Hoffer (1998) found that reduced vegetation moisture content tends to increase visible and MWIR reflectance (Todd and Hoffer, 1998).

Vogelmann et al. (2009) examined trends in spectral response in a time series study of the San Pedro Parks Wilderness area in New Mexico for the years 1992 through 2006. Higher elevations were shown to be spectrally stable except for areas infested with western spruce budworm. Some of the lower elevation shrub regions had declines in their short-wave infrared (SWIR)/NIR ratios as did patches of conifer trees suffering from high mortality rates (Vogelmann et al., 2009). Loss of available moisture significantly impacts

forest growth and overall ecosystem health (Williams et al., 2013). Higher temperatures may also promote pest infestation. Williams et al. (2013) found that bark beetle populations increased during warmer periods, especially in forests already suffering moisture deficits induced by higher temperatures. This study determined that maximum temperature (T_{MAX}) is an ideal surrogate for determining vapor pressure deficit induced forest stress (Williams et al., 2013). Higher temperatures combined with moisture deficits are expected to result in new vegetative assemblages (Williams et al., 2010).

The ecological response to elevated temperatures is complex and will be affected by other factors such as water and other nutrient resource availability. In cold alpine regions where water availability is not limiting, higher temperatures are expected to increase the habitable zones for several species, allowing for upslope migration and increased vegetative cover; provided other essential resources are not limited (Skre and Naess, 1999). Conversely, where water is limited, higher temperatures will increase plant stress resulting in reduced vegetative cover (Chmura et al., 2011). An ongoing study of 76 forest plots in the western US has shown increased tree mortality rates correlated with increased regional temperatures over the last three decades (van Mantgem et al., 2009). This study also found that while mortality rates have increased, recruitment rates have not, resulting in an overall decline in forest density (van Mantgem et al., 2009).

In this paper we examine an alpine watershed using time series analysis of Landsat imagery to determine the impact recent climate change has had on the ecosystem. The Landsat imagery is processed to derive observed surface reflectance

values. We apply a statistical approach to determine the presence of trends in the reflectance and meteorological data that would validate the hypothesis of increased vegetative surface cover resulting from higher temperatures.

2.0 Study Area and Data

2.1 Study Area Description

Figure 1 below shows the Big Pine Creek watershed located in California's Eastern Sierra Mountains. Big Pine Creek is a major tributary to the Owens River which is a significant source of fresh water for Los Angeles. The Owens River valley straddles the Great Basin and Mojave deserts with vegetation consisting primarily of pine forests at higher elevations and xeric species at lower elevations. Areas bordering streams and the Owens River are primarily grass dominated meadows (Elmore et al., 2003). Elevation within the watershed increases from East to West with the higher regions dominated by barren rock and woodlands with the lower regions dominated by mixed desert shrubs.

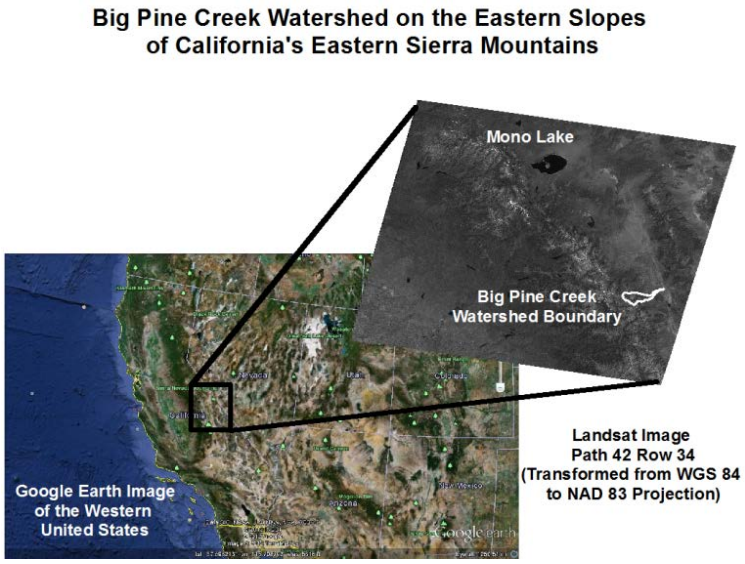

Figure 1. Study area location showing the boundary of the Big Pine Creek watershed.

The Big Pine Creek watershed ecosystem owes its existence to snow melt and melt-water from the Palisade Glacier. In addition to being the southern-most glacier in the United States, it is also the largest glacier in the Sierras with a surface area of 1.3 km^2. It was formed about 3,200 years ago, reaching a maximum extent as recently as 170 years ago (Bowerman and Clark, 2011). It has been generally in retreat ever since. The Big Pine Creek watershed drainage area covers approximately 82 km^2 and its average flow is 1.8 m^3/s. Measurements taken in the 1980's indicate that the creek is a gaining stream at the lower elevations in contrast to most other Owens River tributaries which are losing streams (Kondolf, 1989). Since all of the living species within this watershed depend on the glacier and snow melt for their survival, the impact of temperature and

precipitation variations on the biodiversity of the Big Pine Creek watershed is the focus of this study.

There are 34 land cover classes in the Big Pine Creek watershed with the ten most abundant covering 93% of the total surface area. These top ten land cover classes are listed in table 1 along with their relative abundance. The United States Geological Survey (USGS) provides land cover information to the public through the GAP analysis program; an online mapping service hosted by the University of Idaho (http://www.gap.uidaho.edu/landcoverviewer.html). In order to ensure a representative sample of the numerous vegetative species present in the watershed, three sample sites at different elevations, from each of the ten most abundant land cover classes are selected for a total of 30 sample sites. These ten land cover classes fall into four types, barren, woodland, shrub, and developed. Differences in how the various land types have responded to climate change will provide insight into which ecological processes are being most affected by recent variation in environmental parameters.

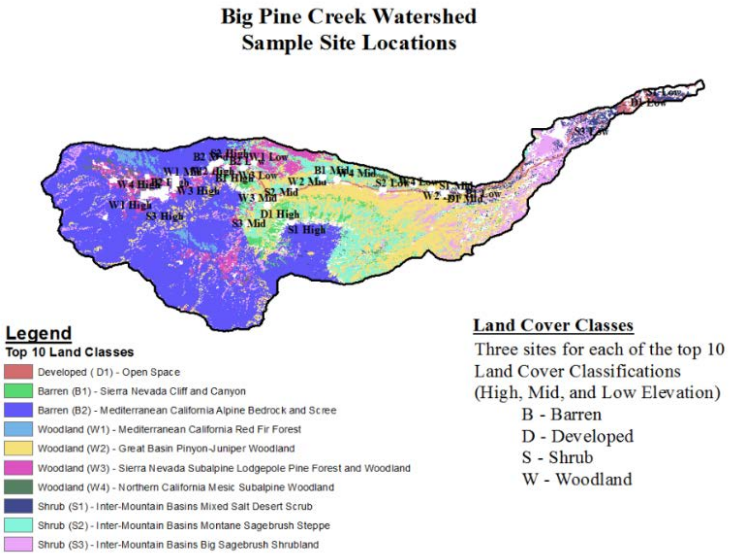

Figure 2. Land Cover Classes of the study area and location of sample sites.

Table 1

Land Cover Classes in the Big Pine Creek Watershed

USGS Land Class Level 3	Land Type	Class ID	PIXEL COUNT	% of Pixels
Mediterranean California Alpine Bedrock and Scree	Barren (B2)	3504	46547	39.16
Great Basin Pinyon-Juniper Woodland	Woodland (W2)	4514	25196	21.19
Inter-Mountain Basins Montane Sagebrush Steppe	Shrub (S2)	5308	10597	8.91
Inter-Mountain Basins Big Sagebrush Shrubland	Shrub (S3)	5706	9925	8.35
Sierra Nevada Subalpine Pine Forest and Woodland	Woodland (W3)	4533	6819	5.73
Sierra Nevada Cliff and Canyon	Barren (B1)	3215	2857	2.40
Inter-Mountain Basins Mixed Salt Desert Scrub	Shrub (S1)	5205	2827	2.37
Developed, Open Space	Developed (D1)	1201	1966	1.65
Mediterranean California Red Fir Forest	Woodland (W1)	4318	1872	1.57
Northern California Mesic Subalpine Woodland	Woodland (W4)	4608	1585	1.33

2.2 Data

The data in this study includes Landsat spectral reflectance data, meteorological data including PRISM generated precipitation, maximum temperatures, minimum temperatures, and dew point temperatures and Big Pine Creek stream flow data.

2.2.1 Spectral data.

The Landsat 5 TM imagery used in this analysis was acquired for 28 dates in the month of July from 1984 (year of launch) through 2011 (year turned off). Most of the imagery used in this analysis is from Path 42, Row 34 with four of the images from Path 41, Row 34. Both image ID ground swaths cover the entire study area. This imagery was obtained from the EarthExplorer web site operated by the USGS (http://earthexplorer.usgs.gov/). Since the period of maximum leaf area index generally occurs in the mid-June to mid-August time frame (Gond et al., 1999), only imagery in the July time frame was considered for this analysis in order to minimize the impacts of the phenological cycle on the reflectance data.

We use only Landsat 5 TM imagery since that sensor has collected data for the entire 28 year period of the study. Using a single sensor ensures maximum consistency of the data and eliminates errors associated with correlating data from multiple sensors. The six reflective bands of the TM sensor cover the blue, green, red, near infrared (NIR), short-wave infrared (SWIR), and mid-wave infrared (MWIR) regions of the spectrum as well as their ecological applications. Bands 5 and 7 are sometimes referred to as SWIR1

and SWIR2. However, in this study, we refer to band 5 as the SWIR and band 7 as the MWIR. Band 6 covers the thermal infrared (TIR) and the data from this region is not used in this study.

2.2.2 Meteorological data.

Meteorological data examined in this study is obtained from the University of Oregon's Parameter-elevation Regressions on Independent Slopes Model (PRISM) web site (http://www.prism.oregonstate.edu/). According to its website, PRISM data are modeled estimates based on point data and a digital elevation model and is available for the entire continental US at 4 km resolution. All 30 sample sites in this study fall within 5 PRISM grid cells as shown in Figure 3.

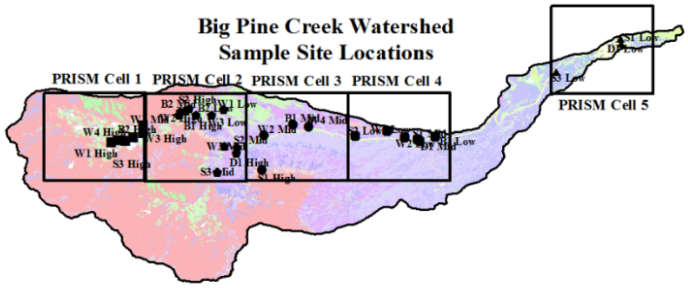

PRISM Meteorological Cell

Cell 1 ■	Cell 2 ⬟	Cell 3 ●	Cell 4 ●	Cell 5 ▲
B2 (High)	B2 (Mid)	W2 (Mid)	W2 (Low)	S3 (Low)
S3 (High)	B2 (Low)	B1 (Mid)	S2 (Low)	S1 (Low)
W3 (High)	W2 (High)	S1 (High)	B1 (Low)	D1 (Low)
W1 (High)	S2 (High)	W4 (Mid)	S1 (Mid)	
W1 (Mid)	S2 (Mid)		D1 (Mid)	
W4 (High)	S3 (Mid)		W4 (Low)	
	W3 (Mid)			
	W3 (Low)			
	B1 (High)			
	D1 (High)			
	W1 (Low)			

Figure 3. PRISM Cell locations and the sample sites within each cell

3.0 Research Approach and Methods

3.1 Statistical Trend Analysis

The non-parametric Mann-Kendall (MK) trend test is used to establish the presence of trends in the surface reflectance observations, meteorological data, and stream flow data over the last 28 years. This analysis essentially determines if a set of values (y) are increasing or decreasing over time. Mann-Kendall analysis looks at the sums of the signs of the differences between successive data points and calculates a score or "S" statistic with the following properties: for S < 0 (values are decreasing over time); for S > 0 (values are increasing over time). The magnitude of the S-statistic is a measure of the strength of the trend. For a sample size of 28, S values of ±100 indicate a statistically significant trend with a p value of < 0.05. This means the null hypothesis of no-trend in the data can be discarded with the risk of committing a Type II (rejection of a true null or H_0) error at less than 5%. The MK S-statistic is calculated using

$$S = \sum_{i=1}^{n-1} \sum_{j=i+1}^{n} sign\,(y_j - y_i)\,, \tag{1}$$

where n is the number of observations and y_i ($i = 1 \ldots n$) is the value at time T_i and y_j ($i = 1, \ldots, n$) is the value at time T_j (De Beurs and Henebry, 2005). Variance in the S statistic is calculated as

$$Var\,(S) = \frac{n(n-1)(2n+5)}{18}. \tag{2}$$

This variance assumes there are no tied pairs in the data. If tied pairs are identified, the software program applies a continuity equation which assumes a normal distribution for S with a mean zero. The variance is used to determine the probability (p) of obtaining a value of S greater than that calculated for the given number of data points when no trend is present. The probability statistic is determined from the Z score which is defined as:

$$Z = \begin{cases} \dfrac{S-1}{\sqrt{Var(S)}} & \text{, for } S > 0 \\ 0 & \text{, for S = 0} \\ \dfrac{S+1}{\sqrt{Var(S)}} & \text{, for } S < 0 \end{cases} \tag{3}$$

In addition to the trend statistic (S), Kendall's tau (τ) is determined from the equation

$$\tau = \frac{S}{\frac{n(n-1)}{2}}. \tag{4}$$

where n is the number of observations. Kendall's tau is similar to the correlation coefficient in linear regression. The magnitude of the trend is determined using the Sen's slope estimation with confidence intervals defined as the upper and lower estimate for the mean value of the slope. Sen's slope is determined by calculating the slope at each data point and taking the median of those slopes as the magnitude of the trend as shown;

$$Sen's\ Slope = median\left(\frac{y_j - y_i}{Time_j - Time_i}\right). \tag{5}$$

These calculations are carried out in Excel using the XLSTAT add-in statistical application. This program generates the S statistic as well as the probability (*p*) value which is used to quantify the statistical significance of the trend. The confidence factor (risk of rejecting a true null) is defined as (1-*p*)*100%. Trend analysis is performed on the spectral reflectance data for the six TM reflectance bands, the meteorological data including precipitation, maximum temperature, minimum temperature, dew point temperature, and stream flow data.

3.2 Landsat Data Processing

The Landsat imagery was processed to observed surface reflectance by first converting the digital numbers to at sensor radiance values by removing the gain and offset caused by the sensors themselves (Chavez, 1996). The digital numbers (DN) from the Landsat Level 1 imagery used in this study are converted to at-sensor radiance values using the band specific rescaling factors provided by the header file of each image (Chander and Markham, 2003). The spectral radiance at the sensor's aperture (L_λ), in W/m^2•sr•μm, is determined using

$$L_\lambda = \left(\frac{L_{Max\,\lambda} - L_{Min\,\lambda}}{Q_{Cal\,max}}\right) \cdot Q_{Cal} + L_{Min\,\lambda}, \quad (6)$$

where Q_{cal} is the calibrated digital number, $L_{Max\lambda}$ is the spectral radiance scaled to $Q_{Cal\,max}$, $L_{Min\lambda}$ is the spectral radiance scaled to $Q_{Cal\,min}$ (Chander and Markham, 2003). The next step is conversion of the at-sensor radiance to top of atmosphere reflectance which

corrects for variation in exoatmospheric solar irradiance due to spectral band differences (Chander and Markham, 2003). Top of atmosphere reflectance (ρ_P) is calculated as

$$\rho_P = \frac{\pi \cdot L_\lambda \cdot d^2}{ESUN_\lambda \cdot Cos\theta_s}, \quad (7)$$

where ρ_P is the unitless planetary reflectance, L_λ is the spectral radiance at the sensor's aperture, d is the earth sun distance in astronomical units, $ESUN_\lambda$ is the mean solar exoatmospheric irradiance, θ_s is the solar zenith angle in degrees (Chander and Markham, 2003).

An atmospheric correction is then applied to obtain surface reflectance using a simple image based method called Dark Object Subtraction (DOS) which is based on the assumption that radiance seen at the satellite for "dark" pixels (i.e. deep water or shadow) result purely from atmospheric path radiance. This allows us to process imagery where atmospheric column data are not available (generally pre-2000). For this analysis DOS is performed using the Cos θ or "COST" technique developed by Chavez (1996). The first step in the DOS method is removal of a reflectance value representing the contribution of the atmospheric scattering effect from the DN recorded at the sensor. Two ways of selecting this value are the histogram approach in which the DN selected is the first below 1000 pixels for a typical Landsat image, or a simpler approach in which a known dark object is selected using the assumption that any DN from that pixel is the result of the atmospheric contribution.

Use of the histogram method typically requires analysis of the entire image (Chavez, 1988). Therefore, for this effort, the selection of the minimum pixel value representing the atmospheric haze was accomplished by selecting the minimum DN for each band over Black Lake. This mountain snowmelt fed water body is surrounded by trees and mountain shadow representing an ideal zero reflectance surface for the DOS method. The first step in the COST technique is to calculate the minimum radiance ($L_{\lambda,min}$) using:

$$L_{\lambda,min} = L_{Min\,\lambda} + \left(\frac{L_{Max\,\lambda} - L_{Min\,\lambda}}{Q_{Cal\,max}}\right). \quad (8)$$

Since no targets are completely black, even the dark object will contain some radiance value. Therefore, the COST method assigns a 1% reflectance value to the selected dark object (Chavez, 1996). The theoretical radiance ($L_{\lambda,1\%}$) of a dark object (assuming a 1% reflectance) is calculated using:

$$L_{\lambda,1\%} = \frac{0.01 \cdot d^2 \cdot Cos^2\theta}{\pi \cdot ESUN_\lambda}, \quad (9)$$

A haze correction factor ($L_{\lambda,haze}$) is then calculated using:

$$L_{\lambda,haze} = L_{Min\,\lambda} - L_{\lambda,1\%}, \quad (10)$$

(Chavez, 1996). The corrected surface reflectance value (ρ_P) is then calculated by

$$\rho_P = \frac{\pi \cdot d^2 \cdot \left(L_\lambda - L_{\lambda,haze}\right)}{TAU_v \cdot ESUN_\lambda \cdot Cos\,\theta \cdot TAU_z}, \quad (11)$$

where TAU_v represents the atmospheric transmittance from the ground to the sensor and TAU_z is the atmospheric transmittance from the sun to the ground (Lu et al., 2002). Since

Landsat images are taken at a nadir angle, TAU_v is equal to Cos 0^o or 1.0. For the COST method, TAU_z is equal to the cosine of the solar zenith angle or Cos θ^o (Chavez, 1996). Therefore, the surface reflectance is calculated as:

$$\rho_P = \frac{\pi \cdot d^2 \cdot \left(L_\lambda - L_{\lambda,haze}\right)}{ESUN_\lambda \cdot Cos^2\,\theta}, \tag{12}$$

The procedure detailed above provides us with observed surface reflectance values for each of the six reflectance bands for all sample sites in each year of the study. In order to identify patterns across all the vegetation types in the study area, spectral reflectance data are averaged for all the sites in each band and then analyzed for trends. Additional analysis is performed by averaging the reflectance data by land type; barren, developed, woodland and shrub. We also examine relationships between the spectral bands by considering the trends in vegetation indices resulting from the spectral reflectance data. Vegetation indices are often used to establish vegetation cover in remote sensing studies. We consider both ratio indices which analyze the large difference in the red and NIR bands characteristic of vegetation and weighted ratios which focus on physical parameters such as surface brightness, greenness and wetness. In this analysis we look at the following indices:

Normalized Difference Vegetation Index (*NDVI*), defined as

$$NDVI = \frac{\rho_{NIR} - \rho_{RED}}{\rho_{NIR} + \rho_{RED}}, \tag{13}$$

(Rouse at al., 1974), where ρ_{NIR} is the reflectance in band 4 and ρ_{RED} is the reflectance in band 3;

Soil Adjusted Vegetation Index (*SAVI*), defined as

$$SAVI = (1 + L)\,\frac{\rho_{NIR} - \rho_{RED}}{\rho_{NIR} + \rho_{RED} + L}, \tag{14}$$

where L is a soil correction factor set at 0.5 (Huete, 1988);

Modified Soil Adjusted Vegetation Index ($MSAVI_2$), defined as

$$MSAVI_2 = \frac{2\rho_{NIR} + 1 - \sqrt{(2\rho_{NIR} + 1)^2 - 8(\rho_{NIR} - \rho_{RED})}}{2}, \tag{15}$$

(Qi et al., 1994); and Tasseled Cap transformations for Brightness (TC_B), Greenness (TC_G), and Wetness (TC_W) which are defined as

$$TC_B = 0.2043\rho_1 + 0.4185\rho_2 + 0.5524\rho_3 + 0.5741\rho_4 + 0.3124\rho_5 + 0.2303\rho_7 \tag{16}$$

$$TC_G = -0.1603\rho_1 - 0.2819\rho_2 - 0.4934\rho_3 + 0.7940\rho_4 - 0.0002\rho_5 - 0.1446\rho_7 \tag{17}$$

$$TC_W = 0.0315\rho_1 + 0.2021\rho_2 + 0.3102\rho_3 + 0.1594\rho_4 - 0.6806\rho_5 - 0.6109\rho_7 \tag{18}$$

where $\rho_{1...7}$ is the reflectance in band 1 through band 7 respectively (Crist, 1985). As with the spectral reflectance and vegetation index data, the precipitation and temperature data sets were averaged across all five PRISM cells to analyze for trends across the entire watershed.

4.0 Results and Discussion

4.1 Spectral Trend Data

While each individual site has its' own unique response to recent environmental fluctuations, we first look for patterns across all the vegetation in the watershed. To accomplish this, we averaged the observed surface reflectance data over all 30 sample sites and analyzed for trends in each of the six reflective bands (see Figure 4). Table 2

contains the descriptive statistics of the analysis including the MK-S value, *p*-value, Sen's slope and confidence intervals (CI). Error bars are set at the confidence interval for each data set.

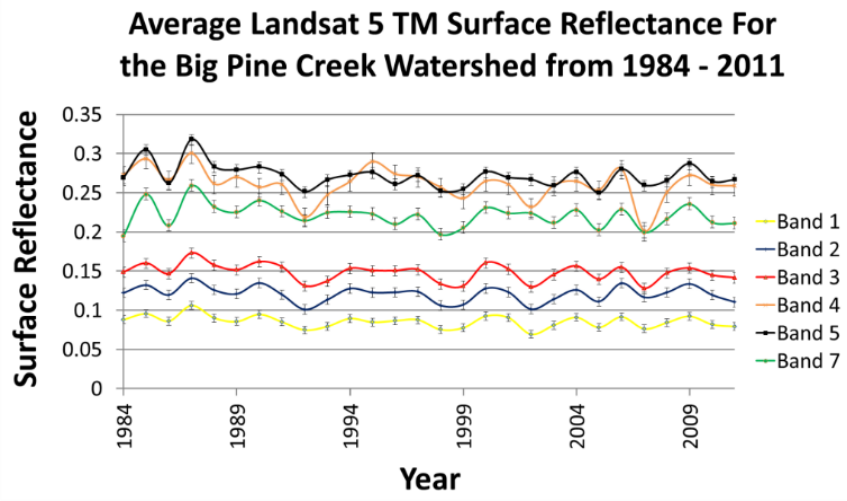

Figure 4. Landsat 5 TM observed surface reflectance averaged over all 30 sample sites.

Table 2

Trend Data for Landsat 5 TM Reflective Bands

Statistic	Band 1	Band 2	Band 3	Band 4	Band 5	Band 7
S	-78	-42	-94	-98	-82	-70
p	0.130	0.422	0.066	0.055	0.110	0.175
Sen's Slope	-0.000291	-0.000243	-0.000465	-0.00059	-0.000544	-0.000639
CI	-0.005 /0.005	-0.006 /0.006	-0.007 /0.006	-0.013 /0.011	-0.008 /0.006	-0.007 /0.008

Figure 4 shows the average spectral response over all 30 sample sites for all six reflective bands of the Landsat 5 TM sensor. For the band 1 data, the S value of -78

indicates values are declining over time. The *p*-value of 0.130 indicates that the risk of rejecting the null hypothesis of no trend is only 13%. A negative trend in the blue region of the spectrum supports our hypothesis of increased vegetative surface cover since higher levels of vegetation would mean increased chlorophyll which has strong blue region absorption features.

For band 2 data, the S value of -42 indicates values are declining over time. The *p*-value of 0.422 indicates that the risk of rejecting the null hypothesis of no trend is 42.2%. Thus while values are in decline, we cannot state there is any significance to the trend. Light in the green region tends to reflect off the surface of the vegetation with not much absorption. Slight declines in the green reflectance values could potentially be due to changes in the physical properties of the vegetation such as reduced surface area from leaf wilting or smaller leaves. Less surface area will result in less green region reflectance.

For the band 3 data, the S value of -94 indicates values are declining over time. The *p*-value of 0.066 indicates that the risk of rejecting the null hypothesis of no trend is only 6.6%. As with the blue region of the spectrum, the red region is strongly absorbed by plant chlorophyll. Thus a negative trend in the red reflectance supports our hypothesis of increased vegetative cover.

For the band 4 data, the S value of -98 indicates values are declining over time. The *p*-value of 0.055 indicates that the risk of rejecting the null hypothesis of no trend is only 5.5%. The negative trend in NIR reflectance is difficult to explain and could suggest

that the surface cover is showing reduced structural complexity since reflectance in this region is due to reflection off the plant cell walls and internal structures (Todd and Hoffer, 1998). This finding is consistent with previous nearby studies showing increased tree mortality and reduced forest stand density (van Mantgem et al., 2009). With reduced tree cover, understory vegetative species with less structural complexity than the trees they replaced would be consistent with the declines in both the visible and NIR regions.

For the band 5 data, the S value of -82 indicates values are declining over time. The *p*-value of 0.110 indicates that the risk of rejecting the null hypothesis of no trend is 11%. The SWIR region is where the water absorption feature can be seen. Reduced SWIR reflectance indicates an increase in water absorption (Todd and Hoffer, 1998). This data supports our hypothesis that increased vegetation is present since more vegetative surface cover would result in higher water content.

For the band 7 data, the S value of -70 indicates values are declining over time. The *p*-value of 0.175 indicates that the risk of rejecting the null hypothesis of no trend is 17.5%. A decline in the MWIR is an indicator of increased absorption by moisture in the soil and vegetation (Asner, 1998) which supports the hypothesis of increased vegetative cover. At the 30 meter resolution of the Landsat imagery, every pixel will include components of the soil and vegetation present. Since soil is much more reflective in this spectral region, an increase in vegetative cover will result in lower overall reflectance.

We next grouped the sample sites into four distinct land types, barren, developed, shrub, and woodland in order to determine if trends are occurring among common vegetative types. Sample site reflectance data was averaged for the four land cover types.

Figure 5 shows how each of these spectral bands has trended for each of the four primary land cover types in the study area. While the barren, woodland, and shrub land types all show a consistent pattern with smaller declines in the green (band 2) region and larger declines in the NIR (band 4), the developed areas show a different pattern across the spectrum with significant declines in the red (band 3) and SWIR/MWIR (bands 5 and 7) while showing much lower declines in the NIR (band 4). Developed areas consist of settings such as city parks, golf courses, and single family residences. This difference in the developed areas can be explained by the significant increase in trees and shrubs at one of the developed area sample sites included in this study. In the visible bands, the largest declines in observed surface reflectance are in the developed and shrub areas while the declines in the woodlands and barren areas show less significance.

The significant declines in reflectance in the MWIR and SWIR for developed land cover suggests that surface water content in the soil and vegetation is increasing which is consistent with residential irrigation taking place. Similar significant declines in the visible, SWIR and MWIR in shrub areas are consistent with more surface cover and increased water content. The declines in the NIR are consistent with new growth that has yet to develop the structural complexity that will increase the NIR reflectance. Reduced

NIR levels are consistent with declines in surface complexity that one would expect if species are transitioning from trees to less complex understory vegetation.

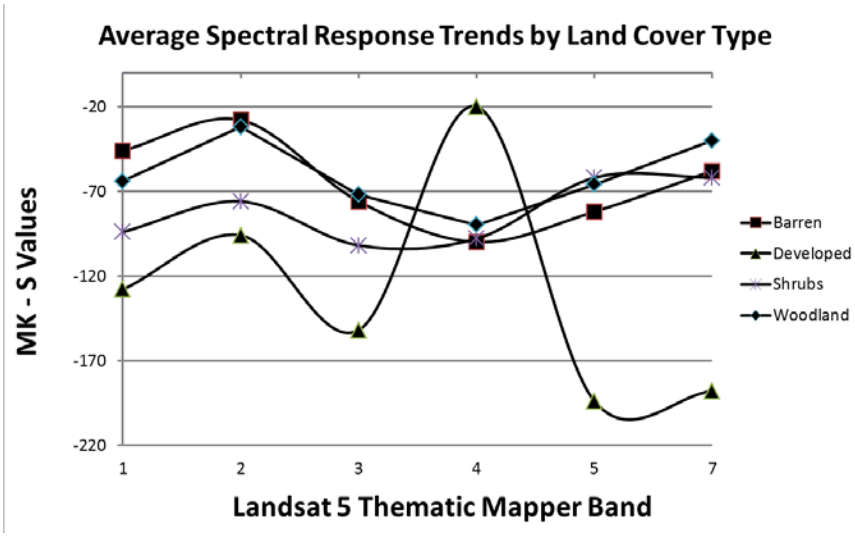

Figure 5. Observed surface reflectance trends averaged over all 30 sample sites of each Landsat 5 TM reflectance band for the four land types.

While also declining in the other land cover types, the strength of the trends is not as significant. For the barren land types, the statistically significant decline in NIR reflectance suggests that what sparse vegetation does exist is in retreat. However, the declines in the visible, SWIR and MWIR while not statistically significant, is an indication vegetative cover is increasing. Similar to the developed and shrub land cover types, these responses are consistent with woody shrubs with their high NIR reflectance being supplanted with less structurally complex species. The woodland land cover sites show similar trends to the barren sites.

We next consider how the trends in reflectance data are manifested in three common vegetation indices and the Tasseled Cap transformation. Figure 6 shows how these indicators have trended during the 28 year study period with the data summarized in table 3. The *NDVI*, *SAVI*, and $MSAVI_2$ indicators are essentially ratios of the NIR and Red bands with corrections for soil contribution for *SAVI* and $MSAVI_2$. As we would expect, the fact that both our red and NIR reflectance's are declining make deriving conclusions from these ratio indices difficult at best. Since the Tasseled Cap transformation considers all six reflective bands, it is better suited to provide useful information regarding trends in vegetation for this study area. In particular, the TC_B (surface brightness) and TC_W (wetness) trends both indicate an increase in vegetation over the time period of the study. The strong decline in surface brightness and strong increase in wetness are consistent with our finding or increased vegetative cover. The small declines in the TC_G (greenness) are not consistent with increases in green vegetation. This finding is consistent with our analysis of each of the six reflectance bands.

Table 3

Trend Data for Vegetation Indices

Statistic	*NDVI*	*SAVI*	*MSAVI2*	TC_B	TC_G	TC_W
S	-6	-48	-58	-80	-36	80
p	0.922	0.357	0.469	0.120	0.493	0.120
Sen's Slope	-0.00003	-0.00024	-0.00031	-0.001	-0.00016	0.00045
CI	-0.014 /0.016	-0.011 /0.010	-0.011 /0.011	-0.017 /0.016	-0.006 /0.006	-0.007 /0.006

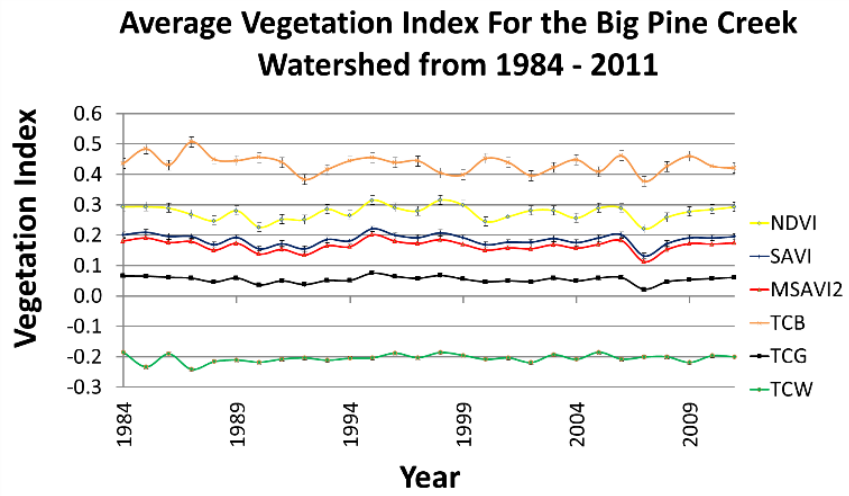

Figure 6. Trends in Vegetation Indices over the 28 year study period.

The trends in observed spectral reflectance are consistent with increased vegetative cover in the study area. The declines in the visible bands indicate the presence of increased photosynthetic compounds that will accompany increased vegetative cover. Declines in the SWIR indicate more water in the scene; another indicator of increased vegetation. Declines in the MWIR are also consistent with increased vegetative surface cover since an increase would suggest higher soil fraction in the land cover. To determine what is driving the increased vegetative surface cover indicated by the observed surface reflectance data, we examine the environmental parameters of precipitation, and temperature.

4.2 Meteorological Data

The meteorological data analyzed in this study include precipitation (*PPT*), maximum temperature (T_{MAX}), minimum temperature (T_{MIN}) and the dew point temperature (T_{DEW}). Big Pine Creek stream flow trends are also analyzed. Precipitation

and temperature data are averaged for each month over the 28 years of the study period. Looking at the monthly trends lets us identify patterns in the seasonality of the study area climate. In addition to monthly precipitation trends, we examine the annual precipitation quantities and Big Pine Creek stream flow data to see if there is evidence of divergence which would suggest increased melting of the Palisade glacier.

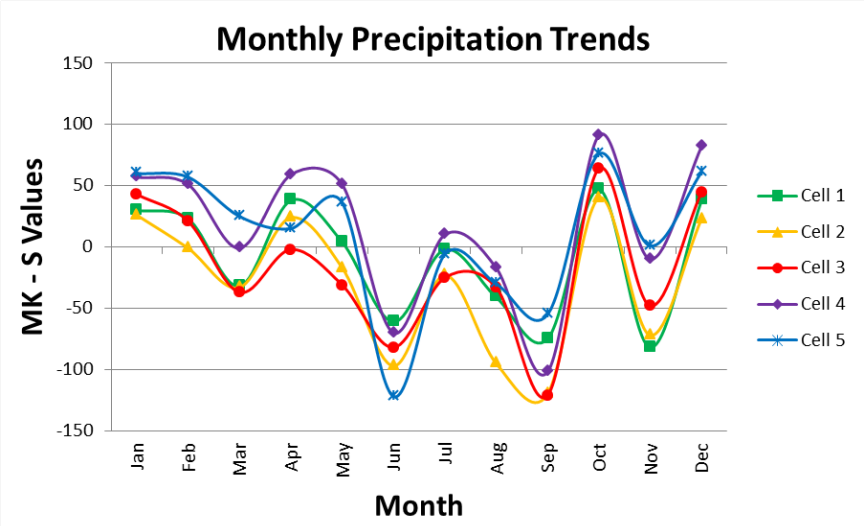

Figure 7. Trends in the monthly precipitation data for the study area for each of the five PRISM cells.

Figure 7 shows the trends in precipitation over the study area for the last 28 years. The PRISM cells are oriented west to east with cell 1 being at the highest elevation near the glacier and cell 5 located in the lowest elevation near the valley floor. The precipitation trends are very consistent across all the PRISM cells with each showing similar seasonal patterns. For this time period, 50% show negative trends and 50% show

positive trends. Only 7% of the precipitation data sets show statistically significant trends (negative).

Looking at seasonal trends, the precipitation appears to be increasing in January, February, October and December while decreasing in March, June, July, and August, (wetter winters and dryer summers). As with the precipitation, there are no statistically significant trends in the stream flow data. However, the months of January, February, April, and August appear to show reduced flow rates while the remainder of the year appears to indicate increased stream flows.

The trends in precipitation, while not statistically significant, do indicate that moisture availability has not significantly changed during the 28 year study period. Even though the monthly precipitation patterns are consistent with development of a late summer moisture deficit, the observed surface reflectance data does not indicate any water resource limitation impacts on the vegetation. This finding suggests that the trends observed in surface reflectance are being driven by other environmental variables such as temperature. As with the precipitation data, the temperature data consists of modelled results based on point measurements. Trends in average maximum, minimum and dew point temperature are presented below.

Figure 8 shows the annual averaged maximum, minimum, and dew point temperatures for all five PRISM cells across the Big Pine Creek study area. The trend statistics shown in table 4 demonstrate that there are very strong positive trends in the

maximum and minimum temperatures and a slight negative trend in the dew point temperatures.

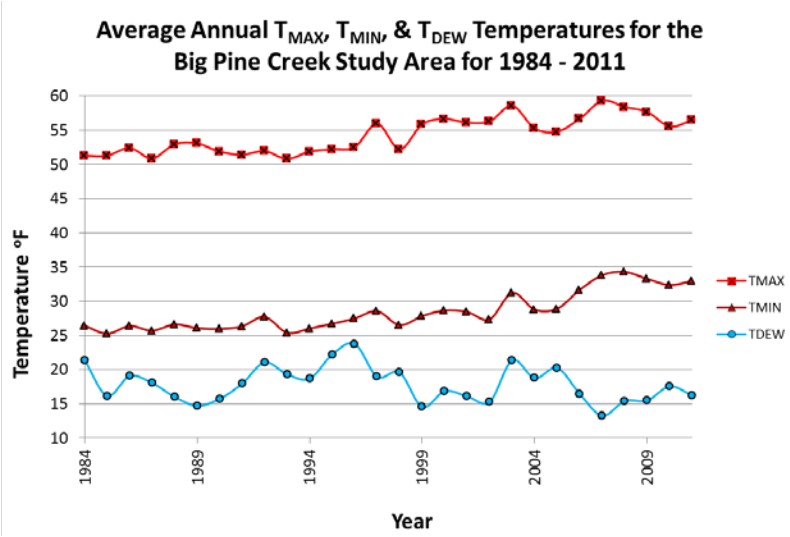

Figure 8. Temperature data for the Big Pine Creek watershed (1984 – 2011).

Table 4

Trend Data for Temperatures

Statistic	T_{MAX}	T_{MIN}	T_{DEW}
S	227	270	-60
p	<0.0001	<0.0001	0.247
Sen's Slope	0.256	0.275	-0.075
CI	-0.544 /1.072	-0.319 /0.964	-1.618 /1.49

Looking further into the monthly temperature trends, we see that for the maximum temperatures, the largest increases are taking place in the summer with smaller increases in the winter; see Figure 9. Higher temperatures are an important factor in driving ecological changes since all biological processes are at their essence chemical

reactions and increased temperatures will increase reaction rates. Increased biological activity can alter vegetative composition by changing the availability essential nutrients. Some nutrients will be more available through faster litter breakdown while some nutrients will be consumed at faster rates. This change in resource availability will drive changes in species composition to those species that are better suited to the new environmental conditions and resource make-up.

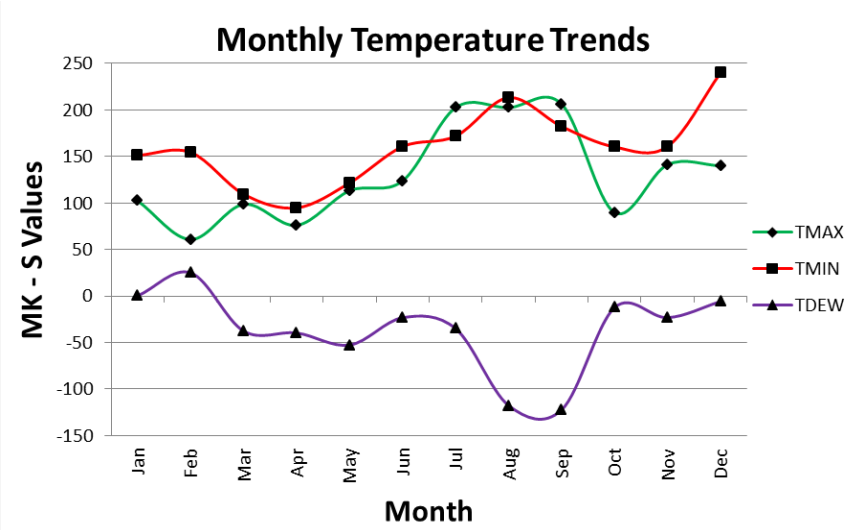

Figure 9. Trends in the monthly temperature data for the study area averaged for all five PRISM cells.

In addition to driving biological activity, higher temperatures will also increase evapotranspiration. This will reduce moisture availability and stress vegetative species, especially those that are not drought tolerant. Species with less dependence on soil moisture will be favored. However, based on the trends in the SWIR and MWIR discussed earlier, soil moisture deficits have not developed. The declines in these spectral

regions are consistent with higher surface moisture content since water absorption is a primary factor in the reflectance of these bands.

For the monthly minimum temperature trends, we see the largest increases are taking place in the summer and fall with smaller increases in the winter and spring. What these data demonstrate is that the summers are getting warmer and the winters are getting milder. This is an important finding since as discussed earlier, warmer summers will increase evapotranspiration during the dry season, increasing potential water stress in the vegetation. Milder winters will also result in reduced water storage capacity as less precipitation will fall as snow, which also results in reduced water supplies in the warmest time of the year.

Figure 9 shows the dew point temperatures (T_{DEW}), which are an indication of atmospheric moisture content show a preponderance of negative S values (85%) indicating a reduction in humidity levels. There are statistically significant declines in T_{DEW} in the months of August and September. The seasonal trends found in this analysis closely align with future climate regimes predicted by general circulation models showing milder wetter winters and hotter drier summers (Lenihan et al., 2003). Lenihan et al. (2003) show that these future climate scenarios can produce shifts in the vegetative composition. In particular, their biological distribution model simulations suggest a shift from shrubs to grasslands under these conditions (Lenihan et al., 2003). All the temperature trends, maximum, minimum, and dew point demonstrate that the Big Pine

Creek watershed is at heightened risk from climate change and highlight the need to develop strategies to adapt to the new climate paradigm.

Higher temperature is an essential factor in the growth of additional vegetation within the study area. While the trends of warmer and dryer summers suggest potential vegetative moisture stress, the observed spectral reflectance data (reduced SWIR and MWIR) does not find any evidence that those conditions have affected the vegetation. The negative trends in the blue and red regions of the spectrum suggest increased absorption by plant pigments from which we infer increased vegetation. The trends in the NIR are more difficult to explain and may, in fact may contradict the conclusion that vegetation is increasing.

4.3 Confidence Levels

Multitemporal satellite imagery is impacted by several factors including changes in sensor response, sensor stability, atmospheric effects, and illumination effects (Vicente-Serrano et al., 2008). To account for geometric pixel registration errors, which are generally below 0.5 pixels (Schueler and Salomonson, 1985), the pixel values for each sample site were resampled by averaging the eight adjacent pixel values along with the sample site pixel value. Radiometric uncertainty for the TM data is approximately 5% (Chander et al., 2009). The USGS has recently published surface reflectance data sets for all of the Landsat 5 imagery analyzed in this study. Future work will include comparison of the USGS surface reflectance data with the reflectance data developed in this study.

The meteorological data used in this analysis is modeled data that is based on interpolation of point data between measurement stations and averaged over 4 km^2 grids. Analysis of how well the model predictions correlate against the actual point sampling locations shows errors generally in the 10 to 20% range (Daly, 2006). While the Landsat reflectance data only covers a 28 year time span, the PRISM data extends back to 1895. Temperature trends over the last century show significant warming through the end of the 1940's, followed by a down trend lasting into the mid 1970's. Since that time, the study area has seen a consistent climb in temperatures across all five PRISM cells.

5.0 Summary and Conclusions

This study examined the changes in the ecosystem of the Big Pine Creek watershed as measured by trends in observed surface reflectance values at 30 sample sites over a 28 year time span from 1984 through 2011. Observed surface reflectance shows declining trends in each band when averaged across all 30 sample sites. Lower surface reflectance in the visible bands is an indication of increased vegetation cover. However, the fact that the NIR reflectance is also decreasing suggests that any additional vegetative cover is structurally less dense.

Examination of ratio based vegetation indices including *NDVI*, *SAVI*, and $MSAVI_2$ do not show significant trends primarily due to the fact that both the Red and NIR bands are both declining. Looking at the Tasseled Cap transformation however, we see additional support for our conclusion that vegetative cover has been increasing based on strong declines in surface brightness and strong increases in wetness. These findings are

consistent with existing regional (California Sierra Nevada) studies showing increased rates of tree mortality resulting in reduced forest stand density (van Mantgem et al., 2009). The reduced tree cover allows for increased understory growth. Reduced forest density is also consistent with the strong NIR declines found in the study.

To determine what is driving the lower surface reflectance, we examined trends in the environmental parameters of precipitation and temperature. Average monthly minimum and maximum temperatures show statistically significant upward trends. Increased temperatures support increased photosynthetic activity as long as that process is not limited by other factors such as lack of water availability. In areas without water or other nutrient resource limitations, these conditions are conducive for increased vegetative surface cover resulting in stronger absorption in the visible region of the spectrum. The statistically significant declines in late summer dew point temperatures suggest a moisture deficit may be developing during the least rainy months of the year.

However, while the NIR reflectance would be expected to decline in moisture stressed vegetation, the SWIR (band 5) is expected to increase from reduced water absorption in the SWIR band. The data in this analysis do not reflect increased SWIR reflectance. The reduced MWIR values we observe are another indicator of increased vegetation since this region is highly reflective in barren areas and reduced in vegetated areas. All of these observations are consistent with an increase of ecosystem vegetative surface cover with reduced structural complexity.

References

Adams, H.D., Guardiola-Claramonte, M., Barron-Gafford, G.A., Villegas, J.C., Breshears, D.D., Zou, C.B., Troch, P.A., and Huxman, T.E., (2009). Temperature sensitivity of drought-induced tree mortality portends increased regional die-off under global-change-type drought. *PNAS*, 106 (17), pp. 7063 – 7066.

Asner, G.P., (1998). Biophysical and Biochemical Sources of Variability in Canopy Reflectance. *Remote Sensing of Environment*, 64, pp. 234-253.

Barnett, T.P., Adam, J.C., and Lettenmaier, D.P., (2005). Potential impacts of a warming climate on water availability in snow-dominated regions. *Nature, Reviews* 438 (17), pp. 303 – 309.

Bowerman, N.D. and Clark, D.H., (2011). Holocene glaciation of the central Sierra Nevada, California. *Quaternary Science Reviews*. 30, pp. 1067-1085.

Chander, G. and Markham, B., (2003). Revised Landsat-5 TM radiometric calibration procedures and post calibration dynamic ranges. *IEEE Transactions on Geoscience and Remote Sensing*, 41 (11), pp. 2674-2677.

Chander, G., Markham, B., and Helder, D.L., (2009). Summary of current radiometric calibration coefficients for Landsat MSS, TM, ETM+, and EO-1 ALI sensors. *Remote Sensing of Environment*, 113, pp. 893-903.

Chavez, P.S., (1996). Image-based atmospheric corrections–revisited and improved. *Photogrammetric Engineering and Remote Sensing*, 62 (9), pp. 1025-1036.

Chavez, P.S., (1988). An Improved Dark-Object Subtraction Technique for Atmospheric Scattering Correction of Multispectral Data. *Remote Sensing of Environment*, 24, pp. 459-479.

Chmura, D.J., Anderson, P.D., Howe, G.T., Harrington, C.A., Halofsky, J.E., Peterson, D.L., Shaw, D.C., and St. Clair, B.J., (2011). Forest responses to climate change in the northwestern United States: Ecophysiological foundations for adaptive management. *Forest Ecology and Management*, 261, pp. 1121–1142.

Chung, S.Y., Ehrenfreund, P., Rummel, J.D., and Peter, N., (2010). Synergies of earth science and space exploration. *Advances in Space Research*, 45, pp. 155–168.

Crist, E.P., (1985). Short Communication: A TM Tasseled Cap Equivalent Transformation for Reflectance Factor Data. *Remote Sensing of the Environment*, 17, pp. 301-306.

Daly, C., (2006). Guidelines for assessing the suitability of spatial climate data sets. *International Journal of Climatology*, 26, pp. 707-721.

De Beurs, K.M. and Henebry, G.M., (2005). A statistical framework for the analysis of long image time series. *International Journal of Remote Sensing*, 26 (8), pp. 1551-1573.

Elmore, A.J., Mustard, J.F., and Manning, S.J., (2003). Regional patterns of plant community response to changes in water: Owens Valley, California. *Ecological Applications*, 13 (2), pp. 443-460.

Gond, V., De Pury, D.G., Veroustraete, F., and Cuelemans, R., (1999). Seasonal variation in leaf area index, leaf chlorophyll and water content; scaling up to estimate fAPAR and carbon balance in a multilayer, multispecies temperate forest. *Tree Physiology*, 19, pp. 673-679.

Huete, A.R., (1988). A Soil-adjusted Vegetation Index. *Remote Sensing of the Environment*, 25, pp. 295-309.

Jackson, R.D., Pinter, P.J., Jr., Reginato, R.J., and Idso, S.B., (1986). Detection and evaluation of plant stresses for crop management decisions. *IEEE Transactions on Geoscience and Remote Sensing*, GE-24 (1), pp. 99-106.

Kondolf, G.M., (1989). Stream-groundwater interactions along streams of the Eastern Sierra Nevada California: Implications for assessing potential impacts of flow diversions. *USDA Forest Service Gen. Tech. Rep. PSW-110*, pp. 352 – 359.

Lenihan, J.M., Drapek, R., Bachelet, D., Kremer, and Nelson, R.P., (2003). Climate change effects on vegetation distribution, carbon, and fire in California. *Ecological Applications*, 13 (6), pp. 1667 – 1681.

Lindner, M., Maroschek, M., Netherer, S., Kremer, A., Barbati, A., Garcia-Gonzalo, J., Seidl, R., Delzon, S., Corona, P., Kolstrom, M., Lexer, M.J., and Marchetti, M., (2010). Climate change impacts, adaptive capacity, and vulnerability of European forest ecosystems. *Forest Ecology and Management*, 259, pp. 698 – 709.

Lu, D., Mausel, P. Brondizio, E., and Moran, E., (2002). Assessment of atmospheric correction methods for Landsat TM data applicable to Amazon basin LBA research, *International Journal of Remote Sensing*, Vol. 23, No. 13, pp. 2651 – 2671.

Musick, H.B. and Pelletier, R.E., (1988). Response to soil moisture spectral indexes derived from bidirectional reflectance in thematic mapper wavebands. *Remote Sensing of Environment*, 25, pp. 167-184.

Qi, J., Chehbouni, A., Huete, A.R., Kerr, Y.H., and Sorooshian, S., (1994). A Modified Soil-adjusted Vegetation Index. *Remote Sensing of the Environment*, 48, pp. 119-126.

Rouse, J.W., Haas, R.H. Schell J.A. and Deering, D.W., (1974). Monitoring vegetation systems in the Great Plains with ERTS. Proc. Third ERTS-1 Symposium, NASA Goddard, NASA SP-351 pp. 309-317.

Schueler, C.F., and Salomonson, V.V., (1985). Landsat Image Data Quality Studies. *Advances in Space Research*, 5 (5), pp. 1-11.

Skre, O. and Naess, M., (1999). CO_2 and winter temperature effects on white birch. *Chemosphere: Global Change Science*, 1, pp. 469-483.

Todd, S.W. and Hoffer, R.M., (1998). Responses of spectral indices to variations in vegetation cover and soil background. *Photogrammetric Engineering & Remote Sensing*, 64 (9), pp. 915-921.

Vicente-Serrano, S.M., Perez-Cabello, F., and Lasanta, T., (2008). Assessment of radiometric correction techniques in analyzing vegetation variability and change using time series of Landsat imagery. *Remote Sensing of Environment*, 112, pp. 3916-3934.

van Mantgem, P.J., Stephenson, N.L., Byrne, J.C., Daniels, L.D., Franklin, J.F., Fule, P.Z., Harmon, M.E., Larson, A.J., Smith, J.M., Taylor, A.H., and Veblen, T.T., (2009). Widespread Increase of Tree Mortality Rates in the Western United States. *Science*, 323, pp. 521-524.

Vogelmann, J.E., Tolk, B., and Zhu, Z., (2009). Monitoring forest changes in the southwestern United States using multitemporal Landsat data. *Remote Sensing of Environment*, 112, pp. 1739-1748.

Wessman, C.A., (1992). Imaging spectrometry for remote sensing of ecosystem processes. *Advances in Space Research*, 12 (7), pp. 361-368.

Williams, A.P., Allen, C.D., Millar, C.L., Swetnam, T.W., Michaelsen, J., Still, C.J., and Leavitt, S.W., (2010). Forest responses to increasing aridity and warmth in the southwestern United States. *PNAS*, 107 (50), pp. 21289-21294.

Williams, A.P., Allen, C.D., Macalady, A.K., Griffin, D., Woodhouse, C.A., Meko, D.M., Swetnam, T.W., Rauscher, S.A., Seager, R., Grissino-Mayer, H.D., Dean, J.S., Cook, E.R., Gangodagamage, C., Cai, M., and McDowell, N.G., (2013). Temperature as a potent driver of regional forest drought stress and tree mortality. *Nature Climate Change*, 3, pp. 292-297.

Chapter 3: Comparison of Surface Reflectance Values from the USGS Landsat 5 TM Climate Data Record (CDR) with Values Generated using a Simple Dark Object Subtraction (DOS) Method in an Alpine Watershed

Contribution of Authors and Co-Authors

This manuscript was co-authored by Patrick Sawyer and Haroon Stephen. Patrick Sawyer was the first author who conceived and implemented the study design, collected and analyzed the data, wrote the manuscript and presented the findings at the International Conference on Advances in Bio-Informatics, Bio-Technology and Environmental Engineering – ABBE 2014 held at Westminster University, London, UK June 2014. Haroon Stephen was the second author who assisted with the study design and provided feedback on statistical analyses and drafts of the manuscript.

Manuscript Information Page

This manuscript has been published by the Institute of Research Engineers and Doctors (IRED) in the peer-reviewed International Journal of Earthquake Engineering, Volume 1, Issue 3, pages 5-13, 30 September 2014. Copyright information can be found in Appendix A or at the IRED web site; (http://journals.theired.org/copyright-policy.html).

This manuscript presents the research performed and findings achieved relating to the use of remote sensing in ecological studies. The purpose of this work is validation of the appropriate method to use for determining surface reflectance. This work supports objective number two to design an analytical methodology that uses remote sensing to determine changes in vegetative surface cover of the ecosystem.

Abstract

Extraction of relevant information from remotely sensed imagery is essential for the identification of changes in the earth's environment. Methods for converting the data collected at the sensor to surface reflectance have been under constant improvement since the beginning of the Landsat program. The time and effort needed to perform this task has recently been eliminated with the publication of the USGS Landsat CDR. This paper compares the data available from the USGS with a simple dark object subtraction method for determining surface reflectance. Our goal is to determine if the USGS data set is comparable to previous methods. We find that the USGS data set is strongly correlated with the simpler DOS method. While clear differences in absolute surface reflectance are observed in the visible and near-IR bands, the trends in the data over time are consistent. This suggests that previous trend studies using the simpler methods do not need to be revisited using the newer data. The findings also suggest that researchers no longer need to perform the labor intensive step of converting raw data to surface reflectance by making use of the USGS surface reflectance data instead.

1.0 Introduction

Understanding changes in Earth's environment is becoming ever more critical as the pace of those changes increases due to factors including anthropogenic influence on global mass and energy balances.

Spaceborne instruments, that can effectively monitor the biosphere, have become essential tools to enhance our ability to adapt to future environmental conditions brought

about by complex processes such as climate change and population growth (Chung et al., 2010). The Landsat program has been indispensable in the analysis of temporal changes in the environment. Landsat earth observation sensors have been in continuous orbit since 1972, providing an unparalleled opportunity to observe changes to the environment and to develop analytical techniques that can relate the Landsat remote sensing data to natural and anthropogenic processes responsible for the observed changes. Examples of how this data is applied to ecological science include: analysis of net primary productivity (NPP) and species richness; monitoring of climate variables such as temperature, precipitation, and soil moisture; determining species distributions and habitat structure including topography (Turner et al., 2003).

The ecological response to elevated temperatures and CO_2 levels is complex and will be affected by other factors such as water and other nutrient resource availability. In cold alpine regions where water availability is not limiting, higher temperatures are expected to increase the habitable zones for several species, allowing for upslope migration and increased vegetative cover. Higher temperatures combined with increased atmospheric CO_2 levels will increase photosynthesis resulting in increased biomass; provided other essential resources are not limited (Skre and Naess, 1999). Conversely, where water is limited, higher temperatures will increase plant stress resulting in reduced vegetative cover (Chmura et al., 2011).

In order to use the wealth of information contained in the Landsat archive database, methods for converting the raw digital numbers recorded by the sensor to actual

surface reflectance must be used. The common methodology for this conversion is to first convert the digital numbers to the at sensor radiance value, followed by conversion to Top-of-Atmosphere (TOA) reflectance and finally applying an atmospheric correction to determine the surface reflectance.

There are many atmospheric correction procedures that have been developed over the last two decades, and with the addition of atmospheric profiling remote sensors, many atmospheric correction algorithms are now available that include actual upwelling and downwelling radiance values in the analysis. However, in order to take advantage of the older Landsat imagery (<2000), other methods, typically imaged based, are used. One of the most common atmospheric correction methods is known as “Dark Object Subtraction or DOS”. This method is based on the assumption that radiance seen at the satellite for “dark” pixels (i.e. deep water) result purely from atmospheric path radiance. A derivation of the DOS technique known as the Cos θ or “COST” method is used in this analysis due to its simplicity and ease of use. The underlying assumption in this method is that there is a theoretical dark object that is assumed to have a reflectance of 1% (Chavez, 1996).

The determination of surface reflectance from the raw Landsat data can be a time consuming and complicated procedure. Fortunately, the United State Geological Survey (USGS) has automated this task and published a complete set of surface reflectance data derived from raw Landsat 5 Thematic Mapper TM and Landsat 7 Enhanced Thematic Mapper (ETM+) imagery. The data, designated the Climate Data Record (CDR), is available for download free from the USGS EarthExplorer

(http://earthexplorer.usgs.gov/) website. The CDR data set was developed under the Landsat Ecosystem Disturbance Adaptive Processing System (LEDAPS) program. The LEDAPS project made use of the existing MODIS Adaptive Processing System (MODAPS) developed for the Moderate Resolution Imaging Spectroradiometer (MODIS) sensor to convert raw at-sensor data to surface reflectance (Masek et al., 2006).

While the availability of this data will no doubt enhance the standardization and utilization of the Landsat data archive, it is important to consider how this data set differs from the surface reflectance values determined in previous studies. This information will allow us to evaluate the usefulness of revisiting those previous studies to determine if their findings may be altered by use of this new data set.

In this study, we compare the surface reflectance data generated by the USGS with the surface reflectance generated using a simple Dark Object Subtraction atmospheric correction based on the COST algorithm developed by Chavez, 1996. The two data sets are compared using simple linear regression. Correlation coefficients are determined for each data set for each of the six reflective bands of the Landsat 5 TM sensor. We analyze the data in several ways included a simple comparison of all data sets and how those comparisons have trended over time. We also compare the data sets based on land class, elevation, and vegetative density to determine which parameters may show significant disagreement. The study area is an ecologically sensitive Alpine watershed in California's Eastern Sierra Nevada Mountains.

2.0 Study Area and Data

2.1 Study Area Description

Figure 10 below shows the Big Pine Creek watershed located in California's Eastern Sierra Mountains. Big Pine Creek is a major tributary to the Owens River which is a significant source of fresh water for Los Angeles. The Owens River valley straddles the Great Basin and Mojave deserts with vegetation consisting primarily of pine forests at higher elevations and xeric species at lower elevations. Areas bordering streams and the Owens River are primarily grass dominated meadows (Elmore et al., 2003). Elevation within the watershed increases from East to West with the higher regions dominated by barren rock and woodlands with the lower regions dominated by mixed desert shrubs.

The Big Pine Creek watershed ecosystem owes its existence to snow melt and melt-water from the Palisade Glacier. In addition to being the southern-most glacier in the United States, it is also the largest glacier in the Sierras with a surface area of 1.3 km^2. It was formed about 3,200 years ago, reaching a maximum extent as recently as 170 years ago (Bowerman and Clark, 2011). It has been generally in retreat ever since. The Big Pine Creek watershed drainage area covers approximately 82 km^2 and its average flow is 1.8 m^3/s. Measurements taken in the 1980's indicate that the creek is a gaining stream at the lower elevations in contrast to most other Owens River tributaries which are losing streams (Kondolf, 1989). Since all of the living species within this watershed depend on the glacier and snow melt for their survival, the impact of temperature and precipitation variations on the biodiversity of the Big Pine Creek watershed can serve as a

predictor of how other ecologically sensitive and critically essential watersheds will respond to future climate regimes.

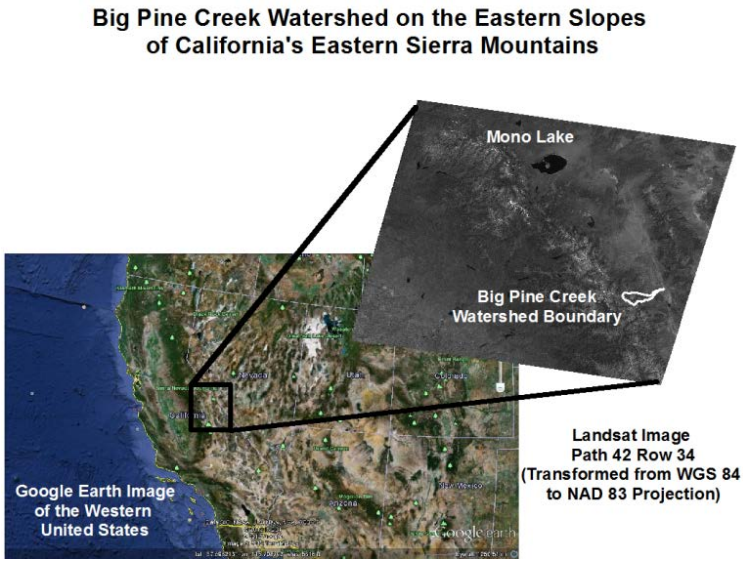

Figure 10. Study area location showing the boundary of the Big Pine Creek watershed.

There are 34 land cover classes in the Big Pine Creek watershed with the ten most abundant covering 93% of the total surface area. These top ten land cover classes are listed in table 5 along with their relative abundance. The USGS provides land cover information to the public through an online mapping service from the University of Idaho (http://www.gap.uidaho.edu/landcoverviewer.html). In order to ensure a representative sample of numerous vegetative species present in the watershed, three sample sites at different elevations, from each of the ten most abundant land cover classes are selected for a total of 30 sample sites. These ten land cover classes fall into four types, barren,

woodland, shrub, and developed. Differences in how the various land types have responded to climate change will provide insight into which ecological processes are being most affected by recent variation in environmental parameters.

In addition to the 30 sites selected by land class, three sites were selected for every 100 meter elevation gradient from 1200 meters MSL to 3600 meters MSL. At each gradient, a densely vegetated site, a moderately vegetated site, and a sparsely vegetated site were selected. These 75 sample sites based on elevation gradient and vegetative density combined with the 30 sites chosen by land class provide a total of 105 sample sites that will be analyzed for comparison between the USGS CDR surface reflectance and the simplified DOS determined surface reflectance.

Table 5

Land Cover Classes in the Big Pine Creek Watershed

USGS Land Class Level 3	Land Type	Class ID	PIXEL COUNT	% of Pixels
Mediterranean California Alpine Bedrock and Scree	Barren (B2)	3504	46547	39.16
Great Basin Pinyon-Juniper Woodland	Woodland (W2)	4514	25196	21.19
Inter-Mountain Basins Montane Sagebrush Steppe	Shrub (S2)	5308	10597	8.91
Inter-Mountain Basins Big Sagebrush Shrubland	Shrub (S3)	5706	9925	8.35
Sierra Nevada Subalpine Pine Forest and Woodland	Woodland (W3)	4533	6819	5.73
Sierra Nevada Cliff and Canyon	Barren (B1)	3215	2857	2.40
Inter-Mountain Basins Mixed Salt Desert Scrub	Shrub (S1)	5205	2827	2.37
Developed, Open Space	Developed (D1)	1201	1966	1.65
Mediterranean California Red Fir Forest	Woodland (W1)	4318	1872	1.57
Northern California Mesic Subalpine Woodland	Woodland (W4)	4608	1585	1.33

2.2 Data

The Landsat program has been providing earth observation remote sensing data to the scientific community for four decades. The first Landsat satellite was placed in orbit in 1972 with Landsat 7 remaining operational today. Landsat 5 was only recently taken off-line. The next generation satellite, the Landsat Data Continuity Mission (Landsat 8), was launched on February 11th, 2013 is now operational. Unfortunately, the Landsat 7 ETM+ imager suffered a scan line correction malfunction in 2003 that causes significant striping across the study area, making data acquired since that event difficult to use. In this analysis, we use only Landsat 5 TM data collected over a 28 year period from 1984 through 2011. Using a single sensor ensures maximum consistency of the data and eliminates errors associated with correlating data from multiple sensors.

Table 6 details the six reflective bands of the TM sensor, covering the blue, green, red, near infrared (NIR), short-wave infrared (SWIR), and mid-wave infrared (MWIR) regions of the spectrum as well as their ecological applications.

Bands 5 and 7 are sometimes referred to as SWIR1 and SWIR2. However, in this study, we refer to band 5 as the SWIR and band 7 as the MWIR. Band 6 covers the thermal infrared (TIR) and the data from this region is not used in this study. These descriptions are retrieved from the Northern Arizona University Infrared Spectrometry Laboratory website (http://www.cefns.nau.edu/seses/llecb/Spectrometer/RemoteSensing.html).

Table 6

Landsat 5 TM Band Description and Ecological Application

Band	Spectral Range (μm)	Resolution (m)	Region	Common Applications
1	0.45 - 0.52	30	Blue	Soil/Vegetation Delineation
2	0.52 - 0.60	30	Green	Assessment of Vegetation Vigor
3	0.63 - 0.69	30	Red	Chlorophyll Absorption for Determining Vegetation
4	0.76 - 0.90	30	NIR	Biomass Survey's, Delineate Water Bodies
5	1.55 - 1.75	30	SWIR	Vegetation and Soil Moisture,
6	10.4 - 12.5	120	TIR	Thermal mapping and estimated soil moisture
7	2.08 - 2.35	30	MWIR	Hydrothermal Mapping

2.2.1 DOS Data.

The Landsat 5 TM imagery used in this analysis was acquired for 28 dates in the month of July from 1984 (year of launch) through 2011 (year turned off). Most of the imagery used in this analysis is from Path 42, Row 34 with four of the images from Path 41, Row 34. Both image ID ground swaths cover the entire study area. The Landsat imagery used in this analysis are listed in table 3 below. This imagery was obtained from the EarthExplorer web site operated by the United States Geological Survey (http://earthexplorer.usgs.gov/). Since the period of maximum leaf area index generally occurs in the mid-June to mid-August time frame (Gond et al., 1999), only imagery in the July time frame was considered for this analysis in order to minimize the impacts of the phenological cycle on the reflectance data.

2.2.2 USGS CDR.

The CDR data set consisted of the same imagery with the raw digital numbers replaced by calculated surface reflectance values for each of the six reflective bands of

the Landsat 5 TM sensor. USGS surface reflectance data is generated from a software package known as the Landsat Ecosystem Disturbance Adaptive Processing System (LEDAPS). The surface reflectance data is generated by applying an atmospheric correction to the raw Landsat 5 TM imagery (USGS, 2013).

This atmospheric correction uses the Second Simulation of a Satellite Signal in the Solar Spectrum (6S) radiative transfer model to account for various atmospheric column constituents including water vapor, ozone, and aerosol optical thickness (Masek et al., 2006).

The LEDAPS process uses average daily lamp brightness history to obtain calibration coefficients based on acquisition date. These calibration coefficients are used to determine the at-sensor radiance values (Masek et al., 2006). The LEDAPS process converts at-sensor radiance to top-of-atmosphere (TOA) by an algorithm that incorporates solar irradiance derived from the MODTRAN model, bandpass, earth sun distance and solar zenith angle (Masek et al., 2006).

The LEDAPS atmospheric correction assumes particle scattering and gaseous absorption can be decoupled (Masek et al., 2006). Surface reflectance is correlated with TOA reflectance using equation 19,

$$\rho_{TOA} = T_g(O_3, O_2, CO_2, NO_2, CH_4)\left[\rho_{R+A} + T_{R+A}T_g(H_2O)\frac{\rho_s}{1+S_{R+A\rho_s}}\right], \tag{19}$$

where ρ_s is the surface reflectance, T_g is the gaseous transmission, T_{R+A} is the Rayleigh and aerosol transmission, ρ_{R+A} is the Rayleigh and aerosol atmospheric intrinsic reflectance, and S_{R+A} is the Rayleigh and aerosol spherical albedo (Masek et al., 2006).

Table 7

Summary of Landsat imagery used in this analysis

Image Acquisition Date	Acquisition Time (Local)	Scene ID (Path/Row)	Image Acquisition Date	Acquisition Time (Local)	Scene ID (Path/Row)
7/18/2011	10:22:49	42/34	7/27/1997	10:04:36	42/34
7/31/2010	10:24:08	42/34	7/8/1996	9:47:45	42/34
7/5/2009	10:16:13	41/34	7/22/1995	9:38:12	42/34
7/25/2008	10:20:14	42/34	7/3/1994	9:52:10	42/34
7/7/2007	10:27:27	42/34	7/16/1993	9:56:07	42/34
7/13/2006	10:20:33	41/34	7/29/1992	9:56:32	42/34
7/1/2005	10:21:20	42/34	7/27/1991	9:57:11	42/34
7/30/2004	10:16:22	42/34	7/8/1990	9:53:51	42/34
7/12/2003	10:10:04	42/34	7/5/1989	9:34:00	42/34
7/25/2002	10:09:02	42/34	7/2/1988	10:04:22	42/34
7/22/2001	10:14:03	42/34	7/25/1987	9:52:56	41/34
7/19/2000	10:10:47	42/34	7/13/1986	9:56:31	42/34
7/17/1999	10:11:26	42/34	7/3/1985	9:57:32	41/34
7/30/1998	10:12:03	42/34	7/7/1984	10:02:17	42/34

3.0 Methodology

This section describes the methods used to derive the data sets and the comparison tests performed.

3.1 Simplified DOS Calculated Surface Reflectance Data

3.1.1 Conversion of Digital Number (DN) to Top-of-Atmosphere Reflectance

The first step in analyzing raw Landsat data is converting the digital numbers to at sensor radiance values by removing the gain and offset caused by the sensors themselves (Chavez, 1996). Conversion of Calibrated Digital Number (Q_{cal}) to at sensor radiance is accomplished using the equation 20,

$$L_\lambda = \left(\frac{L_{Max\lambda} - L_{Min\lambda}}{Q_{Cal\max}} \right) * Q_{cal} + L_{Min\lambda}, \tag{20}$$

where L_λ = spectral radiance at the sensor's aperture in W/m^2•sr•μm (Chander and Markham, 2003). Conversion of Radiance (L_λ) to top-of-atmosphere (TOA) reflectance is accomplished using the following equation 21,

$$\rho_P = \frac{\pi \cdot L_\lambda \cdot d^2}{ESUN_\lambda \cdot COS\theta_s}, \tag{21}$$

where ρ_P = unitless planetary reflectance, L_λ = spectral radiance at the sensor's aperture, d = earth sun distance in astronomical units, $ESUN_\lambda$ = mean solar exoatmospheric irradiances, θ_s = solar zenith angle in degrees (Chander and Markham, 2003).

3.1.2 Atmospheric Correction

An atmospheric correction is applied to obtain surface reflectance using a simple image based method called Dark Object Subtraction (DOS) which is based on the assumption that radiance seen at the satellite for “dark” pixels (i.e. deep water or shadow) result purely from atmospheric path radiance. This allows us to process imagery where atmospheric column data are not available (generally pre-2000). For this analysis DOS is performed using the Cos θ or “COST” technique developed by Chavez (1996). The first

step in the DOS method is removal of a reflectance value representing the contribution of the atmospheric scattering effect from the DN recorded at the sensor. Two ways of selecting this value are the histogram approach in which the DN selected is the first below 1000 pixels for a typical Landsat image, or a simpler approach in which a known dark object is selected using the assumption that any DN from that pixel is the result of the atmospheric contribution.

Use of the histogram method typically requires analysis of the entire image (Chavez, 1988). Therefore, for this effort, the selection of the minimum pixel value representing the atmospheric haze was accomplished by selecting the minimum DN for each band over Black Lake. This mountain snowmelt fed water body is surrounded by trees and mountain shadow representing an ideal zero reflectance surface for the DOS method. The first step in the COST technique is to calculate the minimum radiance ($L_{\lambda,min}$) using:

$$L_{\lambda,\min} = L_{Min\lambda} + \left(\frac{L_{Max\lambda} - L_{Min\lambda}}{Q_{Cal\max}} \right). \tag{22}$$

Since no targets are completely black, even the dark object will contain some radiance value. Therefore, the COST method assigns a 1% reflectance value to the selected dark object (Chavez, 1996). The theoretical radiance ($L_{\lambda,1\%}$) of a dark object (assuming a 1% reflectance) is calculated using equation 23,

$$L_{\lambda,1\%} = \frac{0.01 \cdot d^2 \cdot Cos^2\theta}{\pi \cdot ESUN_\lambda}. \tag{23}$$

A haze correction factor ($L_{\lambda,haze}$) is then calculated using equation 24,

$$L_{\lambda,haze} = L_{Min\lambda} - L_{\lambda,1\%}, \tag{24}$$

(Chavez, 1996). The corrected surface reflectance value (ρ_P) is then calculated using equation 25,

$$\rho_P = \frac{\pi \cdot d^2 \cdot (L_\lambda - L_{\lambda,haze})}{TAU_v \cdot ESUN_\lambda \cdot Cos\theta \cdot TAU_z}, \tag{25}$$

where TAU_v represents the atmospheric transmittance from the ground to the sensor and TAU_z is the atmospheric transmittance from the sun to the ground. Since Landsat images are taken at a nadir angle, TAU_v is equal to Cos 0^o or 1.0. For the COST method, TAU_z is equal to the cosine of the solar zenith angle or Cos θ^o (Chavez, 1996). Therefore, the surface reflectance is calculated from equation 26 as:

$$\rho_P = \frac{\pi \cdot d^2 \cdot (L_\lambda - L_{\lambda,haze})}{ESUN_\lambda \cdot Cos^2\theta}. \tag{26}$$

3.2 Comparison Methods

Linear regression is used to determine the level of agreement between the two data sets. Surface reflectance values from each data set are plotted against each other and the regression statistics are calculated by Excel statistical analysis tool. In this study, we consider the adjusted Coefficient of Determination (R^2) and the Standard Error (SE).

The adjusted R^2 value is determined from the Pearson product correlation coefficient as shown in equation 27,

$$R = \frac{\sum (x-\bar{x})(y-\bar{y})}{\sqrt{\sum (x-\bar{x})^2 \cdot \sum (y-\bar{y})^2}} \tag{27}$$

where x and y are the sample means. The closer R^2 is to 1.0, the closer the data is to the more linear the relationship between the two variables. Adjusted R^2 value is then determined as shown in equation 28,

$$\text{Adjusted } R^2 = 1 - \frac{(1-R^2)\cdot(n-1)}{(n-k-1)}, \tag{28}$$

where n is the number of observations and k is the number of predictors. The adjusted R^2 value is used in this study due to the large number of predictors which may artificially raise the true goodness of fit between the data sets if the unadjusted R^2 value is used.

The *SE* is the square root of the variance of the regression coefficient. It is a measure of how much variation exists in the data points about the regression line. It is another indicator of the general agreement between the variables with a smaller *SE* indicating closer agreement. The *SE* is calculated as shown in equation 29,

$$SE = \sqrt{\frac{1}{(n-2)}\left[\sum (y-\bar{y})^2 - \frac{\left[\sum (x-\bar{x})(y-\bar{y})\right]^2}{\sum (x-\bar{x})^2}\right]}\ , \tag{29}$$

where n is the number of observations and k is the number of predictors. The adjusted R^2 value is used in this study due to the large number of predictors which may artificially raise the true goodness of fit between the data sets if the unadjusted R^2 value is used.

The *SE* is the square root of the variance of the regression coefficient. It is a measure of how much variation exists in the data points about the regression line. It is

another indicator of the general agreement between the variables with a smaller *SE* indicating closer agreement. The *SE* is calculated as shown in equation 30,

$$SE = \sqrt{\frac{1}{(n-2)}\left[\sum (y-\bar{y})^2 - \frac{\left[\sum (x-\bar{x})(y-\bar{y})\right]^2}{\sum (x-\bar{x})^2}\right]} \quad , \tag{30}$$

where *n* is the number of observations.

The results of the linear regression are examined for trends in the data over time. Trends in the data based on elevation gradient and vegetative density are also examined. Presence of trends in the correlation between the data sets may indicate a bias in the methodology used to derive the surface reflectance values. Trends are calculated using the non-parametric Mann-Kendall (MK) trend test. This analysis essentially determines if a set of values (*y*) are increasing or decreasing over time. Mann-Kendall analysis looks at the sums of the signs of the differences between successive data points and calculates a score or "S" statistic with the following properties: for S < 0 (values are decreasing over time); for S > 0 (values are increasing over time). The magnitude of the S-statistic is a measure of the strength of the trend. S values of + or – 100 indicate a statistically significant trend with a *p* value of < 0.05. This means the null hypothesis of no-trend in the data can be discarded with the risk of committing a Type II (rejection of a true null or H_0) error at less than 5%. The MK S-statistic is calculated using equation 31,

$$S = \sum_{i=1}^{n-1} \sum_{j=i+1}^{n} sign\left(y_j - y_i\right), \tag{31}$$

where n is the number of observations and y_i ($i = 1…n$) is the value at time T_i and y_j ($j = 1…n$) is the value at time T_j (De Beurs and Henebry, 2005). These calculations are carried out in Excel using the XLSTAT add-in statistical application. This program generates the S statistic as well as the probability (p) value which is used to quantify the statistical significance of the trend. The p value is defined as the probability of obtaining a value of S equal or greater than the calculated value for n when no trend is present. The confidence factor (risk of rejecting a true null) is defined as (1-p)*100%.

4.0 Results and Discussion

This section presents the results obtained from our comparison of the surface reflectance values published in the USGS CDR data set and those surface reflectance values calculated using the simplified DOS method using the COST approach.

4.1 Comparison of all data sets

This study examined the surface reflectance data for 105 sample sites for 28 dates. This provides a total of 2,940 individual data pairs in each of the six reflective bands of the Landsat 5 TM sensor. Figure 11 shows the DOS and USGS derived data sets plotted against each other for each of the six reflective bands of the TM sensor. Table 8 summarizes the results of comparison between all the data pairs for each band.

Table 9 summarizes the means of the surface reflectance values by each method for each band and shows the difference in those mean reflectance values. We next provide a brief summary of the results of our comparison for each band.

For band 1, an adjusted R^2 value of 0.9082 combined with a *SE* of only 1.17% suggests very strong agreement between the two methods. The mean value of the USGS data set is approximately 10% higher than the DOS derived reflectance mean value for band 1. This suggests the DOS technique is over estimating the atmospheric contribution to the at-sensor radiance measurement for the band 1 region (0.45 – 0.52 μm).

Similar results are seen in bands 2, 3, 5, and 7 with very strong agreement in surface reflectance values derived by each method. Band 4 had the lowest agreement between the two methods. However, with an adjusted R^2 value of 0.8602 combined with a *SE* of only 1.69% strong agreement exists between the two methods in this region also.

Table 8

Adjusted R^2 and SE values for all data sets from 1984 through 2011

Band 1	Band 2	Band 3	Band 4	Band 5	Band 7
Adjusted R^2 Values					
0.9082	0.9246	0.9341	0.8602	0.9667	0.9628
SE Values					
0.0117	0.0132	0.0147	0.0169	0.0132	0.0149

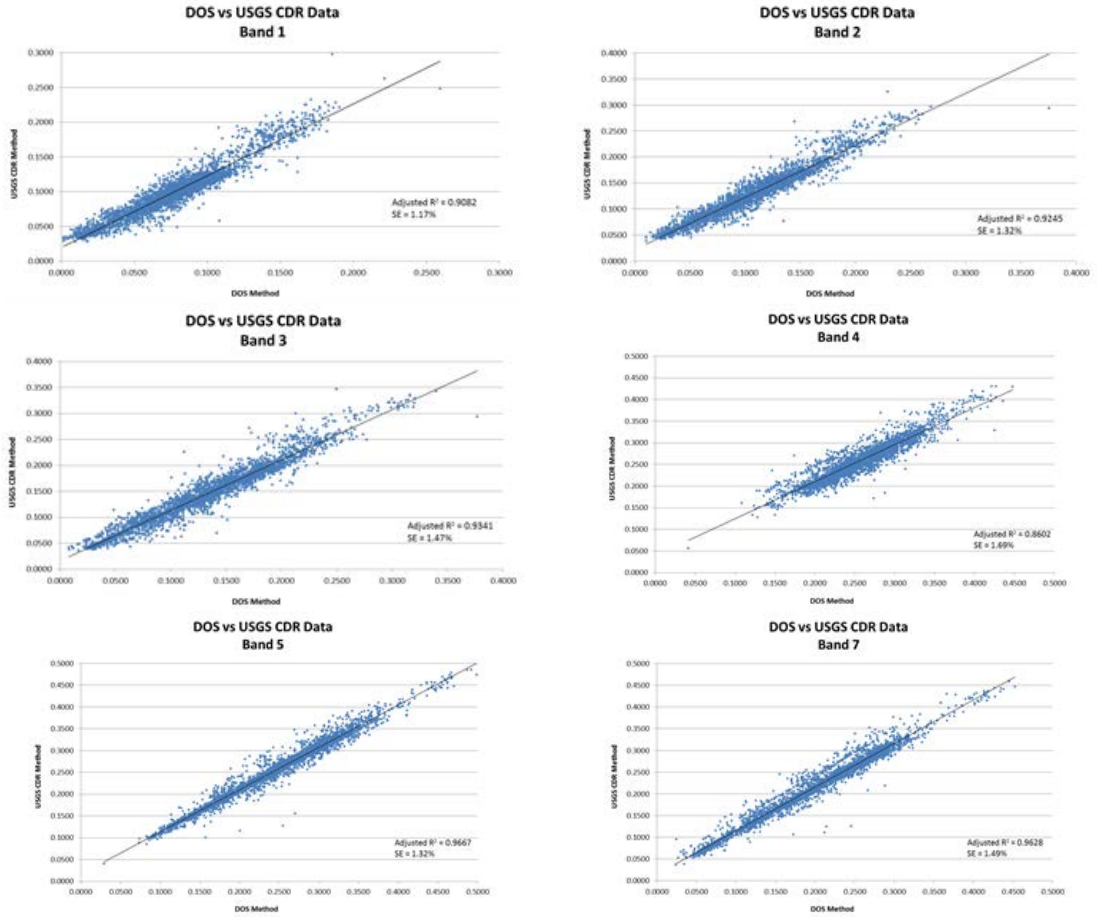

Figure 11. Comparison of surface reflectance values all 105 sample sites for Landsat 5 TM Bands 1, 2, 3, 4, 5, & 7.

Table 9

Mean values and difference between the means for each band

TM Band	Method		Δ (%)
	DOS	USGS	
1	0.078	0.100	10.05
2	0.111	0.133	16.57
3	0.136	0.148	8.40
4	0.257	0.259	0.73
5	0.248	0.256	3.42
7	0.198	0.213	7.26

4.2 Comparison of data sets over time

We next looked at the influence time has had on the different methods of deriving surface reflectance. Table 10 shows the trends in the adjusted R^2 and *SE* values for 105 sample sites in each band over the 28 year period from 1984 through 2011. Trends in the adjusted R^2 values are statistically significant in each band except band 5. Band 5 was strongly correlated throughout the 28 years study period, and the trend is also positive for this region of the spectrum.

This finding demonstrates that the agreement between the two methods has increased significantly over the time period of the study. This suggests that there is a difference in how the DOS and USGS methods accounted for variables such as sensor gain and offset. Several corrections to these values have taken place over the 28 year time span of this study. However, even though the agreement between the two methods has increased, the agreement in the early years of the study also showed R^2 values or 0.9 or better. The variation in how the DOS and USGS methods calculate surface reflectance values are not sufficient to produce tangibly different results.

Table 10

Trends in adjusted R^2 and values for all data sets from 1984 through 2011

Trend	Band 1	Band 2	Band 3	Band 4	Band 5	Band 7
S	196	205	183	144	65	101
p	<0.0001	<0.0001	0.0003	0.004	0.206	0.048

4.3 Comparison of data sets by Land Class

Table 11 shows the results of the comparison between the USGS data set and the DOS derived surface reflectance for each of the top ten land cover classes present in the study area.

Table 11

Trends in adjusted R^2 values for all data sets from 1984 through 2011

Land Class	Adjusted R^2 Values					
	Band 1	Band 2	Band 3	Band 4	Band 5	Band 7
3504	0.9347	0.9327	0.9357	0.8573	0.9449	0.9432
4514	0.8764	0.8909	0.9220	0.7876	0.8787	0.8811
5308	0.6546	0.7314	0.7840	0.5600	0.8308	0.8104
5706	0.8682	0.8200	0.6909	0.2662	0.6598	0.5966
4533	0.5951	0.6424	0.6320	0.5380	0.4558	0.4177
3215	0.6401	0.4533	0.1735	0.5629	0.8646	0.5224
5205	0.9518	0.9516	0.9309	0.8639	0.5513	0.7174
1201	0.8072	0.4984	0.4870	0.2896	0.8075	0.7814
4318	0.9482	0.9523	0.9511	0.8412	0.9653	0.9640
4608	0.7182	0.8090	0.8577	0.7614	0.7755	0.8819

There are 30 sample sites (3 for each land cover class), for each of the 28 years of the study providing a total of 840 data pairs for each band in this analysis. The results of this analysis shows that the correlation between the USGS data sets and the DOS methodology varies significantly based on land cover classification. While most of the data sets show good agreement, Land class 3215 (Sierra Nevada Cliff and Canyon) in particular shows poor correlation between the two methods for determining surface reflectance. This is especially true in Band 3 (Red) where there is significant scatter among the data points as shown in Figure 12.

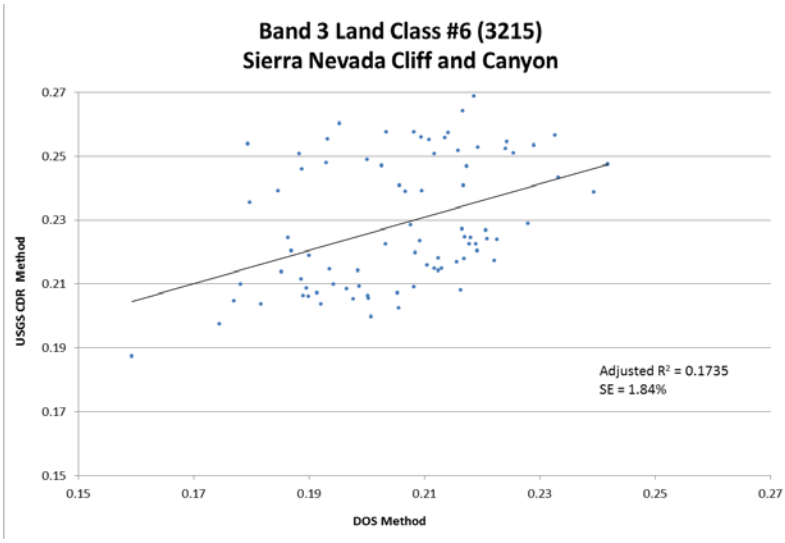

Figure 12. Comparison of surface reflectance values Sierra Nevada Cliff and Canyon Land Class for Landsat 5 TM Band 3 (RED 0.63 – 0.69 μm).

Sierra Nevada Cliff and Canyon land cover consist of rocky barren areas located in the foothills and sub alpine areas of the Sierra Nevada's. Typically less than 10% of the surface contains any vegetative species. The geography consists of steep cliff faces, rock outcrops, canyon walls and some talus (SWReGAP 2003). This suggests that extreme topographic variation within individual pixels has an impact on the surface reflectance determinations between the two approaches.

4.4 Comparison of data sets at elevation gradients

Next, we examine the results of the comparison between the USGS data set and the DOS derived surface reflectance at each elevation from 1200 meters MSL to 3600 meters MSL. There are 84 pairs of data at each elevation, (3 sites x 28 years).

Table 12

Trends in adjusted R^2 and values for all data sets by elevation

Trend	Band 1	Band 2	Band 3	Band 4	Band 5	Band 7
S	90	86	47	90	8	2
p	0.037	0.047	0.283	0.037	0.870	0.982

Table 12 shows that the correlation between the USGS data sets and the DOS methodology increase with elevation. Trends in the adjusted R^2 values in the SWIR and MWIR bands are not statistically significant and we can only infer that the USGS and DOS data sets show closer agreement at higher elevations from the positive S values. Although not statistically significant, the trends in the visible and NIR regions is strong suggesting closer agreement between the two surface reflectance methodologies at higher elevations.

4.5 Comparison of data sets based on vegetative density

Table 13 shows the results of the comparison between the USGS data set and the DOS derived surface reflectance for densely, medium, and sparsely vegetated sites. There are 700 pairs of data for each vegetative density, (25 elevations x 28 years). This analysis indicates that the agreement between the USGS data and the DOS methodology declines with increasing vegetation density with the exception of band 7. Since the sparse areas have a higher absolute reflectance, the data shown here indicate correlation between the USGS data and the DOS data increases with absolute surface reflectance.

This observation is consistent with the previous finding for trends in the agreement between the two methods based on elevation gradient since vegetation density tends to decline at higher elevation; we observe the R^2 value increase with elevation.

Table 13

Adjusted R^2 and SE values for densely, medium and sparsely vegetated sites

Vegetative Density	Adjusted R^2 Values					
	Band 1	Band 2	Band 3	Band 4	Band 5	Band 7
Dense	0.7926	0.8507	0.8726	0.8356	0.9541	0.9394
Medium	0.8080	0.8664	0.8683	0.8745	0.9548	0.9335
Sparse	0.8853	0.8877	0.8931	0.9093	0.9770	0.9354

4.6 Confidence Levels

Multitemporal satellite imagery is impacted by several factors including changes in sensor response, sensor stability, atmospheric effects, and illumination effects (Vicente-Serrano et al., 2008). Radiometric uncertainty for the TM data is approximately 5% (Chander et al., 2009).

The USGS surface reflectance data set has been assessed against MODIS surface reflectance data and found to be highly correlated with discrepancies between 2.2 to 3.5 % (Feng et al., 2013).

5.0 Summary and Conclusions

This study compared the surface reflectance values published in the USGS Climate Data Record archive with surface reflectance calculated using a simple Dark Object Subtraction method. The ecologically sensitive Big Pine Creek watershed served

as the study site and 105 sample locations within that watershed were examined for 28 dates in each of the six reflective bands of the Landsat 5 TM imager. Simple linear regression was used to compare the surface reflectance values determined by each method. In addition to looking at a complete comparison of all the data pairs, sample sites were analyzed based on land cover class, elevation, and vegetative density. Trends in the data over time and by elevation were also determined.

The overall comparison of the two methods showed very close agreement in the surface reflectance values, with band 5 showing the closest agreement (adjusted R^2 = 0.9667) and band 4 shown the least (adjusted R^2 = 0.8602). Mean surface reflectance values from the USGS CDR data set are generally higher than the values determined by the DOS method with band 2 showing the highest difference between the means (16.57%) while band 4 showed the least difference between the means (0.73%). The statistically significant positive trends in the level of agreement between the two methodologies over time suggests differences in the values used for the gains and offset values for the Landsat 5 TM sensor. These values were revised periodically to correct for changes in the radiometric response of the sensor over time or for improved calibration data sets (Chander and Markham, 2003).

The greatest discrepancy between the two methodologies is found in comparisons of surface reflectance over the land class 3215 (Sierra Nevada Cliff and Canyon). This may be the result of the large topographical variations within individual pixels that can occur for this land cover class. While this one result makes it clear that discrepancies do

exist in the two methodologies, the primary conclusion we draw from the results of this study is that the USGS derived CDR data base shows good agreement with the data generated using previous methods. This suggests that the need to revisit past studies using the newly available surface reflectance data set would not result in new findings or altered conclusions.

References

Bowerman, N.D. and Clark, D.H., (2011). Holocene glaciation of the central Sierra Nevada, California. *Quaternary Science Reviews,* 30, pp. 1067-1085.

Chander, G. and Markham, B., (2003). Revised Landsat-5 TM radiometric calibration procedures and post calibration dynamic ranges. *IEEE Transactions on Geoscience and Remote Sensing,* 41 (11), pp. 2674-2677.

Chander, G., Markham, B., and Helder, D.L., (2009). Summary of current radiometric calibration coefficients for Landsat MSS, TM, ETM+, and EO-1 ALI sensors. *Remote Sensing of Environment,* 113, pp. 893-903.

Chavez, P.S., (1988). An Improved Dark-Object Subtraction Technique for Atmospheric Scattering Correction of Multispectral Data. *Remote Sensing of Environment,* 24, pp. 459-479.

Chavez, P.S., (1996). Image-based atmospheric corrections–revisited and improved. *Photogrammetric Engineering and Remote Sensing,* 62 (9), pp. 1025-1036.

Chmura, D.J., Anderson, P.D., Howe, G.T., Harrington, C.A., Halofsky, J.E., Peterson, D.L., Shaw, D.C., and St. Clair, B.J., (2011). Forest responses to climate change in the northwestern United States: Ecophysiological foundations for adaptive management. *Forest Ecology and Management*, 261, pp. 1121–1142.

Chung, S.Y., Ehrenfreund, P., Rummel, J.D., and Peter, N., (2010). Synergies of earth science and space exploration. *Advances in Space Research*, 45, pp. 155–168.

De Beurs, K.M. and Henebry, G.M., (2005). A statistical framework for the analysis of long image time series. *International Journal of Remote Sensing,* 26 (8), pp. 1551-1573.

Elmore, A.J., Mustard, J.F., and Manning, S.J., (2003). Regional patterns of plant community response to changes in water: Owens Valley, California. *Ecological Applications,* 13 (2), pp. 443-460.

Feng, M., Sexton, J.O., Huang, C., Masek, J.G., Vermote, E.F., Gao, F., Narasimhan, R., Channan, S., Wolfe, R.E., and Townshend, J.R., (2013). Global surface products from Landsat: Assessment using coincident MODIS observations. *Remote Sensing of Environment,* 134, pp. 276-293.

Gond, V., De Pury, D.G., Veroustraete, F., and Cuelemans, R., (1999). Seasonal variation in leaf area index, leaf chlorophyll and water content; scaling up to estimate fAPAR and carbon balance in a multilayer, multispecies temperate forest. *Tree Physiology,* 19, pp. 673-679.

Kondolf, G.M., (1989). Stream-groundwater interactions along streams of the Eastern Sierra Nevada California: Implications for assessing potential impacts of flow diversions, *USDA Forest Service Gen. Tech. Rep. PSW-110*, pp. 352-359.

Masek, J.G., Vermote, E.F., Saleous, N., Wolfe, R., Hall, F.G., Huemmrich, F., Gao, F., Kutler, J., and Lim, T.K., (2006). A Landsat surface reflectance data set for North America, 1990-2000. *IEEE Geoscience and Remote Sensing Letters*, 3, pp. 68-72.

Skre, O. and Naess, M., (1999). CO_2 and winter temperature effects on white birch. *Chemosphere: Global Change Science*, 1, pp. 469-483.

SWReGAP, (2003). Southwest Regional Gap Analysis Project Land Cover Legend, Ecological Systems and Alliance Descriptions. *The Nature Conservancy* 1815 N. Lynn Street Arlington, Virginia 22209.

Turner, W., Spector, S., Gardiner, N., Fladeland, M., Sterling, E., and Steininger, M., (2003). Remote sensing for biodiversity science and conservation. *Trends in Ecology and Evolution*, 18 (6), pp. 306–314.

United States Geological Survey, (2013). Landsat Climate Data Record (CDR) Surface Reflectance Version 2.0. *US Department of Interior Product Guide*, March 2013.

Vicente-Serrano, S.M., Perez-Cabello, F., and Lasanta, T., (2008). Assessment of radiometric correction techniques in analyzing vegetation variability and change using time series of Landsat imagery. *Remote Sensing of Environment*, 112, pp. 3916-3934.

Chapter 4: Vegetative response to climate change in the Big Pine Creek Watershed along a 2,500 meter elevation gradient using Landsat data

Contribution of Authors and Co-Authors

This manuscript was co-authored by Patrick Sawyer and Haroon Stephen. Patrick Sawyer was the first author who conceived and implemented the study design, collected and analyzed the data, and wrote the manuscript. Haroon Stephen was the second author who assisted with the study design and provided feedback on statistical analyses and drafts of the manuscript.

Manuscript Information Page

This manuscript has been published by the Science Publishing Group in the peer-reviewed journal Earth Sciences, Volume 3, Number 6, pages 137-146, 2014. Copyright information can be found in Appendix A or at the Science Publishing Group web site; (http://www.sciencepublishinggroup.com/journal/copyright?journalid=183).

This manuscript presents the research performed and findings achieved relating to the effect of elevation on climate driven ecological changes in an alpine ecosystem. This work supports objective number one to identify those changes. The study demonstrates objective two by employing multiple indices to determine climate driven changes in the surface cover of the study area.

Abstract

This paper presents a time series study of an alpine ecosystem in the Big Pine Creek watershed in California's Eastern Sierra Nevada Mountain's. Seventy five sample sites along a 2,500 meter elevation gradient are analyzed for trends in surface reflectance based on vegetative density using USGS data derived from Landsat imagery for the 1984 through 2013 time frame. Three vegetative indices, *NDVI, SAVI*, and $MSAVI_2$ as well as the Tasseled Cap transformations for Brightness (TC_B), greenness (TC_G), and wetness (TC_W) are explored. We found that over the time period of the study, significant increases in vegetation are occurring at densely vegetated sites at almost all elevations within the watershed while less change and even some significant declines in vegetation are seen in moderately and sparsely vegetated sites. Sparsely vegetated sites show distinct bifurcation in their response with the lower elevations seeing declines and the upper elevations seeing increases in vegetation. Several sites show significant declines in both the visible and near infrared regions suggesting there are compositional changes taking place consistent with climate induced range shifts. This study provides a useful insight into the ecological response of the Big Pine Creek watershed to recent climate change.

1.0 Introduction

Alpine ecosystems are crucial laboratories for the study of how changing climatic variables will impact local species assemblages. The steep elevation gradients in these regions provides for analysis of several ecotones within a small area. The biomes that inhabit these areas are particularly susceptible to changing environmental parameters

since many exist at the limits of their ranges (Lindner et al., 2010). While many studies have identified biotic response to climate change over large regions, the response at the local and individual ecosystem level are necessary to understand population dynamics that underlie range shifts (Opdam and Wascher, 2004; Gasner et al., 2010).

Existing research has focused on the response of individual species, often overlooking important biotic and abiotic interactions that drive community assembly. All the life forms within a local community interact with each other and their physical world forming a complex intricate fabric that identifies the characteristic traits of that assemblage. The predicted trend in climate induced range shifts is for increased extinctions at the warm boundaries and species expansions at the cold range limits (Opdam and Wascher, 2004). However, in alpine regions, the loss of space with elevation will lead upslope migrating species into a summit trap which will drive extinction rates higher (Wilson et al., 2005; Vittoz et al., 2013).

Since the response rate to altered environmental conditions varies among each member of the local assemblage, climate change will drive significant alteration of the interactions between the individual components and the overall functioning of the local community. Changes in the timing and availability of resources can have significant negative impacts on individual species survival rates while at the same time providing opportunities for competition to allow replacement species to prosper (Walther, 2010). An ongoing study of the Global Observation Research Initiative in Alpine Environments

(GLORIA) site in the European Alps demonstrates this process as species richness has shown a 12% increase in only a 10 year period (Salick et al., 2009).

Previous studies have examined the climate induced shift in range limits for species. Kelly and Goulden, (2008) found that the average elevation of the dominant plant species rose by about 65 meters over a 30 year period along an elevation gradient of 2,314 meters in the Santa Rosa Mountains of Southern California. The study area consisted of arid to semi-arid regions dominated by desert scrub in the lower reaches, pinyon-juniper woodlands as you move upslope, followed by chaparral shrubland and conifer forest in the higher reaches. Total plant cover was stable over the study period. Half of the sample sites had modest increases while half showed modest declines (Kelly and Goulden, 2008).

However, while total cover was stable, species distribution showed significant change with an average elevation gain of 65 meters. This study found that instead of migration of new species into new territory, most of the observed changes were related to a shift in dominance within local assemblages (Kelly and Goulden, 2008). This is an important finding in that significant compositional changes were observed even though overall range limits were stable. Regional studies that focus on range shifts may miss important changes at the local community level.

Habitat density plays an essential role in determining the local response to climate change. Once the critical population for a specific resource falls below sustainment levels, a chain reaction can occur that fundamentally alters the composition and

functioning of the local grouping. Altered environmental parameters such as warmer temperatures or reduced moisture availability can leave individual species in a weakened state, allowing for rapid infestation of predator or competitor species. While natural selection can lead to the development of tolerance traits that enhance the survivability of individual species, this process will most likely take much longer than the changes to the habitat which are driving species extinction (Walther, 2010).

Spectral characteristics measured with remote sensing instruments such as the Landsat 5 Thematic Mapper (TM) and Landsat 7 Enhanced Thematic Mapper (ETM^{+}) enable us to analyze ecological properties of vegetation. Vegetation has characteristic spectral responses such as low red reflectance due to chlorophyll absorption and high near infrared (NIR) reflectance due to the reflectance of the internal structures of the canopy (Wessman, 1992). Changes in surface reflectance can thus be correlated with variation in vegetative cover and plant health. Since the constituents of the plants vary over their phenological cycle, it is also possible to identify the various stages of the cycle such as spring flowering and fall senescence. Changes in the timing of these cycles can serve as an indicator of climate change.

Soil also demonstrates unique spectral characteristics depending on properties such as its moisture, organic matter content and texture (Jackson et al., 1986). Lower soil moisture content, a possible indicator of water stress in vegetation, would cause higher surface reflectance in the mid-wave infrared (MWIR) region that can be detected using Landsat data (Musick and Pelletier, 1988). Higher temperatures combined with lower

humidity levels will increase evapotranspiration resulting in less soil and vegetation moisture which will place additional burden on ecosystem vegetation. These effects are heightened in regions experiencing historic droughts such as the southwestern United States (Adams et al., 2009). Jackson et al. (1986) found that plant water stress will decrease the NIR response while increasing the reflectance in the red region of the spectrum. In addition to altering the spectral reflectance properties of the vegetation, plant stress can alter the geometry of the plant through processes such as drooping or wilting, resulting in a higher soil fraction component of the response signal (Jackson et al., 1986). Todd and Hoffer (1998) found that reduced vegetation moisture content tends to increase visible and MWIR reflectance (Todd and Hoffer, 1998).

Vogelmann et al. (2009) examined trends in spectral response in a time series study of the San Pedro Parks Wilderness area in New Mexico for the years 1992 through 2006. Higher elevations were shown to be spectrally stable except for areas infested with western spruce budworm. Some of the lower elevation shrub regions had declines in their short-wave infrared (SWIR)/NIR ratios as did patches of conifer trees suffering from high mortality rates (Vogelmann et al., 2009). Loss of available moisture significantly impacts forest growth and overall ecosystem health (Williams et al., 2013). Higher temperatures may also promote pest infestation. Williams et al. (2013) found that bark beetle populations increased during warmer periods, especially in forests already suffering moisture deficits induced by higher temperatures. This study determined that maximum

temperature (T_{MAX}) is an ideal surrogate for determining vapor pressure deficit induced forest stress (Williams et al., 2013).

The ecological response to elevated temperatures and CO_2 levels is complex and will be affected by other factors such as water and other nutrient resource availability. In cold alpine regions where water availability is not limiting, higher temperatures are expected to increase the habitable zones for several species, allowing for upslope migration and increased vegetative cover. In alpine regions, higher temperatures combined with increased atmospheric CO_2 levels will increase photosynthesis resulting in increased biomass; provided other essential resources are not limited (Skre and Naess, 1999). Conversely, where water is limited, higher temperatures will increase plant stress resulting in reduced vegetative cover (Chmura et al., 2011).

In this study we explore ecosystem response to recent climate change by analyzing trends in surface reflectance across a 2,500 meter elevation gradient in an alpine watershed using time series analysis of Landsat surface reflectance data. We apply a statistical approach to determine the presence of trends in the data that would validate the hypothesis of increased biomass resulting from higher temperature and atmospheric CO_2 levels in resource rich areas. Increased biomass is inferred by evidence of increased vegetative surface cover. We also look for evidence that species composition has been changing as evidenced by changes in the spectral fingerprint for each sample site over time. We present this information by first describing the study area and the data used in the analysis, we then discuss the research approach and methods used to collect and

process the data, followed by our results and conclusions. We hypothesize that sites with no resource limitations, (i.e. those nearest a water source), will show an increase in vegetative cover while sites with limited resources will show a decrease in the vegetative cover. We also hypothesize that sites at the limits of species ranges will show compositional change.

2.0 Study Area and Data

2.1 Study Area Description

Figure 13 below shows the Big Pine Creek watershed located in California's Eastern Sierra Mountains. Big Pine Creek is a major tributary to the Owens River which is a significant source of fresh water for Los Angeles. The Owens River valley straddles the Great Basin and Mojave deserts with vegetation consisting primarily of pine forests at higher elevations and xeric species at lower elevations. Areas bordering streams and the Owens River are primarily grass dominated meadows (Elmore et al., 2003). Elevation within the watershed increases from East to West with the higher regions dominated by barren rock and woodlands with the lower regions dominated by mixed desert shrubs.

The Big Pine Creek watershed ecosystem owes its existence to snow melt and melt-water from the Palisade Glacier. In addition to being the southern-most glacier in the United States, it is also the largest glacier in the Sierras with a surface area of 1.3 km^2. It was formed about 3,200 years ago, reaching a maximum extent as recently as 170 years ago (Bowerman and Clark, 2011). It has been generally in retreat ever since. The Big Pine Creek watershed drainage area covers approximately 82 km^2 and its average

flow is 1.8 m^3/s. Measurements taken in the 1980's indicate that the creek is a gaining stream at the lower elevations in contrast to most other Owens River tributaries which are losing streams (Kondolf, 1989). Since all of the living species within this watershed depend on the glacier and snow melt for their survival, the impact of temperature and precipitation variations on the biodiversity of the Big Pine Creek watershed is the focus of this study.

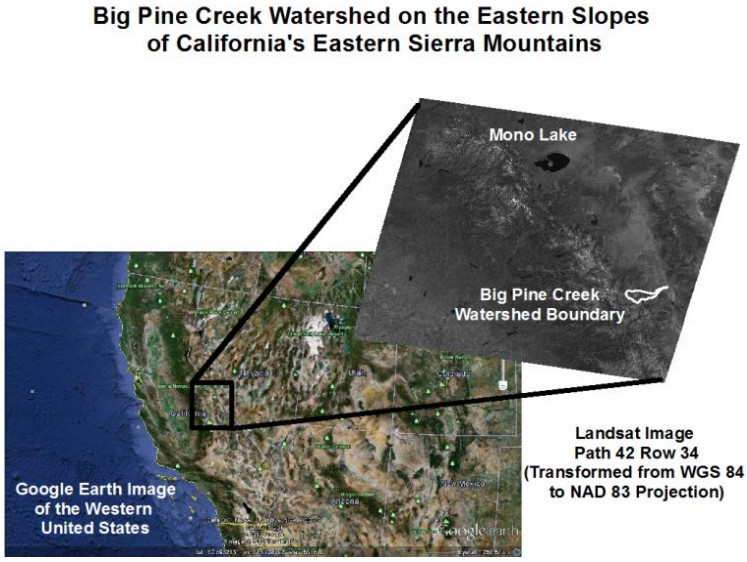

Figure 13. Study area location showing the boundary of the Big Pine Creek watershed.

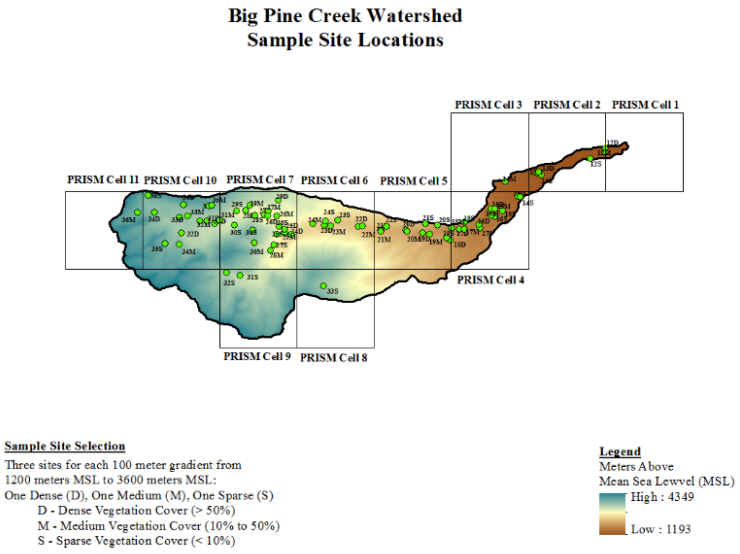

Figure 14. Sample Site Locations.

Three sample sites were selected at each 100 meter elevation gradient from 1200 meters above sea level (asl) at the base of the watershed to 3600 meters asl at the top. At each elevation, a densely vegetated site, a moderately vegetated site and a sparsely vegetated site were selected. Vegetation density at each elevation was determined by visual analysis of Google Earth satellite imagery. In general, the densely vegetated sites show surface cover exceeding 50%, the moderately vegetated sites had 10% to 50% surface cover and the sparsely vegetated sites were typically barren with less than 10% cover. The percentage vegetative cover closely correlated to the distance from a water source such as the Big Pine Creek, one of its tributaries, or one of the watershed lakes.

2.2 Data

The data in this study includes Landsat surface reflectance data obtained from the USGS EarthExplorer website. The Landsat program has been providing earth observation remote sensing data to the scientific community for four decades. The first Landsat satellite was placed in orbit in 1972 with Landsat 7 remaining operational today. Landsat 5 was only recently taken off-line. The latest generation satellite, Landsat 8, was launched on February 11th, 2013 and is now operational. Data for this study includes imagery from both the Landsat 5 TM and Landsat 7 ETM^{+} sensors.

Table 14

Summary of Landsat imagery used in this analysis

Image Date	Time	Scene ID (Path/Row)	Image Date	Time	Scene ID (Path/Row)
7/13/2013	10:28	42/34	7/30/1998	10:12	42/34
7/28/2012	10:28	42/34	7/27/1997	10:04	42/34
7/18/2011	10:22	42/34	7/24/1996	9:48	42/34
7/31/2010	10:24	42/34	7/31/1995	9:31	41/34
7/5/2009	10:16	41/34	7/3/1994	9:52	42/34
7/25/2008	10:20	42/34	7/16/1993	9:56	42/34
7/7/2007	10:27	42/34	7/29/1992	9:56	42/34
7/13/2006	10:20	41/34	7/27/1991	9:57	42/34
7/26/2005	10:15	41/34	7/8/1990	9:53	42/34
7/30/2004	10:16	42/34	7/5/1989	9:34	42/34
7/12/2003	10:10	42/34	7/2/1988	10:04	42/34
7/25/2002	10:09	42/34	7/25/1987	9:52	41/34
7/22/2001	10:14	42/34	7/29/1986	9:55	42/34
7/19/2000	10:10	42/34	7/3/1985	9:57	41/34
7/17/1999	10:11	42/34	7/7/1984	10:02	42/34

This surface reflectance data product for each of these imagers was obtained from the EarthExplorer web site operated by the United States Geological Survey (http://earthexplorer.usgs.gov/). Since the period of maximum leaf area index generally occurs in the mid-June to mid-August time frame (Gond et al., 1999), only imagery in the July time frame was considered for this analysis in order to minimize the impacts of the phenological cycle on the reflectance data.

3.0 Research Approach and Methods

3.1 Research Approach

This study examines how the surface reflectance of the watershed has changed over the last 30 years. To determine if climate change impacts to the vegetation in the study area have already occurred, we look for trends in the data that indicate alteration of the vegetative composition, health, or quantity. Sample sites are selected at 100 meter elevation gradients to determine if there are specific elevations where changes are most likely to occur. This is accomplished by performing a time series trend analysis of the surface reflectance values in each of the six reflectance bands of the Landsat sensors. Trends in the environmental parameters of precipitation and temperature are performed to correlate observed surface reflectance changes to altered climatic parameters.

3.2 Research Methods

The research methodology consists of data collection; data processing; and statistical analysis. Each step is described below.

3.2.1 Data Collection

In order to perform a temporal study comparing the physiological changes over time at each of the sample sites, surface reflectance values for each year of the study period were obtained from the USGS Climate Data Record (CDR) archive.

3.2.2 Statistical Trend Analysis

The non-parametric Mann-Kendall (MK) trend test is used to establish the presence of trends in the surface reflectance and meteorological data over the last 30 years. This analysis essentially determines if a set of values (y) are increasing or decreasing over time. Mann-Kendall analysis looks at the sums of the signs of the differences between successive data points and calculates a score or "S" statistic with the following properties: for S < 0 (values are decreasing over time); for S > 0 (values are increasing over time). The magnitude of the S-statistic is a measure of the strength of the trend. For a sample size of 30, S values of ±111 indicate a statistically significant trend with a p value of < 0.05. This means the null hypothesis of no-trend in the data can be discarded with the risk of committing a Type II (rejection of a true null or H_0) error at less than 5%. The MK S-statistic is calculated using (32)

$$S = \sum_{i=1}^{n-1} \sum_{j=i+1}^{n} sign\,(y_j - y_i)\,, \tag{32}$$

where n is the number of observations and y_i ($i = 1 \ldots n$) is the value at time T_i and y_j ($i = 1, \ldots, n$) is the value at time T_j (De Beurs and Henebry, 2005). Variance in the S statistic is calculated as

$$Var\ (S) = \frac{n(n-1)(2n+5)}{18}. \tag{33}$$

This variance assumes there are no tied pairs in the data. If tied pairs are identified, the software program applies a continuity equation which assumes a normal distribution for S with a zero mean. The variance is used to determine the probability (p) of obtaining a value of S greater than that calculated for the given number of data points when no trend is present. The probability statistic is determined from the Z score which is defined as:

$$Z = \begin{cases} \frac{S-1}{\sqrt{Var(S)}} & \text{, for } S > 0 \\ 0 & \text{, for S = 0} \\ \frac{S+1}{\sqrt{Var(S)}} & \text{, for } S < 0 \end{cases} \tag{34}$$

In addition to the trend statistic (S), Kendall's tau (τ) is determined from the equation

$$\tau = \frac{S}{\frac{n(n-1)}{2}}, \tag{35}$$

where n is the number of observations. Kendall's tau is similar to the correlation coefficient in linear regression. The magnitude of the trend is determined using the Sen's slope estimation with confidence intervals defined as the upper and lower estimate for the mean value of the slope. Sen's slope is determined by calculating the slope at each data point and taking the median of those slopes as the magnitude of the trend as shown;

$$Sen's\ Slope = median\left(\frac{y_j - y_i}{Time_j - Time_i}\right). \tag{36}$$

These calculations are carried out in Excel using the XLSTAT add-in statistical application. This program generates the S statistic as well as the probability (*p*) value which is used to quantify the statistical significance of the trend. The confidence factor (risk of rejecting a true null) is defined as (1-*p*)*100%.

3.2.3 Surface Reflectance Data

USGS surface reflectance data is generated from a software package known as the Landsat Ecosystem Disturbance Adaptive Processing System (LEDAPS). The surface reflectance data is computed by applying an atmospheric correction to the raw Landsat imagery (USGS, 2013). This atmospheric correction uses the Second Simulation of a Satellite Signal in the Solar Spectrum (6S) radiative transfer model to account for various atmospheric column constituents including water vapor, ozone, and aerosol optical thickness (Masek et al., 2006).

The LEDAPS process uses average daily lamp brightness history to obtain calibration coefficients based on acquisition date. These calibration coefficients are used to determine the at-sensor radiance values (Masek et al., 2006). The LEDAPS process converts at-sensor radiance to top-of-atmosphere (TOA) by an algorithm that incorporates solar irradiance derived from the MODTRAN model, bandpass, earth sun distance and solar zenith angle (Masek et al., 2006). The LEDAPS atmospheric correction assumes particle scattering and gaseous absorption can be decoupled (Masek et al., 2006). LEADAPS applies Moderate Resolution Imaging Spectroradiometer

(MODIS) atmospheric correction routines to Landsat data that correlates surface reflectance is with TOA reflectance using (37),

$$\rho_{TOA} = T_g(O_3, O_2, CO_2, NO_2, CH_4)\left[\rho_{R+A} + T_{R+A}T_g(H_2O)\frac{\rho_S}{1 + S_{R+A}\rho_S}\right] \quad (37)$$

where ρ_s is the surface reflectance, T_g is the gaseous transmission, T_{R+A} is the Rayleigh and aerosol transmission, ρ_{R+A} is the Rayleigh and aerosol atmospheric intrinsic reflectance, and S_{R+A} is the Rayleigh and aerosol spherical albedo (Masek et al., 2006).

The 6S radiative transfer model is used to derive surface reflectance from (6) with the input of aerosol optical thickness (AOT), atmospheric pressure and water vapor. The Total Ozone Mapping Spectrometer (TOMS) carried by the Nimbus 7, Meteor 3 and Earth Probe satellites provides the ozone concentration data. For the 1994 through 1996 time period when TOM's data was unavailable, vertical sounder data from the National Oceanic and Atmospheric Administration (NOAA) was used. Rayleigh scattering is adjusted to local conditions using surface pressure data from NOAA's National Center for Environmental Protection (NCEP) (Masek et al., 2006).

This atmospheric correction methodology uses a dark dense vegetation procedure developed by Kaufman et al., (1997) to determine AOT from the imagery. This technique is based on the assumption of a linear relationship between surface reflectance in the visible bands and the surface reflectance in the short wave band (2.2 μm where surface reflectance is not affected by the atmosphere) based on the physical correlation between bound water absorption and chlorophyll absorption. Using this procedure to calculate

surface reflectance in the visible bands then allows for the determination of AOT by comparing the TOA reflectance to the surface reflectance. Since this technique only determines the AOT in the blue region, a continental aerosol model is used to determine AOT in the other spectral regions. The AOT, atmospheric pressure, ozone and water vapor data are then processed by the 6S model to convert TOA reflectance to surface reflectance (Masek et al., 2006).

The USGS CDR data set provides us with observed surface reflectance values for each of the six reflectance bands for all sample sites in each year of the study. In order to identify the effect of elevation on the ecosystem's response to climate change, we examine trends in surface reflectance at 100 meter gradients from 1200 meters to 3600 meters asl. Additional analysis is performed by examining trends based on vegetative density. We also examine relationships between the spectral bands by considering the trends in vegetation indices resulting from the surface reflectance data.

Vegetation indices are often used to establish vegetation cover in remote sensing studies. We consider both ratio indices which analyze the large difference in the red and NIR bands characteristic of vegetation and weighted ratios which focus on physical parameters such as surface brightness, greenness and wetness. In this analysis we look at the following indices:

Normalized Difference Vegetation Index (*NDVI*), defined as

$$NDVI = \frac{\rho_{NIR} - \rho_{RED}}{\rho_{NIR} + \rho_{RED}}, \tag{38}$$

(Rouse at al., 1974), where ρ_{NIR} is the reflectance in band 4 and ρ_{RED} is the reflectance in band 3; Soil Adjusted Vegetation Index (*SAVI*), defined as

$$SAVI = (1 + L)\ \frac{\rho_{NIR} - \rho_{RED}}{\rho_{NIR} + \rho_{RED} + L}, \tag{39}$$

where *L* is a soil correction factor set at 0.5 (Huete, 1988); Modified Soil Adjusted Vegetation Index ($MSAVI_2$), defined as

$$MSAVI_2 = \frac{2\rho_{NIR} + 1 - \sqrt{(2\rho_{NIR} + 1)^2 - 8(\rho_{NIR} - \rho_{RED})}}{2}, \tag{40}$$

(Qi et al., 1994); and Tasseled Cap transformations for Brightness (TC_B), Greenness (TC_G), and Wetness (TC_W) which are defined as

$$TC_B = 0.2043\rho_1 + 0.4185\rho_2 + 0.5524\rho_3 + 0.5741\rho_4 + 0.3124\rho_5 + 0.2303\rho_7, \tag{41}$$

$$TC_G = -0.1603\rho_1 - 0.2819\rho_2 - 0.4934\rho_3 + 0.7940\rho_4 - 0.0002\rho_5 - 0.1446\rho_7, \tag{42}$$

$$TC_W = 0.0315\rho_1 + 0.2021\rho_2 + 0.3102\rho_3 + 0.1594\rho_4 - 0.6806\rho_5 - 0.6109\rho_7, \tag{43}$$

where $\rho_{1...7}$ is the reflectance in band 1 through band 7 respectively (Crist, 1985).

4.0 Results and Discussion

4.1 Spectral Trend Data

Figure 15 summarizes the trends in surface reflectance data for densely vegetated sites by elevation gradient. These graphs demonstrate significant declines in the visible bands 1, 2, and 3 below the 2600 meter level. Declines in the visible bands are consistent with increased vegetation due to higher chlorophyll absorption. The near infrared, band 4, shows positive trends at most elevations. This finding is consistent with increased structural complexity at those sites as near infrared reflectance increases with increasing

surface structural features. The trends in band 5 reflectance are mixed with no consistent pattern. This spectral region is where the water absorption feature exists which means sites showing significant declines are indicative of higher water content from which we infer increased vegetation cover. In the band 7 region, most of the sites show declines regardless of elevation which is consistent with increased surface cover as this region is correlated with surface brightness.

Figure 16 summarizes the trends in surface reflectance data for moderately vegetated sites by elevation gradient. These graphs demonstrate that for moderately vegetated sites, the most significant changes are taking place at the upper reaches of the watershed at the 3300 meter to 3600 meter asl elevations. Below that level, the trends do not show a distinct elevational dependency. However, in the band 5 and band 7 regions, the lower reaches of the watershed show decreased surface moisture along with increased surface brightness respectively. These findings are consistent with declines in vegetation for moderately vegetated sited below 1800 meters asl.

Figure 15. Trends in surface reflectance for densely vegetated sites.

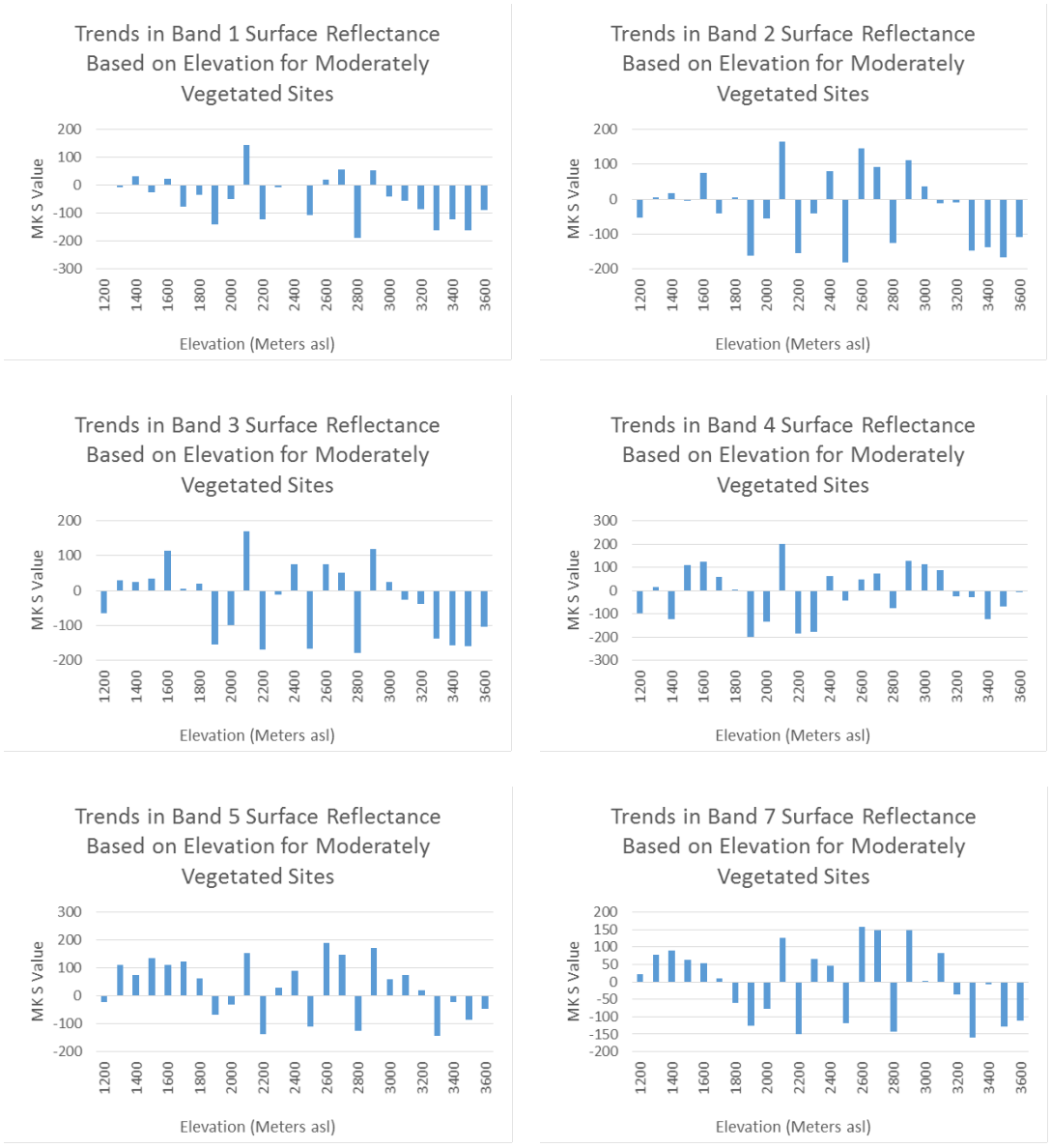

Figure 16. Trends in surface reflectance for moderately vegetated sites.

Although no clear elevational correlation is seen in the middle third of the study area (1900 meters to 2900 meters asl), several of the moderately vegetated sites show statistically significant changes with the data suggesting declining vegetation at the 2100

meter and 2900 meter asl sites and significant increases at the 1900 meter, 2200 meter, 2500 meter, and 2800 meter asl sites. The variation in the individual band responses suggests compositional changes are also taking place.

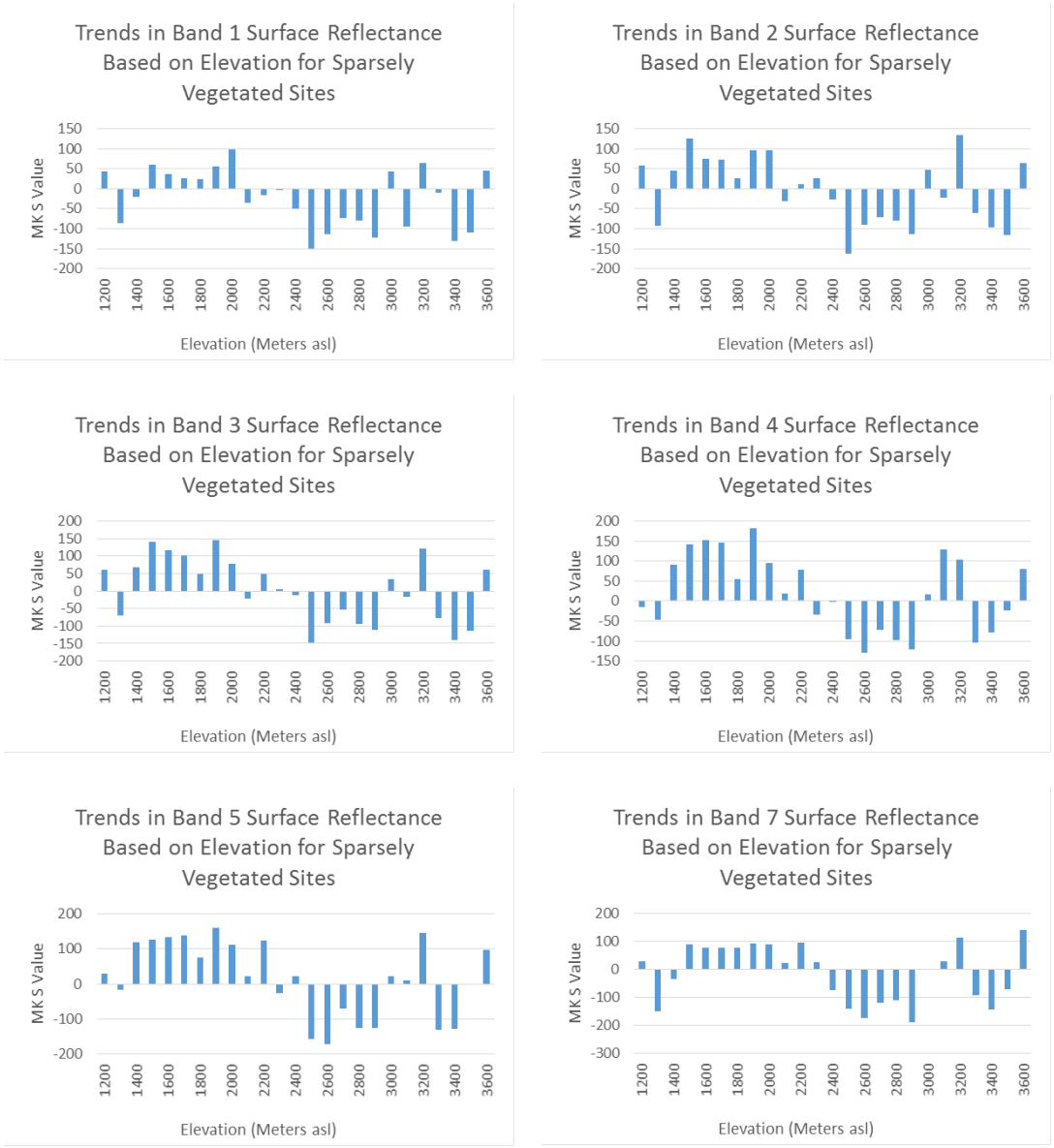

Figure 17. Trends in surface reflectance for sparsely vegetated sites.

Figure 17 summarizes the trends in surface reflectance data for sparsely vegetated sites by elevation gradient. These graphs demonstrate that for sparsely vegetated sites, there is a distinct bifurcation in spectral responses by elevation with increasing surface reflectance in the lower half of the watershed and decreasing reflectance in the upper half of the watershed for all six bands. There is a distinct transition range from 2200 meters to 2400 meters asl where the increases in reflectance switch to declines.

These findings suggest that in sparsely vegetated sites, vegetative surface cover is declining in the lower elevations while increasing at the higher elevations. The fact that the near infrared region response matches the visible response is consistent with a change in composition over the time period of the study. These findings support the hypothesis of upslope migration at the upper limits into newly habitable zones and an associated decline in population at the lower range limits where heat and moisture stressors are reducing habitability.

Figure 18 shows the trends for vegetation indices and Tasseled Cap transformations for densely vegetated sites. These results suggest a nearly uniform increase in vegetation with the exception of the 3000 meter to 3400 meter asl zone. The three indices (*NDVI*, *SAVI*, and $MSAVI_2$) along with the tasseled cap greenness transformation (TC_G) show consistent patterns. The general declines in tasseled cap brightness (TC_B) are also consistent with increased vegetative surface cover as are the general increases in tasseled cap wetness (TC_W).

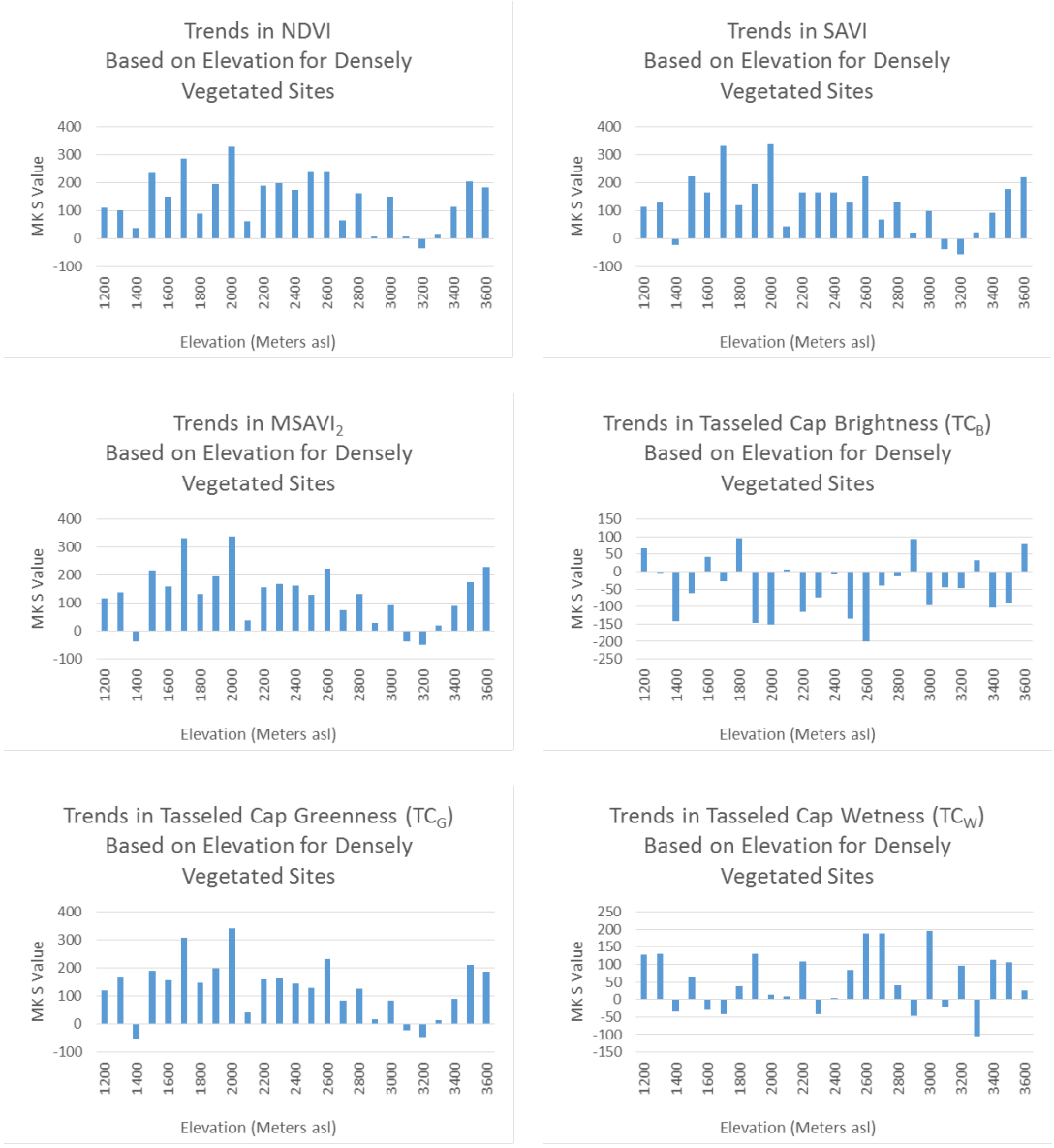

Figure 18. Trends in vegetation indices for densely vegetated sites.

These results mirror the trends in the spectral response. Both the spectral trends and the trends in the vegetation indices and transformations are consistent with a significant increase in vegetation throughout the study area in densely vegetated sites. This supports our hypothesis that sites without resource limitations, higher temperatures and CO_2 levels will boost photosynthetic activity resulting in increased vegetation and biomass.

The lack of change in the 3000 meter to 3400 meter asl zone is most likely due to unique characteristics of those sites and suggests that those locations lack the resources to take advantage of the increases temperature and CO_2 levels.

Figure 19 shows that for moderately vegetated sites, the vegetation indices and tasseled cap transformations do not indicate any significant patterns associated with elevation gradient. As with the trends in spectral response, these findings suggest an increase in vegetation at the higher elevations (above 2800 meters asl). The declines in the wetness values along with the increases in brightness values below 1800 meters asl suggest declining vegetative surface cover resulting from increased moisture stress at those sites.

Figure 19. Trends in vegetation indices for moderately vegetated sites.

The strong declines at the 2100 meter asl site seen in the spectral response is also reflected in the trends in the vegetation indices while the evidence for significant declines at the 2900 meter asl site suggested by the spectral trend data are not evident in the

vegetation indices. For the sites where spectral trends suggest significant increases, (1900 meter, 2200 meter, 2500 meter, and 2800 meter asl), trends in vegetation indices are not as significant. However, the tasseled cap brightness values for those sites do show significant declines suggesting increased ground cover. The fact that the vegetation indices do not coincide with the spectral response trends is consistent with a compositional change taking place at those sites.

Figure 20 shows that in the sparsely vegetated sites, the trends in vegetation indices and tasseled cap transformations are not as distinct as the spectral response. While the brightness and wetness transform trends are in good agreement, the vegetative indices show a more varied response. For example, the spectral responses in the visible bands suggest a decline in vegetation in the lower reaches of the watershed while the vegetation indices suggest an increase.

Since the near infrared response at the lower elevations is increasing, the structural complexity of the surface at these sites is increasing. These findings suggest that the compositions of the vegetation at the sites in the lower elevation are changing. The increase in TC_B is consistent with a decline in overall surface cover in the lower elevations, while the decline in TC_B is consistent with increased surface cover at the higher elevations. These data are consistent with the hypothesis of upslope migration suggested by the findings of the spectral response trend analysis for sparsely vegetated sites.

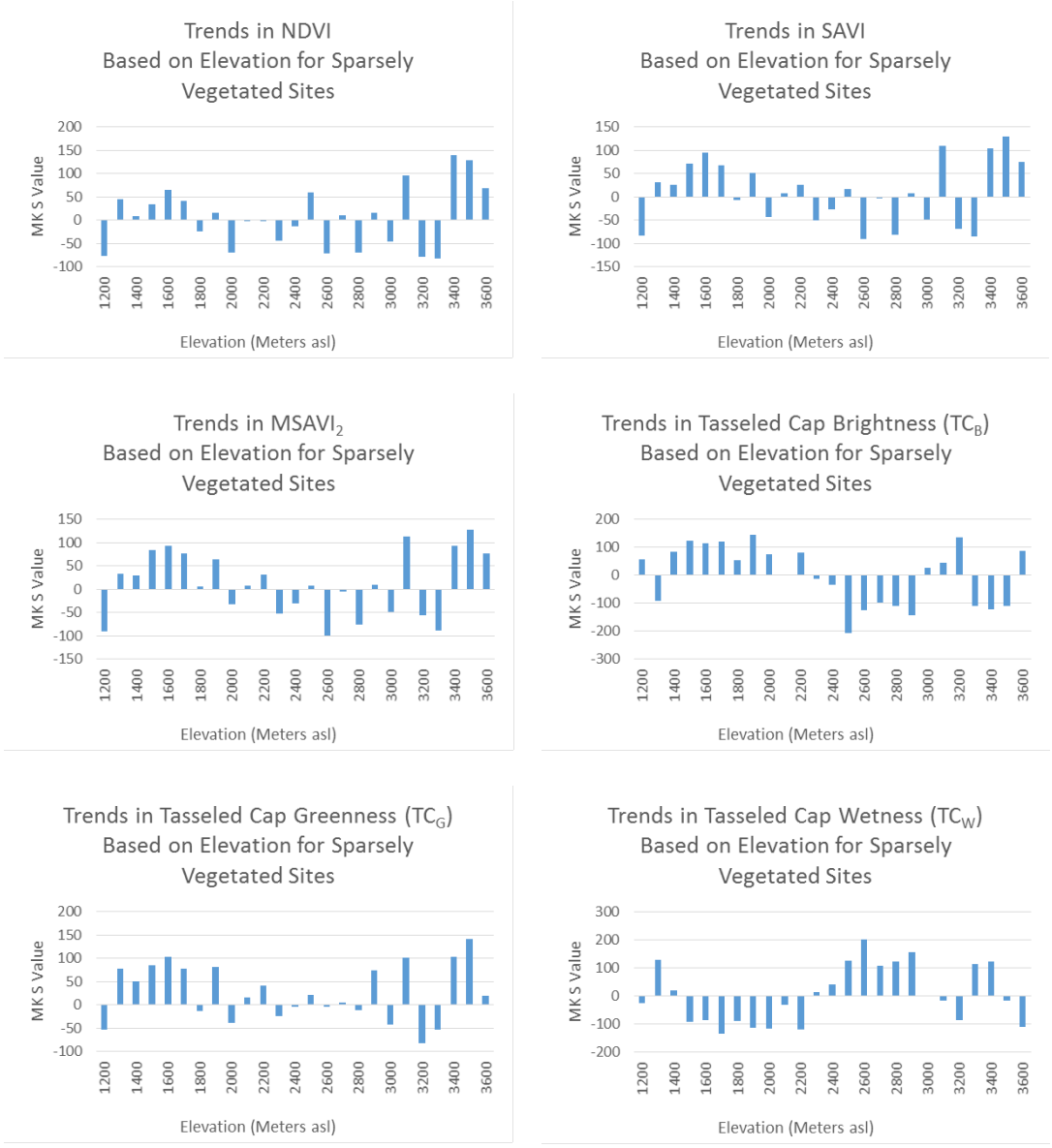

Figure 20. Trends in vegetation indices for sparsely vegetated sites.

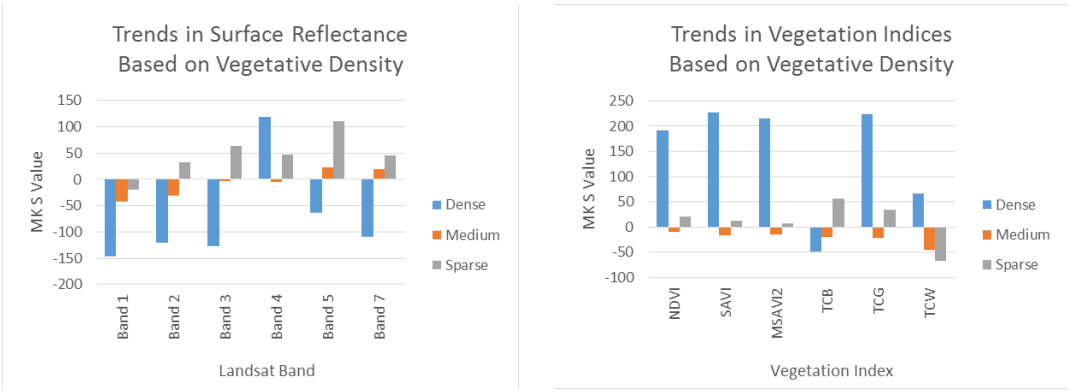

Figure 21. Trends in surface reflectance and vegetation indices based on vegetative density.

Looking at trends in surface reflectance and vegetation indices based solely on vegetative density, we see clear differences in the responses. As Figure 21 demonstrates, densely vegetated sites show clear evidence of increases over the 30 year study period. Moderately and sparsely vegetated sites show no statistically significant change. This does not mean that change is not taking place at those sites, only that when averaged together, any changes are washed out. For example, with the sparsely vegetated sites, we observe declines in the lower half of the watershed and increases in the upper half. Therefore, when averaged across all sites, there appears to be no change. The primary finding from this comparison is that densely vegetated sites are seeing increased growth regardless of elevation.

The trends in surface reflectance and vegetative indices demonstrate significant changes are taking place across all regions of the watershed. Densely vegetated sites are seeing increases in growth at most elevation gradients with the exception of the 3000 meter to 3400 meter asl zone. Meanwhile, the least vegetated sites are seeing a distinct

shift with increased vegetative cover in the upper half of the watershed and declines in the lower half of the watershed. Trends in the moderately vegetated sites do not show distinctive patterns based on elevation gradient.

4.2 Meteorological Data

Ecological changes we have identified in the Big Pine Creek watershed are consistent with warming temperatures. In our previous paper, we identified statistically significant increases across the study area in both the maximum temperature (T_{MAX}) and minimum temperature (T_{MIN}). Looking at monthly trends, we found that for the maximum temperatures, the largest increases are taking place in the summer with smaller increases in the winter. Higher temperatures are an important factor in driving ecological changes since all biological processes are at their essence chemical reactions and increased temperatures will increase reaction rates. Increased biological activity can alter vegetative composition by changing the availability essential nutrients. Some nutrients will be more available through faster litter breakdown while some nutrients will be consumed at faster rates. This change in resource availability will drive changes in species composition to those species that are better suited to the new environmental conditions and resource make-up (Sawyer and Stephen, 2014).

Precipitation and Big Pine Creek stream flow trends were also examined to determine if the moisture deficit conditions were impacting ecological responses over the study period. Here we found that although there was a slight decline in precipitation in the watershed, stream flow was slightly increasing which is consistent with warmer

temperatures increasing the melt water contribution to the stream flow from the Palisade glacier (Sawyer and Stephen, 2014). In addition to driving biological activity, higher temperatures will also increase evapotranspiration. This will reduce moisture availability and stress vegetative species, especially those that are not drought tolerant.

For the monthly minimum temperature trends, we see the largest increases are taking place in the summer and fall with smaller increases in the winter and spring. What these data demonstrate is that the summers are getting warmer and the winters are getting milder. This is an important finding since as discussed earlier, warmer summers will increase evapotranspiration during the dry season, increasing potential water stress in the vegetation. Milder winters will also result in reduced water storage capacity as less precipitation will fall as snow, which also results in reduced water supplies in the warmest time of the year (Sawyer and Stephen, 2014). The seasonal trends found in this analysis closely align with future climate regimes predicted by general circulation models showing milder wetter winters and hotter drier summers (Lenihan et al., 2003). Lenihan et al. (2003) show that these future climate scenarios can produce shifts in the vegetative composition (Lenihan et al., 2003). In particular, their biological distribution model simulations suggest a shift from shrubs to grasslands under these conditions (Lenihan et al., 2003). The temperature trends demonstrate that the Big Pine Creek watershed is at heightened risk from climate change and highlight the need to develop strategies to adapt to the new climate paradigm.

4.3 Confidence Levels

Multitemporal satellite imagery is impacted by several factors including changes in sensor response, sensor stability, atmospheric effects, and illumination effects (Vicente-Serrano et al., 2008). Geometric pixel registration errors are generally less than ½ pixel (Schueler and Salomonson, 1985). Radiometric uncertainty for the TM data is approximately 5% (Chander et al., 2009). The USGS surface reflectance data set has been assessed against MODIS surface reflectance data and found to be highly correlated with discrepancies between 2.2 to 3.5 percent (Feng et al., 2013).

5.0 Summary and Conclusions

This study examined the changes in the ecosystem of the Big Pine Creek watershed as measured by trends in observed surface reflectance values along a 2500 meter elevation gradient at 75 sample sites over a 30 year time span from 1984 through 2013. Densely vegetated sites demonstrated significant increases in vegetative growth as evidenced by both declines in visible reflectance and increases in vegetative indices. Sparsely vegetated sites show a distinctive response pattern with vegetation increasing in the upper half of the watershed and declining in the lower half. Moderately vegetated sites show a mixed response with a few sites experiencing significant increases and a few showing significant declines. No elevation dependent pattern was evident for moderately vegetated sites.

Based on the findings of this study, we conclude that for densely vegetated sites, (those nearest permanent water sources), increased temperatures are driving increased

vegetative growth with little evidence of compositional change. At sparsely vegetated sites, (those farthest from permanent sources of water), vegetation is moving upslope. At the upper reaches of the watershed, warmer temperatures are increasing the habitable zone for these sites while at the lower reaches, increased temperatures are driving an alteration of vegetative composition towards more drought tolerant species. The mixed responses seen at the moderately vegetated sites appear to be site specific with changes dictated by local conditions.

To determine what is driving the changes in vegetative surface cover, we examined trends in the environmental parameters of precipitation and temperature. Average monthly minimum and maximum temperatures show statistically significant upward trends (Sawyer and Stephen, 2014). Increased temperatures support increased photosynthetic activity as long as that process is not limited by other factors such as lack of water availability. In areas without water or other nutrient resource limitations, these conditions are conducive for increased vegetative surface cover resulting in stronger absorption in the visible region of the spectrum.

This study has clearly identified numerous changes taking place in the Big Pine Creek watershed over the last 30 years. Many of these changes are consistent with previous research related to climate change impacts on montane habitats. While this study has identified coarse trends in vegetative response, more detailed analysis of individual study sites is needed to both validate the findings from this study as well as to delineate the specific compositional changes that are occurring. Identifying how the

individual components of each sample site have responded to altered environmental parameters will provide critical information on the ecological response to climate change in Alpine environments.

References

Adams, H.D., Guardiola-Claramonte, M., Barron-Gafford, G.A., Villegas, J.C., Breshears, D.D., Zou, C.B., Troch, P.A., and Huxman, T.E., (2009). Temperature sensitivity of drought-induced tree mortality portends increased regional die-off under global-change-type drought. *PNAS*, 106 (17), pp. 7063 – 7066.

Bowerman, N.D. and Clark, D.H., (2011). Holocene glaciation of the central Sierra Nevada, California. *Quaternary Science Reviews*. 30, pp. 1067-1085.

Chander, G., Markham, B., and Helder, D.L., (2009). Summary of current radiometric calibration coefficients for Landsat MSS, TM, ETM+, and EO-1 ALI sensors. *Remote Sensing of Environment*, 113, pp. 893-903.

Chmura, D.J., Anderson, P.D., Howe, G.T., Harrington, C.A., Halofsky, J.E., Peterson, D.L., Shaw, D.C., and St. Clair, B.J., (2011). Forest responses to climate change in the northwestern United States: Ecophysiological foundations for adaptive management. *Forest Ecology and Management*, 261, pp. 1121–1142.

Crist, E.P., (1985). Short Communication: A TM Tasseled Cap Equivalent Transformation for Reflectance Factor Data. *Remote Sensing of the Environment*, 17, pp. 301-306.

De Beurs, K.M. and Henebry, G.M., (2005). A statistical framework for the analysis of long image time series. *International Journal of Remote Sensing*, 26 (8), pp. 1551-1573.

Elmore, A.J., Mustard, J.F., and Manning, S.J., (2003). Regional patterns of plant community response to changes in water: Owens Valley, California. *Ecological Applications*, 13 (2), pp. 443-460.

Feng, M., Sexton, J.O., Huang, C., Masek, J.G., Vermote, E.F., Gao, F., Narasimhan, R., Channan, S., Wolfe, R.E., and Townshend, J.R., (2013). Global surface products from Landsat: Assessment using coincident MODIS observations. *Remote Sensing of Environment*, 134, pp. 276-293.

Gasner, M.R., Jankowski, J.E., Ciecka, A.L., Kyle, K.O., and Rabenold, K.N., (2010). Projecting the local impacts of climate change on a Central American montane avian community. *Biological Conservation*, 143, pp. 1250-1258.

Gond, V., De Pury, D.G., Veroustraete, F., and Cuelemans, R., (1999). Seasonal variation in leaf area index, leaf chlorophyll and water content; scaling up to estimate fAPAR and carbon balance in a multilayer, multispecies temperate forest. *Tree Physiology*, 19, pp. 673-679.

Huete, A.R., (1988). A Soil-adjusted Vegetation Index. *Remote Sensing of the Environment,* 25, pp. 295-309.

Jackson, R.D., Pinter, P.J., Jr., Reginato, R.J., and Idso, S.B., (1986). Detection and evaluation of plant stresses for crop management decisions. *IEEE Transactions on Geoscience and Remote Sensing*, GE-24 (1), pp. 99-106.

Kaufman, Y.J., Wald, A.E., Remer, L.A., Gao, B.C., Li, R.R., and Flynn, L., (1997). The MODIS 2.1 μm channel – Correlation with visible reflectance for use in remote sensing of aerosol. *IEEE Transactions on Geoscience and Remote Sensing*, 35 (5), pp. 1286-1298.

Kelly, A.E. and Goulden, M.L, (2008). Rapid shifts in plant distribution with recent climate change. *Proceedings of the National Academy of Sciences (PNAS)*, 105(33), pp. 11823-11826.

Kondolf, G.M., (1989). Stream-groundwater interactions along streams of the Eastern Sierra Nevada California: Implications for assessing potential impacts of flow diversions. *USDA Forest Service Gen. Tech. Rep. PSW-110*, pp. 352 – 359.

Lenihan, J.M., Drapek, R., Bachelet, D., Kremer, and Nelson, R.P., (2003). Climate change effects on vegetation distribution, carbon, and fire in California. *Ecological Applications*, 13 (6), pp. 1667 – 1681.

Lindner, M., Maroschek, M., Netherer, S., Kremer, A., Barbati, A., Garcia-Gonzalo, J., Seidl, R., Delzon, S., Corona, P., Kolstrom, M., Lexer, M.J., and Marchetti, M., (2010). Climate change impacts, adaptive capacity, and vulnerability of European forest ecosystems. *Forest Ecology and Management*, 259, pp. 698 – 709.

Masek, J.G., Vermote, E.F.., Saleous, N., Wolfe, R., Hall, F.G., Huemmrich, F., Gao, F., Kutler, J., and Lim, T.K., (2006). A Landsat surface reflectance data set for North America, 1990-2000. *IEEE Geoscience and Remote Sensing Letters*, 3, pp. 68-72.

Musick, H.B. and Pelletier, R.E., (1988). Response to soil moisture spectral indexes derived from bidirectional reflectance in thematic mapper wavebands. *Remote Sensing of Environment*, 25, pp. 167-184.

Opdam, P. and Wascher, D., (2004). Climate change meets habitat fragmentation: linking landscape and biogeographical scale levels in research and conservation. *Biological Conservation*, 117, pp. 285-297.

Qi, J., Chehbouni, A., Huete, A.R., Kerr, Y.H., and Sorooshian, S., (1994). A Modified Soil-adjusted Vegetation Index. *Remote Sensing of the Environment*, 48, pp. 119-126.

Rouse, J.W., Haas, R.H. Schell J.A. and Deering, D.W., (1974). Monitoring vegetation systems in the Great Plains with ERTS. *Proc. Third ERTS-1 Symposium, NASA Goddard*, NASA SP-351 pp. 309-317.

Salick, J., Zhendong, F., and Byg, A., (2009). Eastern Himalayan alpine plant ecology, Tibetan ethnobotany, and climate change. *Global Environmental Change*, 19, pp. 147-155.

Sawyer, P.S., and Stephen, H., (2014). The Big Pine Creek watershed and climate change: A trend analysis of Landsat surface reflectance and PRISM datasets over the last three decades. *Advances in Space Research*, 54, pp. 37-48.

Schueler, C.F., and Salomonson, V.V., (1985). Landsat Image Data Quality Studies. *Advances in Space Research*, 5 (5), pp. 1-11.

Skre, O. and Naess, M., (1999). CO_2 and winter temperature effects on white birch. *Chemosphere: Global Change Science*, 1, pp. 469-483.

Todd, S.W. and Hoffer, R.M., (1998). Responses of spectral indices to variations in vegetation cover and soil background. *Photogrammetric Engineering & Remote Sensing*, 64 (9), pp. 915-921.

United States Geological Survey, (1994). Standardized national vegetation classification system. *The Nature Conservancy* 1815 N. Lynn Street Arlington, Virginia 22209, Prepared for the United States Department of Interior, United States Geological Survey and National Park Service.

Vicente-Serrano, S.M., Perez-Cabello, F., and Lasanta, T., (2008). Assessment of radiometric correction techniques in analyzing vegetation variability and change using time series of Landsat imagery. *Remote Sensing of Environment*, 112, pp. 3916-3934.

Vittoz, P., Cherix, D., Gonseth, Y., Lubini, V., Maggini, R., Zbinden, N., and Zumbach, S., (2013). Climate change impacts on biodiversity in Switzerland: A review. *Journal for Nature Conservation*, 21, pp. 154-162.

Vogelmann, J.E., Tolk, B., and Zhu, Z., (2009). Monitoring forest changes in the southwestern United States using multitemporal Landsat data. *Remote Sensing of Environment*, 112, pp. 1739-1748.

Walther, G-R., (2010). Community and ecosystem responses to recent climate change. *Philosophical Transactions of The Royal Society B*, 365, pp. 2019-2024.

Wessman, C.A., (1992). Imaging spectrometry for remote sensing of ecosystem processes. *Advances in Space Research*, 12 (7), pp. 361-368.

Williams, A.P., Allen, C.D., Macalady, A.K., Griffin, D., Woodhouse, C.A., Meko, D.M., Swetnam, T.W., Rauscher, S.A., Seager, R., Grissino-Mayer, H.D., Dean,

J.S., Cook, E.R., Gangodagamage, C., Cai, M., and McDowell, N.G., (2013). Temperature as a potent driver of regional forest drought stress and tree mortality. *Nature Climate Change*, 3, pp. 292-297.

Wilson, R.J., Gutierrez, D., Gutierrez, J., Martinez, D., Agudo, R., and Monserrat, V.J., (2005). Changes to the elevational limits and extent of species ranges associated with climate change. *Ecology Letters*, 8, pp. 1138-1146.

Chapter 5: Surface Cover Spectra of the Big Pine Creek Watershed

Contribution of Authors and Co-Authors

This manuscript was co-authored by Patrick Sawyer and Haroon Stephen. Patrick Sawyer was the first author who conceived and implemented the study design, collected and analyzed the data, and wrote the manuscript. Haroon Stephen was the second author who assisted with the study design and provided feedback on drafts of the manuscript. Additional collaboration was provided by Dr. David Charlet from the College of Southern Nevada. Dr. Charlet assisted with species identification of the ground cover vegetative samples.

Manuscript Information Page

This manuscript has been officially submitted to a peer-reviewed journal for publication.

This manuscript presents the research performed and findings achieved relating to the collection and analysis of field ground cover samples. The purpose of this work is the production of data needed to determine climate driven ecological changes. This work supports objective number two to design an analytical methodology that uses remote sensing to determine changes in vegetative surface cover of the ecosystem.

Abstract

This paper presents a set of spectral reflectance data of numerous surface cover types of the Big Pine Creek watershed in California's Eastern Sierra Nevada Mountains. Ground cover vegetative types include several samples of deciduous broad leaf and narrow leaf trees, needle leaf conifers, sages, and needle leaf and broad leaf shrubs. In addition, several litter samples as well as soil and rock spectra are presented. Samples were collected in July 2014 and analyzed in the laboratory using a 0.35 to 2.5 μm Advanced Spectral Devices (ASD) Flexscan spectroradiometer.

1.0 Introduction

Alpine ecosystems are crucial laboratories for the study of how changing climatic variables will impact local species assemblages. The steep elevation gradients in these regions provides for analysis of several ecotones within a small area. The biomes that inhabit these areas are particularly susceptible to changing environmental parameters since many exist at the limits of their ranges (Lindner et al., 2010). Since alpine ecotones represent bioclimatic transitions, species compositional change is high and susceptible to slight alteration in bioclimatic regimes (Grabherr et al., 2010). Our ability to identify where changes are taking place in these sensitive regions depends upon our ability to exploit existing data sets such as the Landsat Climate Data Record. Understanding the spectral characteristics of the surface cover constituents is essential to being able to identify changes at the local vegetative assembly scale.

Spectral characteristics measured with remote sensing instruments such as the Landsat 5 Thematic Mapper (TM) and Landsat 7 Enhanced Thematic Mapper (ETM+) enable us to analyze ecological properties of vegetation. Vegetation has characteristic spectral responses such as low red reflectance due to chlorophyll absorption and high near infrared (NIR) reflectance due to the reflectance of the internal structures of the canopy (Wessman, 1992). Changes in surface reflectance can thus be correlated with variation in vegetative cover and plant health.

Soil also demonstrates unique spectral characteristics depending on properties such as its moisture, organic matter content and texture (Jackson et al., 1986). Lower soil moisture content, a possible indicator of water stress in vegetation, would cause higher surface reflectance in the mid-wave infrared (MWIR) region that can be detected using Landsat data (Musick and Pelletier, 1988). Remote sensing using multispectral imagers such as the Landsat series provide a wealth of data that can be used to monitor for changes in the environment. Large scale regional change is clearly evident from the 30 meter resolution imagery these instruments provide. However, at this resolution, important details within each pixel remain hidden. For remote sensing applications, unless the image is over human controlled agricultural plots, most Landsat image pixels will include several components that cannot be discerned from the raw data. This necessitates the use of spectral unmixing techniques such as spectral mixture analysis (SMA). With SMA, the radiance measured in each pixel by the sensor in each wave band is composed of a mixture of reflectance exitance given off by each of the individual

components within that pixel. Studies performing subpixel analysis of Landsat imagery often make use of generic spectral libraries of various vegetative species to identify spectral endmembers that make up the constituents of each pixel.

This study is designed to provide a spectral library of the vegetative and other ground cover types present within the Big Pine Creek watershed. Spectral response data of numerous vegetative samples in addition to several litter, soil, and rock samples are presented. Sample collection and analysis procedures are explained and the full spectrum reflectance data are provided for each sample. The field collected spectra developed in this study allow us to decompose the individual spectral components present with each Landsat pixel. From this data, we can then identify the fractional cover of individual species present within each pixel and analyze how those fractions have trended over time. This information can then be used to assess the impact recent climate variations have had on the Big Pine Creek ecosystem.

This research has the added benefit of providing the scientific community with samples of reflectance data commonly encountered in desert and montane environments. Although the samples were obtained from a specific watershed in the Eastern Sierra Nevada Mountains of California, most of the species are ubiquitous throughout the inter-mountain and great basin regions of the western United States.

2.0 Study Area and Sample Description

2.1 Study Area Description

Figure 22 below shows the Big Pine Creek watershed located in California's Eastern Sierra Mountains. Big Pine Creek is a major tributary to the Owens River which is a significant source of fresh water for Los Angeles. The Owens River valley straddles the Great Basin and Mojave deserts with vegetation consisting primarily of pine forests at higher elevations and xeric species at lower elevations. Areas bordering streams and the Owens River are primarily grass dominated meadows (Elmore et al., 2003). Elevation within the watershed increases from East to West with the higher regions dominated by barren rock and woodlands with the lower regions dominated by mixed desert shrubs.

The Big Pine Creek watershed ecosystem owes its existence to snow melt and melt-water from the Palisade Glacier. In addition to being the southern-most glacier in the United States, it is also the largest glacier in the Sierras with a surface area of 1.3 km^2. It was formed about 3,200 years ago, reaching a maximum extent as recently as 170 years ago (Bowerman and Clark, 2011). It has been generally in retreat ever since. The Big Pine Creek watershed drainage area covers approximately 82 km^2 and its average flow is 1.8 m^3/s.

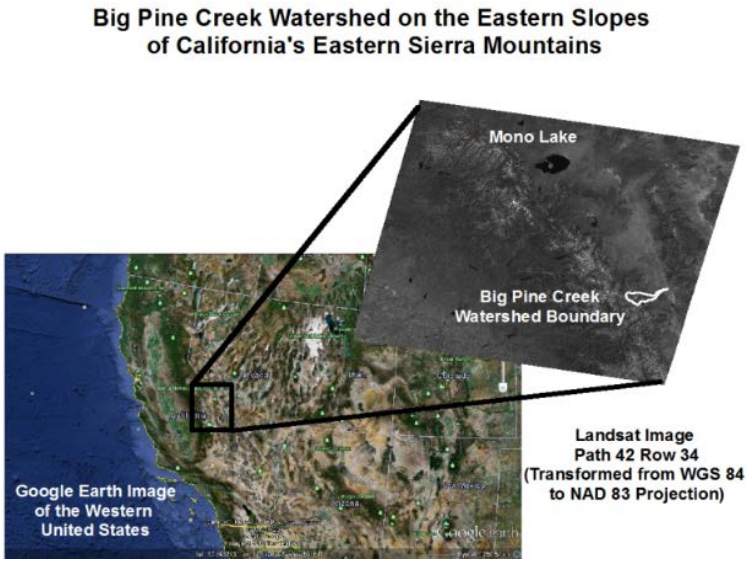

Figure 22. Study area location showing the boundary of the Big Pine Creek watershed

2.2 Sample Collection

The Big Pine Creek watershed consists of mostly undeveloped rugged terrain within the Inyo National Forest. Due to the remoteness and steep gradients, performing the spectral measurements in the field was not practical. Therefore, the vegetative and other surface constituent samples were collected and placed in sealed plastic bags and placed on ice for shipment to the lab. Samples were selected by choosing the top two or three vegetative surface cover types at each site along with a litter or soil sample when practical. Figure 23 shows the locations of each sample site within the watershed. Table fifteen provides the geographic coordinates and elevations of each site.

2.3 Sample Analysis

All of the samples were analyzed within two hours of their arrival at the laboratory. Analysis was performed using an ASD 0.35 – 2.5 μm VNIR-SWIR Flexscan Spectroradiometer (S/N 16232). Composite spectra of each species as well as combined composite spectra for each type were developed by first averaging the spectra of each species and then averaging the composites. These data are presented in section 3.

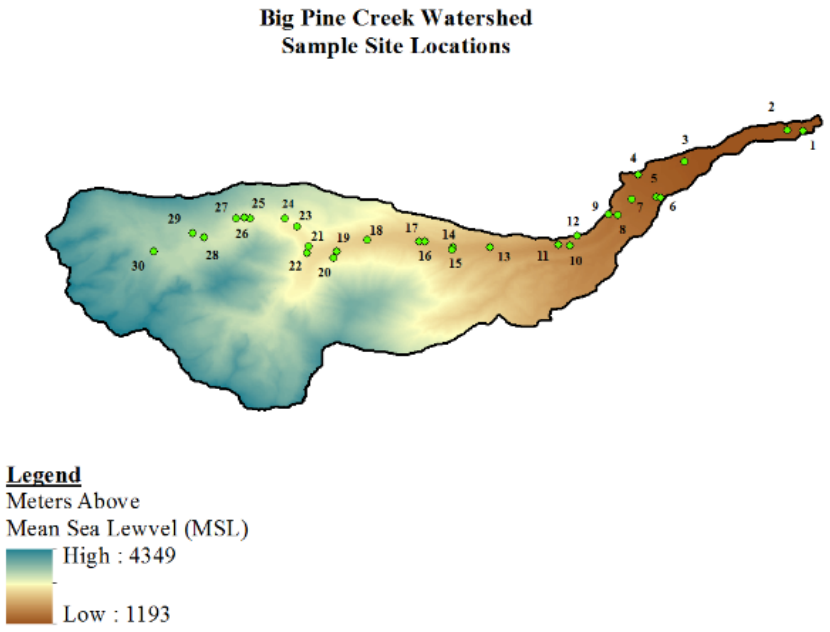

Figure 23. Sample Site Locations

Table 15

Sample Site Locations

Sample Site ID	Latitude (N)	Longitude (W)	Elevation (M MSL)	Sample Site ID	Latitude (N)	Longitude (W)	Elevation (M MSL)
1	37.1675	-118.2657	1201	16	37.1274	-118.4024	2198
2	37.1676	-118.2714	1201	17	37.1275	-118.4044	2208
3	37.1567	-118.3070	1294	18	37.1279	-118.4231	2296
4	37.1516	-118.3251	1397	19	37.1240	-118.4340	2389
5	37.1435	-118.3187	1402	20	37.1221	-118.4421	2408
6	37.1433	-118.3172	1403	21	37.1256	-118.4442	2495
7	37.1426	-118.3274	1460	22	37.1232	-118.4449	2502
8	37.1370	-118.3326	1509	23	37.1328	-118.4485	2603
9	37.1372	-118.3359	1598	24	37.1358	-118.4529	2702
10	37.1258	-118.3499	1707	25	37.1358	-118.4653	2799
11	37.1264	-118.3541	1798	26	37.1359	-118.4675	2836
12	37.1294	-118.3471	1805	27	37.1357	-118.4703	2899
13	37.1252	-118.3788	2009	28	37.1290	-118.4820	3005
14	37.1253	-118.3922	2100	29	37.1305	-118.4863	3099
15	37.1246	-118.3923	2105	30	37.1238	-118.5002	3198

3.0 Data Results

This section presents the results of the sample collection and spectral analysis. The samples collected in this study were for the purpose of performing an analysis of the surface reflectance of the study area and how the reflectance has trended over the last three decades. Endmember spectra were collected from a broad sample of surface cover types at 30 sample sites located throughout the watershed. At each site, three to four samples of the predominant surface covers were collected for analysis. Sample cover types include six categories of photosynthetic vegetation, litter, and barren surface.

3.1 Photosynthetic Vegetation

Photosynthetic vegetation is categorized as trees (three types) or shrubs (three types). The three types of trees include broad leaf, narrow leaf, and needle leaf. The three

shrub types include sages, broad leaf shrubs and needle leaf shrubs. Sedges were also analyzed and categorized as needle leaf shrub for this analysis.

3.1.1 Trees

3.1.1.1 Broad Leaf Trees

Broad leaf tree samples collected include Cottonwood (*Hibiscus tilliaceus*), Red Birch (*Betula occidentalis*), California Poplar (*Populus trichocarpa*), Aspen (*Populus tremuloides*), and Black Oak (*Quercus kelloggii*). Figure 24 shows the composite spectra of each species and a combined composite of all broad leaf tree species. The red data points represent the spectral values at the midpoint of the Landsat 5 TM spectral bands.

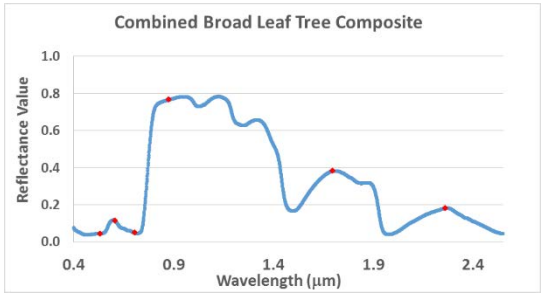

a. Combined full spectrum composite

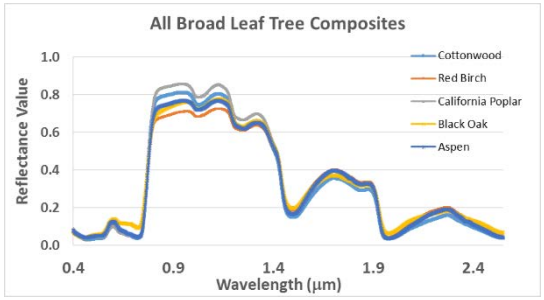

b. Full Spectrum composite of all species

Figure 24. Composite broad leaf tree spectra; full VNIR-SWIR.

3.1.1.2 Narrow Leaf Trees

Narrow leaf tree samples collected include Willow (*Salix sp.*), Sandbar willow (*Salix exigua*), and California Coffeeberry (*Frangula californica ssp. cuspidata*). Figure 25 shows the composite spectra of each species and a combined composite of all narrow

leaf tree species. The red data points represent the spectral values at the midpoint of the Landsat 5 TM spectral bands.

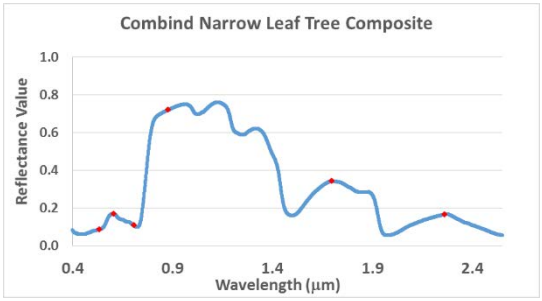

a. Combined full spectrum composite

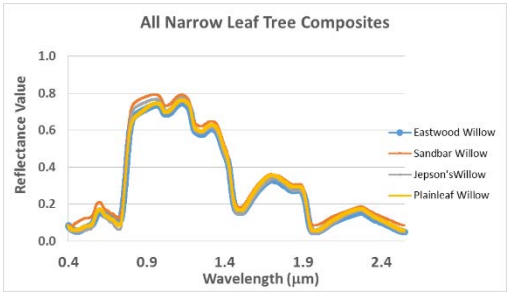

b. Full Spectrum composite of all species

Figure 25. Composite narrow leaf tree spectra; full VNIR-SWIR.

3.1.1.3 Needle Leaf Trees

Needle leaf tree samples collected include Yellow Pine (*Pinus sp.*), White Pine (*Pinus sp.*), and California Lodgepole Pine (*Pinus contorta var. murrayana*). Figure 26 shows the composite spectra of each species and a combined composite of all needle tree species. The red data points represent the spectral values at the midpoint of the Landsat 5 TM spectral bands.

3.1.2 Shrubs

Three broad categories of shrubs were sampled including sages, needle leaf shrubs and broad leaf shrubs. Sedges are grouped with the needle lead shrubs.

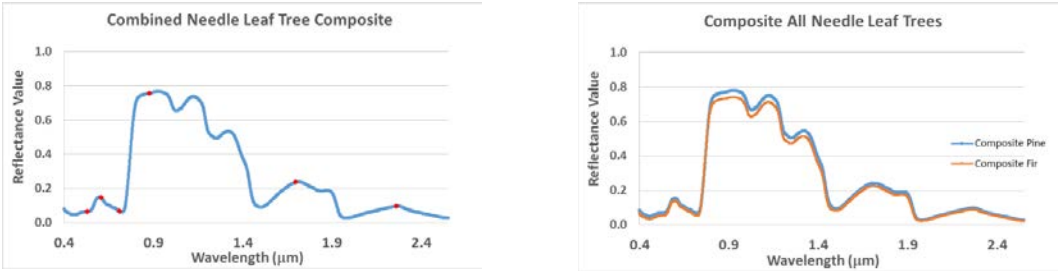

a. Combined full spectrum composite b. Full Spectrum composite of all species

Figure 26. Composite needle leaf tree spectra; full VNIR-SWIR.

3.1.2.1 Sages

Four sage types were identified in this study, Sagebrush (*Artemisia sp.*), Black Sagebrush (*Artemisia nova*), Big Sagebrush (*Artemisia tridentata*), and Low Sagebrush (*Artemisia arbuscula*). Figure 27 shows the composite spectra of each species and a combined composite of all sage shrub species. The red data points represent the spectral values at the midpoint of the Landsat 5 TM spectral bands.

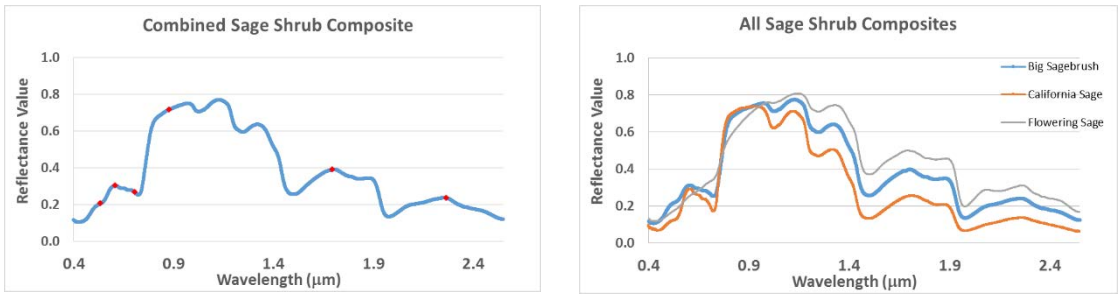

a. Combined full spectrum composite b. Full Spectrum composite of all species

Figure 27. Composite sage shrub spectra; full VNIR-SWIR.

3.1.2.2 Broad Leaf Shrubs

Five broad leaf shrub species were identified in this study, Curlleaf Mountain-Mahogany (*Cercocarpus ledifolius*), Desert peach (*Prunus andersonii*), Greenleaf manzanita (*Arctostaphylos patula*), Borage (*Mertensia oblongifolia*), and California Lilac (*Ceanothus spinosus*). Figure 28 shows the composite spectra of each species and a combined composite of all broad leaf shrub species. The red data points represent the spectral values at the midpoint of the Landsat 5 TM spectral bands.

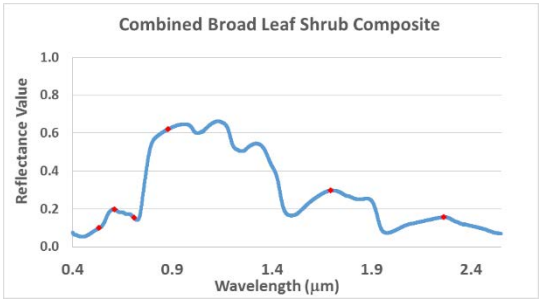

a. Combined full spectrum composite

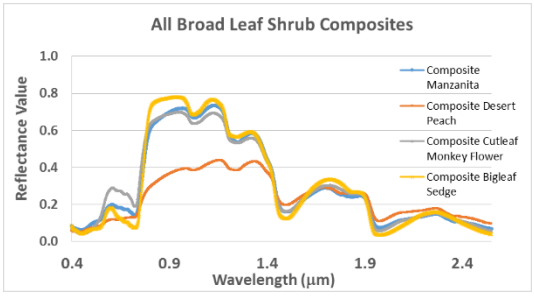

b. Full Spectrum composite of all species

Figure 28. Composite broad leaf shrub spectra; full VNIR-SWIR.

3.1.2.3 Needle Leaf Shrubs

Eight needle leaf shrub species were identified in this study including, Rabbitbrush (*Chrysothamnus (Ericameria)*), Greasewood (*Sarcobatus vermiculatus*), Tumbleweed (*Kali Tragus*), Bitterbrush (*Purshia tridentata*), Green Ephedra (*Ephedra viridis*), Sulphur Flower (*Eriogonum umbellatum*), Buckwheat (*Eriogonum sp.*), and Sedge (*Carex sp.*). Figure 29 shows the composite spectra of each species and a

combined composite of all needle leaf shrub species. The red data points represent the spectral values at the midpoint of the Landsat 5 TM spectral bands.

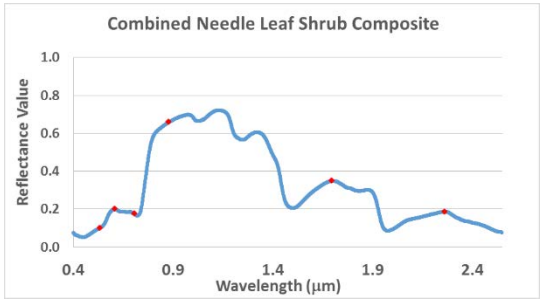

a. Combined full spectrum composite

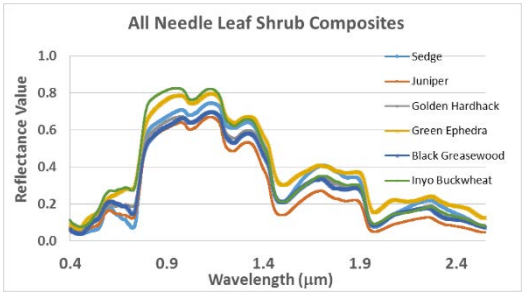

b. Full Spectrum composite of all species

Figure 29. Composite needle leaf shrub spectra; full VNIR-SWIR.

3.2 Litter

A total of fourteen litter samples were collected. Figure 30 shows the composite spectra of all litter samples. The red data points represent the spectral values at the midpoint of the Landsat 5 TM spectral bands.

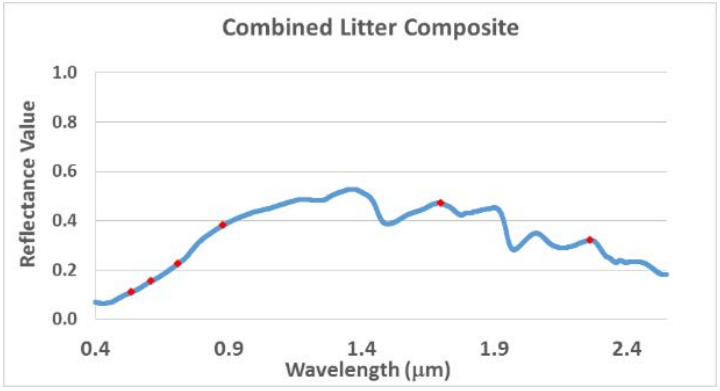

Figure 30. Composite litter spectra; full VNIR-SWIR.

3.3 Barren Surface Cover

Barren surface cover includes seven soil and eight rock samples.

3.3.1 Soil

A total of seven soil samples were collected. Figure 31 shows the composite spectra of all soil samples. The red data points represent the spectral values at the midpoint of the Landsat 5 TM spectral bands.

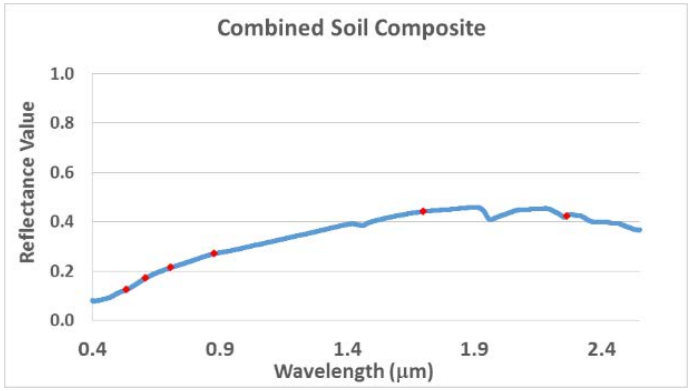

a. Combined full spectrum composite

Figure 31. Composite soil spectra; full VNIR-SWIR.

3.3.2 Rocks

A total of eight rock samples were collected. Figure 32 shows the composite spectra of all rock samples. The red data points represent the spectral values at the midpoint of the Landsat 5 TM spectral bands.

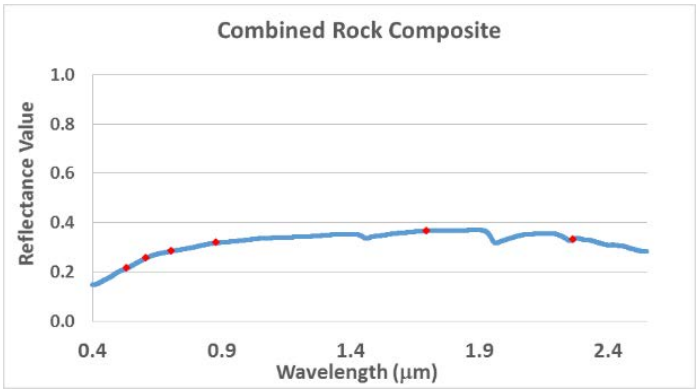

a. Combined full spectrum composite

Figure 32. Composite rock spectra; full VNIR-SWIR.

4.0 Discussion

4.1 Field Collected Endmember spectra

A total of 116 surface cover samples located throughout the study area were collected in situ during July 2014 including three to four samples from each of the 30 sample sites used in this study. The surface cover types are classified as either photosynthetic vegetation (PV), non-photosynthetic vegetation (NPV), or barren surface. There were six broad categories of PV present: broad leaf trees; narrow leaf trees; needle leaf trees; sage bush; broad leaf shrubs; and needle leaf shrubs.

Figure 33 shows examples of the three tree sample types collected and how the samples looked as they were being analyzed in the lab. The three shrub types are shown in Figure 34.

a. Broad leaf (Aspen - *Populus tremuloides*)

Broad leaf sample as analyzed in the lab

b. Narrow leaf (Willow - *Salix sp.*)

Narrow leaf sample as analyzed in the lab

c. Needle leaf (Pine - *Pinus sp.*)

Needle leaf sample as analyzed in the lab

Figure 33. Samples of study area trees; a - *Populus tremuloides*, b - *Salix sp.* and c - *Pinus sp.*

a. Sage (Big sage - *Artemisia tridentata*)

Sage sample as analyzed in the lab

b. Needle leaf shrub (Sedge - *Carex sp.*)

Needle leaf shrub sample as analyzed in the lab

c. Broad leaf shrub (Manzanita - *Arctostaphylos paula*)

Broad leaf shrub sample as analyzed in the lab

Figure 34. Samples of study area shrubs; a - *Artemisia tridentata,* b - *Carex sp.* and c - *Arctostaphylos paula*.

Most of the vegetation spectra have the characteristic vegetation spectral curve shape with subtle differences in amplitude and where specific peak reflectance's are

present which are unique to individual species. One exception was one of the desert peach samples. This is most likely a result of the sampling methodology in which the spectral analyzer fore optics captured more of the stem than the leaf. This resulted in flattened spectra. Another outlier was the Buckwheat sample which produced unique spectra, especially in the visible bands that are distinctly different from all the other shrubs.

5.0 Summary and Conclusions

This paper presents VNIR-SWIR 0.35 μm – 2.5 μm spectra of numerous vegetative, litter and barren surface cover types from the Big Pine Creek watershed. The spectra were analyzed in the lab using an ASD Flexscan Spectroradiometer. Composite spectra for the full VNIR-SWIR for each predominant surface cover type were presented. All of the individual sample spectra are available for download from google drive (Big Pine Creek Surface Cover Spectra.docx).The raw spectral data from each sample are also available for download on google drive (sample site VNIR-SWIR spectra).

The data presented in this paper are intended for public use in the analysis of remote sensed imagery. The spectra can be used to assist analysts in the identification of surface features, especially in remote areas that do not have historical surface cover composition data. Litter and soil samples are provided as these surface cover types will account for a significant percentage of any remote sensed image. Field collected spectra are important elements of successful spectral unmixing studies of remote areas. These studies can take advantage of the more than three decades of continuous Landsat data

covering the globe to identify changes taking place in our environment that pose significant challenges to sustainability.

References

Bowerman, N.D. and Clark, D.H., (2011). Holocene glaciation of the central Sierra Nevada, California. *Quaternary Science Reviews*. 30, pp. 1067-1085.

Elmore, A.J., Mustard, J.F., and Manning, S.J., (2003). Regional patterns of plant community response to changes in water: Owens Valley, California. *Ecological Applications*, 13 (2), pp. 443-460.

Grabherr, G., Gottfried, M., and Pauli, H., (2010). Climate change impacts in Alpine environments. *Geography Compass*, 48, pp. 1133-1153.

Jackson, R.D., Pinter, P.J., Jr., Reginato, R.J., and Idso, S.B., (1986). Detection and evaluation of plant stresses for crop management decisions. *IEEE Transactions on Geoscience and Remote Sensing*, GE-24 (1), pp. 99-106.

Lindner, M., Maroschek, M., Netherer, S., Kremer, A., Barbati, A., Garcia-Gonzalo, J., Seidl, R., Delzon, S., Corona, P., Kolstrom, M., Lexer, M.J., and Marchetti, M., (2010). Climate change impacts, adaptive capacity, and vulnerability of European forest ecosystems. *Forest Ecology and Management*, 259, pp. 698 – 709.

Musick, H.B. and Pelletier, R.E., (1988). Response to soil moisture spectral indexes derived from bidirectional reflectance in thematic mapper wavebands. *Remote Sensing of Environment*, 25, pp. 167-184.

Wessman, C.A., (1992). Imaging spectrometry for remote sensing of ecosystem processes. *Advances in Space Research*, 12 (7), pp. 361-368.

Chapter 6: Ecological response to climate change in the Big Pine Creek watershed from trend analysis of vegetation indices and spectral mixture analysis

Contribution of Authors and Co-Authors

This manuscript was co-authored by Patrick Sawyer and Haroon Stephen. Patrick Sawyer was the first author who conceived and implemented the study design, collected and analyzed the data, and wrote the manuscript. Haroon Stephen was the second author who assisted with the study design and provided feedback on statistical analyses and drafts of the manuscript.

Manuscript Information Page

This manuscript has been officially submitted to a peer-reviewed journal for publication.

This manuscript presents the research performed and findings achieved relating to the determination of climate driven ecological trends. The purpose of this work is the identification of vegetative composition trends as well as the testing and the validation of red-shift theories and vegetation indices and transforms. This work supports objectives one – identification of climate driven ecological changes; objective three - study of red-shift translation in relation to vegetation quantity and composition change; and objective four - measure the performance of vegetative indices and transforms against data from vegetative survey plots.

Abstract

Changing climatic regimes can have significant impacts on vegetative assemblies, especially where species exist near their habitat limits. Understanding how recent changes in environmental parameters, such as temperature and precipitation, have impacted sensitive ecosystems is essential to our ability to adapt to these new regimes and to mitigate their negative consequences. This paper presents a time series study of vegetative composition change in an alpine ecosystem in the Big Pine Creek watershed in California's Eastern Sierra Nevada Mountain's. Thirty sample sites were examined to identify changes in surface cover over the last thirty years. This is accomplished by examining trends in vegetation indices, tasseled cap transformations, and surface composition derived from spectral mixture analysis. These results are used to establish the relationship between trends in spectral reflectance and changes in vegetative composition. Applicability of vegetative indices and tasseled cap transformations in trend analysis is validated against numerous surveyed sample sites. Comparing spectral mixture analysis trends in vegetative cover, trends in vegetation indices and trends in tasseled cap transformations, we found the tasseled cap brightness index showing the highest level of agreement with the red-shift theory (90%) while trends in vegetation cover using spectral mixture analysis showed the lowest agreement with red-shift theory of vegetation cover. The highest levels of agreement between spectral mixture analysis trends and vegetative cover predicted by red-shift theory occur with red-shift upward translation and red-shift downward translation predictions at 75% and 63% agreement

respectively, while agreement levels for the vegetation indices are at their lowest for these two theories. While the vegetative indices and tasseled cap transforms perform remarkably well for simple cases of red-shift stretch and red-shift compression, when analyzing the more complex case of red-shift translation one should consider using spectral mixture analysis to increase the confidence level of the findings.

1.0 Introduction

Alpine ecosystems are crucial laboratories for the study of how changing climatic variables will impact isolated species assemblages. The steep elevation gradients in these regions encompass several ecotones within a small area. The biomes that inhabit these areas are particularly susceptible to changing environmental parameters since many exist at the limits of their ranges (Lindner et al., 2010). Since alpine ecotones represent bioclimatic transitions, species compositional change is high and susceptible to slight alteration in bioclimatic regimes (Grabherr et al., 2010). While many studies have identified biotic response to climate change over large regions, the response at the local and individual ecosystem level are necessary to understand population dynamics that underlie range shifts (Opdam and Wascher, 2004; Gasner et al., 2010).

Existing research has focused on the response of individual species, often overlooking important biotic and abiotic interactions that drive community assembly. All the life forms within a local community interact with each other and their physical world forming a complex intricate fabric that identifies the characteristic traits of that assemblage. The predicted trend in climate induced range shifts is for increased

extinctions at the warm boundaries and species expansions at the cold range limits (Opdam and Wascher, 2004). However, in alpine regions, the loss of space with elevation will lead upslope migrating species into a summit trap which will increase extinction rates (Wilson et al., 2005; Vittoz et al., 2013).

Since the response rate to altered environmental conditions varies among each member of the local assemblage, climate change will drive significant alteration of the interactions between the individual components and the overall functioning of the local community. Since alpine vegetation tends to be long lived, (Grabherr et al., 2010), changes in the timing and availability of resources can have significant negative impacts on individual species survival rates while at the same time providing opportunities for competition to allow replacement species to prosper (Walther, 2010).

The ecological response to elevated temperature and CO_2 levels is complex and will be affected by other factors such as water and other nutrient resource availability. In cold alpine regions where water availability is not limiting, higher temperatures are expected to increase the habitable zones for several species, allowing for upslope migration and increased vegetative cover. Higher temperatures combined with increased atmospheric CO_2 levels will increase photosynthesis resulting in increased biomass; provided other essential resources are not limited (Skre and Naess, 1999). Conversely, where water is limited, higher temperatures will increase plant stress resulting in reduced vegetative cover (Chmura et al., 2011).

Spectral characteristics measured with remote sensing instruments such as the Landsat 5 Thematic Mapper (TM) and Landsat 7 Enhanced Thematic Mapper (ETM^+) enable us to analyze ecological properties of vegetation. Vegetation has characteristic spectral responses such as low red reflectance due to chlorophyll absorption and high near infrared (NIR) reflectance due to the reflectance from the internal structures of the canopy (Wessman, 1992). Soil also demonstrates unique spectral characteristics depending on properties such as its moisture, organic matter content and texture (Jackson et al., 1986). Lower soil moisture content, a possible indicator of water stress in vegetation, would cause higher surface reflectance in the mid-wave infrared (MWIR) region that can be detected using Landsat data (Musick and Pelletier, 1988).

Remote sensing using multispectral imagers such as the Landsat instruments provide a wealth of data that can be used to monitor for changes in the environment. Large scale regional change is clearly evident from the 30 meter resolution imagery these instruments provide. However, at this resolution, important details within each pixel remain hidden. For remote sensing applications, unless the image is over human controlled agricultural plots; most Landsat image pixels will include several components that cannot be discerned from the raw data. For each pixel, the radiance measured by the sensor in each wave band is composed of a mixture of reflectance energies given off by each of the individual components within that pixel.

In order to elicit the sub-pixel information needed to assess vegetative composition change, we need to employ spectral mixture analysis (SMA). The basic

theory of SMA is that in any given pixel, a limited number of dominant components contribute the overwhelming majority of the radiance measured by the sensor. These components are called endmembers (EM). The simplest SMA technique is called Linear Spectral Mixture Analysis (LSMA). For LMSA, the fractional coverage of each EM is proportional to its contribution the overall radiance value of the pixel. This can be expressed mathematically using equation (44),

$$R_i = \sum_{k=1}^{n} f_k R_{ik} + e_i \qquad (44)$$

where R_i is the spectral reflectance for band i of a pixel, f_k is the fraction of endmember k within the pixel, R_{ik} is the known spectral reflectance of endmember $_k$ within that pixel in band i, e_i is the error for band i, and n is the number of endmembers in the pixel (Lu et al., 2004). LMSA can be used to unmix pixel spectra from both multi spectral and hyperspectral data (Tompkins et al, 1997). Two methods for solving for f_k have been used; constrained and unconstrained. In the constrained method, sum of the fractions must equal 1 as shown in equation (45) (Lu et al., 2004).

$$\sum_{k=1}^{n} f_k = 1 \ and \ 0 \leq f_k \leq 1 \qquad (45)$$

In the unconstrained method, f_k is not required to sum to 1 which means the solution will not equal the actual percent cover of each EM (Lu et al., 2004). The error for each band e_i is defined as the root mean square error (*RMSE*) expressed as equation (46),

$$e_i = \sqrt{\frac{\sum_{j=1}^{m}\left(e_{ij}\right)^2}{m}} \qquad (46)$$

where *m* is the spectral band (Myint and Okin, 2010). Models of each pixel are developed by varying the fractions of each EM. The model which produces the lowest *RMSE* is considered the best-fit and those EM fractions are recorded as the solution (Myint and Okin, 2010). The *RMSE* represents the difference between the measured and modelled value. The *RMSE* should be in the range of the noise level of the absolute reflectance. For Landsat TM data, this is 0.56%. The analyst can select an arbitrary threshold for the *RMSE* value for determining when a given pixel has been successfully unmixed; typically 2% (Eibl et al., 1996).

In previous studies, we examined the spectral response at numerous sample sites in the Big Pine Creek watershed to determine how those sites have changed over the last three decades. In our first study we examined the average spectral response across the watershed and found that both the visible and NIR responses were declining (Sawyer and Stephen, 2014). Vegetation indices are useful tools to analyze for the increase or decline in vegetative surface cover. However, these indices are based primarily on the ratio between the red and NIR bands. A decline in the red band surface reflectance from increased visible light absorption combined with an increase in NIR reflectance from higher surface complexity are indicative of increased vegetative surface cover. Likewise, increased surface reflectance in the visible range combined with a decline in the NIR reflectance from less surface complexity is an indicator of a decline in surface vegetative

cover. While the simple ratios are useful in identifying increases or declines in surface characteristics, these indices do not provide clear information on what is taking place when the visible and NIR surface reflectance change in the same direction (translation). In order to determine what is occurring at sites where both the visible and NIR spectral responses are trending in the same direction, we need to decompose the spectral responses of those sites using spectral mixture analysis.

Spectral response over time can demonstrate one of four possible trends; 1) Red-shift stretch in which the red response declines while the NIR increases. This response is consistent with increased vegetative surface cover resulting from higher red absorption from increased chlorophyll content and increased NIR reflectance due to higher reflectance from the internal structures of the increased vegetation cover. 2) Red-shift compression in which the red response increases while the NIR decreases. This response is consistent with decreased vegetative surface cover resulting from lower red absorption from decreased chlorophyll content and decreased NIR reflectance due to lower reflectance from the internal structures of the decreased vegetation cover. 3) Red-shift upward translation in which both the red and NIR response increase. We hypothesize that this complex response is due to both overall declining vegetative cover consistent with lower red absorption along with a change in composition of the vegetative surface cover with the new dominant species showing higher structural complexity that the original species. 4) Red-shift downward translation in which both the red and NIR response decline. We hypothesize that this complex response is due to both overall increasing vegetative cover consistent

with greater red absorption along with a change in composition of the vegetative surface cover with the new dominant species showing lower structural complexity that the original species.

Since the vegetation indices are essentially a measure of the red-shift, trends in vegetation indices are expected to correlate to trends in the spectral response. For the tasselled cap transformations, spectral trends which increase surface brightness are consistent with declining vegetative surface cover as vegetation tends to demonstrate lower reflectance than barren surface. Tasseled cap greenness responds to trends in the visible bands with lower visible reflectance resulting in a higher greenness index. Tasseled cap wetness measures the amount of water absorption in the scene. This correlates to the presence or absence of vegetative cover as vegetation tends to contain more water than barren surface.

In this paper we investigate ecosystem response to climate change by examining trends in vegetation indices and tasseled cap transformations. Trends in vegetative composition are determined by performing a spectral mixture analysis of 30 sample sites. We present this information by first describing the study area and the data used in the analysis, we then discuss the research approach and methods used to collect and process the data, followed by our results and conclusions. We hypothesize that sites where the visible and NIR spectral responses are changing in the same direction will demonstrate compositional changes that account for the spectral response trends. An examination of the accuracy of trend analysis of vegetation indices and tasseled cap transformations is

performed by comparing the trends in these metrics to actual sample site field survey data from fifty long term vegetation monitoring plots located across the western United States.

2.0 Study Area and Data

2.1 Study Area Description

Figure 35 below shows the Big Pine Creek watershed located in California's Eastern Sierra Mountains. Big Pine Creek is a major tributary to the Owens River which is a significant source of fresh water for Los Angeles. The Owens River valley straddles the Great Basin and Mojave deserts with vegetation consisting primarily of pine forests at higher elevations and xeric species at lower elevations (Elmore et al., 2003). Elevation within the watershed increases from East to West with the higher regions dominated by barren rock and woodlands with the lower regions dominated by mixed desert shrubs.

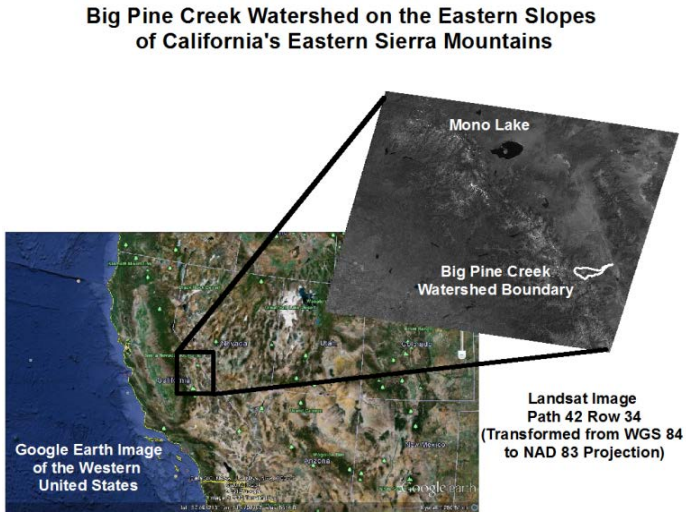

Figure 35. Study area location showing the boundary of the Big Pine Creek watershed.

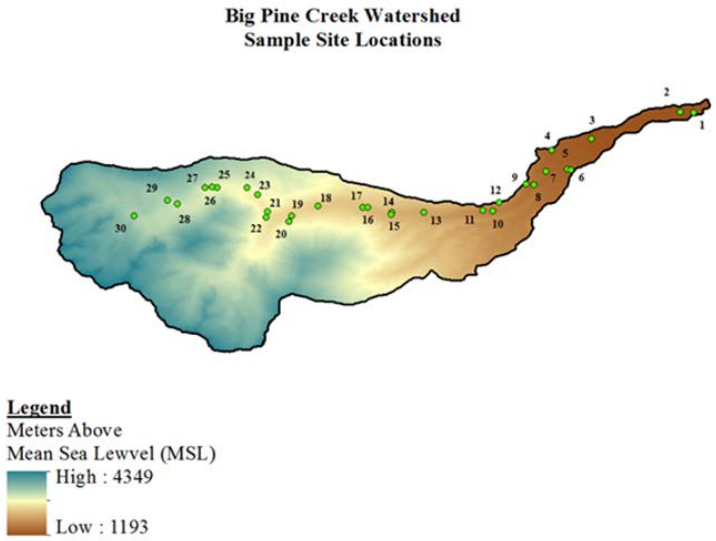

Figure 36. Sample Site Locations.

In previous spectral studies of the Big Pine Creek watershed, we examined 105 sample sites. Three sites for each of the top ten predominant land cover classes present in the watershed and three sites at 100 meter elevation gradients from 1200 meters above sea level to 3600 meters above sea level. At each elevation, a densely vegetated site, a moderately vegetated site and a sparsely vegetated site were selected. While many of the sites demonstrated clear trends in their spectral reflectance consistent with declining or increasing vegetative surface cover, numerous locations exhibited same direction trends in their visible and NIR reflectance bands making interpretation of what is taking place difficult. In this study 30 of those sample sites which were accessible for in situ sampling were chosen for detailed spectral mixture analysis to elicit sub-pixel information which could provide us with evidence of species compositional change not discernable from the

multi-spectral 30 meter resolution Landsat imagery. Sample site locations and elevations for this study are shown in table 16.

Table 16

Sample Site Location

Sample Site ID	Latitude (N)	Longitude (W)	Elevation (M MSL)	Sample Site ID	Latitude (N)	Longitude (W)	Elevation (M MSL)
1	37.1675	-118.2657	1201	16	37.1274	-118.4024	2198
2	37.1676	-118.2714	1201	17	37.1275	-118.4044	2208
3	37.1567	-118.3070	1294	18	37.1279	-118.4231	2296
4	37.1516	-118.3251	1397	19	37.1240	-118.4340	2389
5	37.1435	-118.3187	1402	20	37.1221	-118.4421	2408
6	37.1433	-118.3172	1403	21	37.1256	-118.4442	2495
7	37.1426	-118.3274	1460	22	37.1232	-118.4449	2502
8	37.1370	-118.3326	1509	23	37.1328	-118.4485	2603
9	37.1372	-118.3359	1598	24	37.1358	-118.4529	2702
10	37.1258	-118.3499	1707	25	37.1358	-118.4653	2799
11	37.1264	-118.3541	1798	26	37.1359	-118.4675	2836
12	37.1294	-118.3471	1805	27	37.1357	-118.4703	2899
13	37.1252	-118.3788	2009	28	37.1290	-118.4820	3005
14	37.1253	-118.3922	2100	29	37.1305	-118.4863	3099
15	37.1246	-118.3923	2105	30	37.1238	-118.5002	3198

2.2 Data

The data in this study includes Landsat surface reflectance data obtained from the USGS Earth Explorer web site, field collected spectra from 116 surface cover samples collected in situ throughout the study area during July 2014, field transect data from 50 permanent vegetation plots across the western United States, and modelled endmember spectra and abundance values derived from the Landsat data using the ENVI 5.1 software package. Each data is further described below.

2.2.1 Surface Reflectance Data

The Landsat imagery used in this analysis was acquired for 30 dates in the month of July from 1984 through 2013. Most of the imagery used in this analysis is from Path 42, Row 34 with four of the images from Path 41, Row 34. Both image ID ground swaths cover the entire study area. Data for this study include imagery from both the Landsat 5 TM and Landsat 7 ETM^+ sensors. The imagery acquisition date and time for the data used in this analysis are listed in table 17 below. The surface reflectance data product for each of these imagers was obtained from the EarthExplorer web site operated by the United States Geological Survey (http://earthexplorer.usgs.gov/). The data files are located in the Landsat Climate Data Record folder with the titles "Landsat Surface Reflectance - L4-5 TM and L7 ETM^+".

Table 17

Summary of Landsat imagery used in this analysis

Image Date	Time	Scene ID	Image Date	Time	Scene ID
7/13/2013	10:28	42/34	7/30/1998	10:12	42/34
7/28/2012	10:28	42/34	7/27/1997	10:04	42/34
7/18/2011	10:22	42/34	7/24/1996	9:48	42/34
7/31/2010	10:24	42/34	7/31/1995	9:31	41/34
7/5/2009	10:16	41/34	7/3/1994	9:52	42/34
7/25/2008	10:20	42/34	7/16/1993	9:56	42/34
7/7/2007	10:27	42/34	7/29/1992	9:56	42/34
7/13/2006	10:20	41/34	7/27/1991	9:57	42/34
7/26/2005	10:15	41/34	7/8/1990	9:53	42/34
7/30/2004	10:16	42/34	7/5/1989	9:34	42/34
7/12/2003	10:10	42/34	7/2/1988	10:04	42/34
7/25/2002	10:09	42/34	7/25/1987	9:52	41/34
7/22/2001	10:14	42/34	7/29/1986	9:55	42/34
7/19/2000	10:10	42/34	7/3/1985	9:57	41/34
7/17/1999	10:11	42/34	7/7/1984	10:02	42/34

2.2.2 Field Spectra Data

The Big Pine Creek watershed consists of mostly undeveloped rugged terrain within the Inyo National Forest. Due to the remoteness and steep gradients, performing the spectral measurements in the field was not practical. Therefore, the vegetative and other surface constituent samples were collected and placed in sealed plastic bags and placed on ice for shipment to the lab. Samples were selected by choosing the top two or three vegetative surface cover types at each site along with a litter or soil sample when practical.

2.2.3 Field Transect Survey Data

Validation of the performance of vegetation indices and tasseled cap transformations is accomplished by performing trend analysis of the Landsat imagery over sites of measured vegetation surface cover and composition. Fifty sites including thirteen from California's Owens Valley, five from the Desert Laboratory in Tucson Arizona, one from the Nevada Test Site, and thirty-one from Mt Saint Helens in Washington were used for this analysis.

3.0 Research Approach and Methods

3.1 Research Approach

This study examines how the surface cover in the watershed has varied over the last 30 years at 30 sample sites across the Big Pine Creek watershed. This is accomplished by performing a spectral mixture analysis of each of the sample sites for each year in the study, then performing a time series trend analysis of the endmembers

identified. Trends in surface composition and surface cover are compared against trends in vegetation indices and tasseled cap transformations. A validation study comparing the accuracy of vegetation indices and tasseled cap transformations is performed by comparing trends in those metrics against actual long-term surveyed vegetation plots.

3.2 Research Methods

The research methodology consists of surface reflectance data collection; endmember determination; data processing; and statistical analysis. Each step is described below.

3.2.1 Data Collection.

In order to perform a temporal study comparing the physiological changes over time at each of the sample sites, surface reflectance values for each year of the study period were obtained from the USGS Climate Data Record (CDR) archive. A total of 116 endmember samples were collected in the field. These samples fell into nine broad categories including six types of photosynthetic vegetation, non-photosynthetic vegetation such as litter, and two barren surface cover types, soil and rock. The samples were measured with an Analytical Spectral Devices, Inc. (ASD) 0.35 to 2.5 μm Flexscan spectroradiometer. The 1 nm bandwidth spectra generated by the ASD instrument was rescaled to match the Landsat spectral bands using the spectral resampling application in the ENVI 5.1 software.

3.2.2 Surface Reflectance Data.

USGS surface reflectance data is generated from a software package known as the Landsat Ecosystem Disturbance Adaptive Processing System (LEDAPS). The surface reflectance data is computed by applying an atmospheric correction to the raw Landsat imagery (Schmidt et al., 2013). This atmospheric correction uses the Second Simulation of a Satellite Signal in the Solar Spectrum (6S) radiative transfer model to account for various atmospheric column constituents including water vapor, ozone, and aerosol optical thickness (Masek et al., 2006). The USGS CDR data set provides us with observed surface reflectance values for each of the six reflectance bands for all sample sites in each year of the study.

3.2.3 Spectral Endmember Determination.

Spectral mixture analysis for this study was performed using the spectral hourglass wizard toolkit in the ENVI 5.1 software application. The ENVI Spectral Hourglass Wizard generated a set of endmember spectra for each sample site. In order to determine what each of the endmember spectra represented, the spectra was compared to the spectra derived from samples collected in the field. The abundance of each of the ENVI generated spectral endmembers was determined for each date in the study period and a trend analysis was performed to determine how the fractional coverage of each of the endmembers has changed over the last 30 years.

3.2.4 Statistical Trend Analysis.

The non-parametric Mann-Kendall (MK) trend test is used to establish the presence of trends in the spectral responses, vegetation indices, tasseled cap

transformations and spectral endmembers over the last 30 years. This analysis essentially determines if a set of values (*y*) are increasing or decreasing over time. Mann-Kendall analysis looks at the sums of the signs of the differences between successive data points and calculates a score or "S" statistic with the following properties: for $S < 0$ (values are decreasing over time); for $S > 0$ (values are increasing over time). The magnitude of the S-statistic is a measure of the strength of the trend. These calculations are carried out in Excel using the XLSTAT add-in statistical application. This program generates the S statistic as well as the probability (*p*) value which is used to quantify the statistical significance of the trend.

4.0 Results and Discussion

4.1 Field Collected Endmember spectra

A total of 116 surface cover samples located throughout the study area were collected in situ in July 2014 including three to four samples from each of the 30 sample sites used in this study. The surface cover types are classified as either photosynthetic vegetation (PV), non-photosynthetic vegetation (NPV), or barren surface. There were six broad classes of PV present: broad leaf trees including aspen, birch, and cottonwood; narrow leaf trees including willow and coffeeberry; needle leaf trees including pine; sage bush; needle leaf shrubs including rabbitbrush, bitterbrush and sedges; and leafy shrubs including manzanita, curlleaf mountain-mahogany, and desert peach.

a. Broad Leaf (Aspen - *Populus tremuloides*)

Broad Leaf Sample as analyzed in the lab

b. Narrow Leaf (Willow - *Salix sp.*)

Narrow Leaf Sample as analyzed in the lab

c. Needle Leaf (Pine - *Pinus sp.*)

Needle Leaf Sample as analyzed in the lab

Figure 37. Samples of study area trees. a - *Populus tremuloides*, b - *Salix sp.* and c - *Pinus sp*.

a. Sage (Big sage - *Artemisia tridentata*)

Sage Sample as analyzed in the lab

b. Needle Leaf Shrub (Sedge - *Carex sp.*)

Needle Leaf Shrub Sample as analyzed in the lab

c. Broad Leaf Shrub (Manzanita - *Arctostaphylos paula*)

Broad Leaf Shrub Sample as analyzed in the lab

Figure 38. Samples of study area shrubbery. a - *Artemisia tridentata*, b - *Carex sp.* and c - *Arctostaphylos paula*.

The NPV was composed of litter and dead vegetation. Barren surface included various soil and rock types. All of the field collected samples were categorized into those nine surface types and composite spectra of each surface cover was created. Figure 39 shows the composite field collected spectra of all the PV types collected in the field. Figure 40 shows the composite field collected spectra of non-photosynthetic vegetation (litter) along with composite soil and rock spectra.

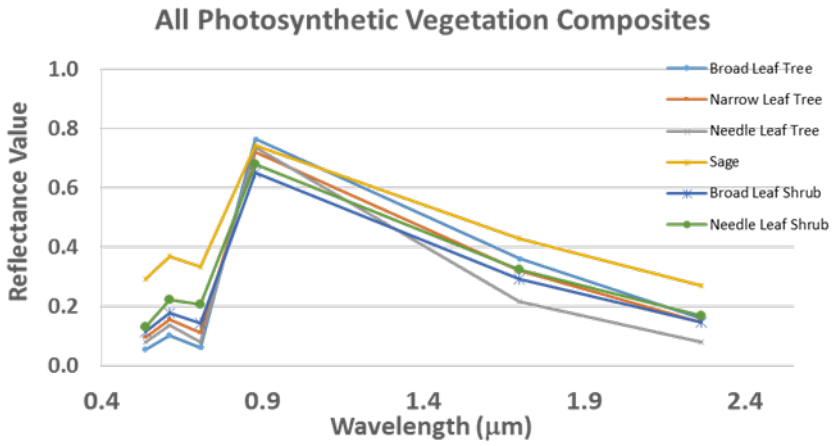

Figure 39. Composite field collected reflectance spectra for photosynthetic vegetation types present in the study area.

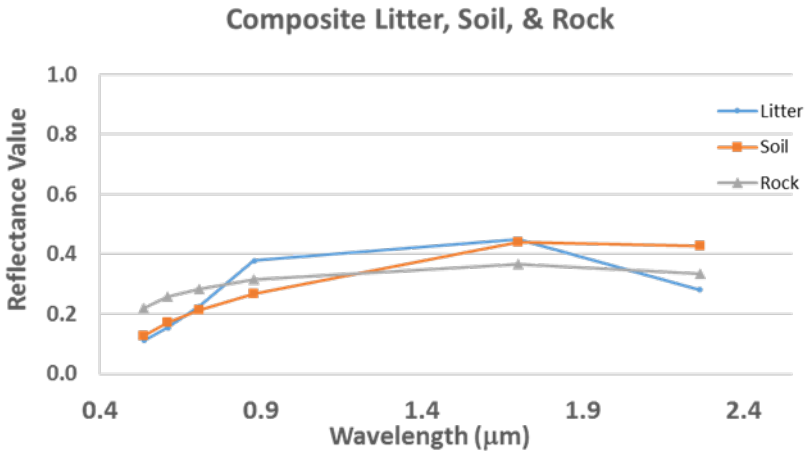

Figure 40. Composite field collected reflectance spectra for non-photosynthetic vegetation, soil, and rock types present in the study area.

For each sample site, the endmember spectra extracted from the ENVI software application were compared against the field collected endmember spectral library to determine their classification. The abundance values for each endmember type, (PV, NPV, and Soil/Rock), were compiled for each sample site for each year and a trend analysis was performed to determine how the surface cover has changed over the last 30 years.

Figures 41 and 42 provide an example of this procedure. In Figure 41, sample site #1 ENVI extracted spectral endmembers for photosynthetic vegetation from the Landsat 5 TM imagery for the year 2000 are compared against the spectra produced from vegetation samples collected at that site. At this particular location, vegetation is primarily Greasewood (*Sarcobatus vermiculatus*) and Rabbitbrush (*Chrysothamnus* (*Ericameria*)). Although the raw reflectance values are significantly different, the shapes of the spectra allow us to clearly identify that the ENVI extracted spectra nD Class #3

matches the field collected spectra for Rabbitbrush while the nD Class #4 matches the field collected spectra for Greasewood.

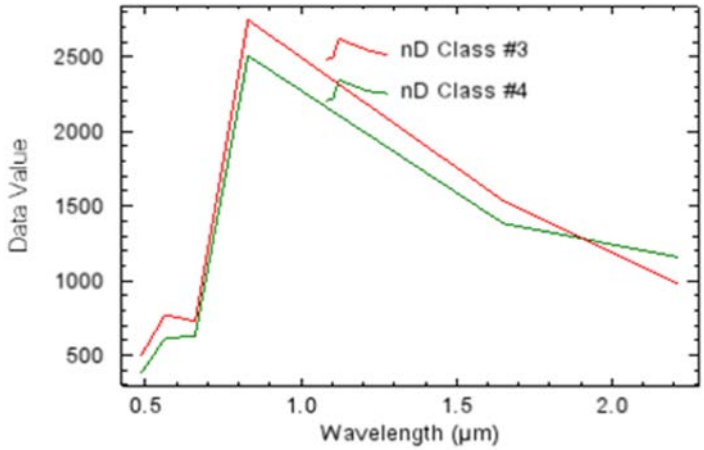

a. ENVI Extracted Spectra for Sample Site #1 PV

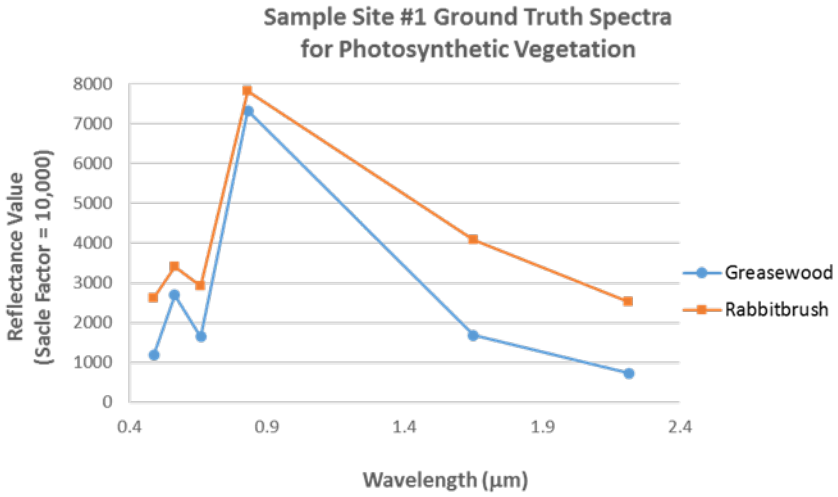

b. Field Collected Spectra for Sample Site #1 PV

Figure 41. Comparison of ENVI extracted spectra for sample site #1 with field collected spectra of the vegetation collected at that site.

In Figure 42, sample site #23 ENVI extracted spectral endmembers for non-photosynthetic vegetation (litter) and soil from the Landsat 5 TM imagery for the year 1994 are compared against composite litter and soil field collected samples. As with the vegetation spectra, the soil and litter spectra differs in their data values, but their distinctive shapes are clearly distinguishable.

In general, the ENVI extracted spectra data values were much lower than those produced by the ASD instrument. The spectra measured in the laboratory are contact samples, meaning there is no atmospheric column between the sample and the detector. This contrasts with the full atmospheric column between the study site and the Landsat sensor orbiting 700 km above the earth.

In addition to the spectra, the ENVI software generated abundance images of each modeled endmember in every pixel. The constrained option was selected so that the abundance values reflected fractional coverage of each endmember within each pixel. The software also produced an *RMS* image indicating the root mean square error associated with the derived endmembers for each individual pixel. Average error values for all 30 years of the study are shown in table 20 for each site.

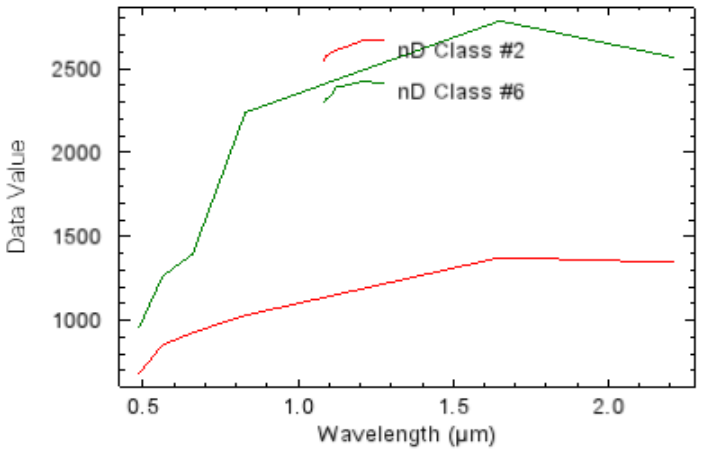

a. ENVI extracted Spectra for Sample Site #23 Soil and Litter

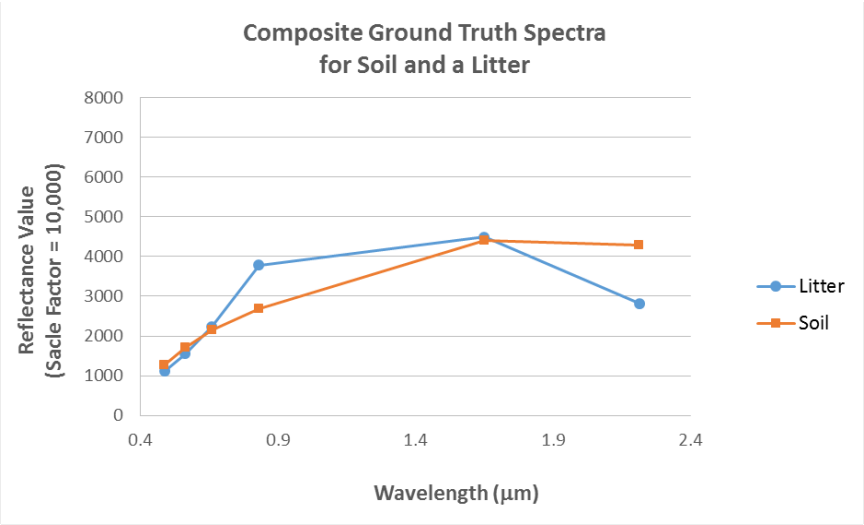

b. Field Collected Spectra for Composite Field Collected Soil and Litter

c.

Figure 42. Comparison of ENVI extracted spectra for sample site #23 with field collected composite spectra of the soil and litter samples collected throughout the watershed.

Table 18 shows the trends in surface cover for the thirty sites in this study. In most instances we see trends in the PV and NPV going in opposite directions. For example, twelve of the sites show declines in PV along with increases in NPV while at eight sites, the PV is increasing while the NPV is in decline. Of the remaining ten sites, five show increases in both PV and NPV while five site show both the PV and NPV are in decline. Ten of the sites demonstrate spectral trends with increasing NIR and declining red values (Red-Shift Stretch), four sites demonstrate spectral trends with decreasing NIR and increasing red values (Red-Shift Compression), eight sites demonstrate spectral trends with increasing NIR and increasing red values (Red-Shift Upward Translation), and eight sites demonstrate spectral trends with decreasing NIR and decreasing red values (Red-Shift Downward Translation).

At sites where the PV and NPV are moving in the same direction, we see barren surface going in the opposite direction as one would expect. Where the PV and NPV are receding, we see increased barren surface contribution to the observed surface reflectance signal. Likewise where PV and NPV are increasing, the barren surface contribution is in decline.

Table 18

Trends in surface cover and reflectance at 30 Big Pine Creek sample sites

Sample Site	Trends in Surface cover for each sample site (S Values)			Trends in CDR Surface Reflectance Data for Landsat Bands (S Values)					
	PV	NPV	Barren	Band 1	Band 2	Band 3	Band 4	Band 5	Band 7
1	33	10	-20	-78	-59	-87	-257	-155	-111
2	-30	95	-83	0	-52	-65	-97	-23	21
3	-26	22	23	-7	5	30	14	110	77
4	-68	81	49	33	16	25	-123	75	89
5	5	-42	7	-121	-160	-158	-124	-52	-55
6	62	-10	-50	-21	46	69	91	118	-35
7	-28	-112	67	-55	-43	7	28	35	-36
8	6	5	-22	-194	-139	-173	127	-53	-119
9	85	-75	-9	-44	-40	-32	-15	103	-46
10	-26	-51	98	-165	-134	-189	197	53	-5
11	-39	82	-70	-35	6	20	5	63	-60
12	-15	54	-5	23	26	48	55	76	77
13	-56	70	-29	-204	-203	-229	78	-62	-155
14	45	-50	25	-67	-65	-44	35	-13	-5
15	-52	4	17	143	164	170	201	153	127
16	23	6	-10	-123	-156	-169	-184	-139	-149
17	-72	83	-9	-137	-133	-156	35	-108	-137
18	12	-16	0	-169	-138	-162	25	37	-53
19	-47	64	-20	66	66	102	-28	78	69
20	62	-66	27	-132	-91	-112	53	-35	-127
21	-3	-14	57	-186	-158	-232	21	-140	-196
22	-25	-54	18	-150	-163	-147	-96	-158	-141
23	148	-14	-59	19	146	75	48	188	157
24	-105	52	16	56	91	51	72	147	147
25	-45	50	25	-67	-109	-119	135	-10	-77
26	13	41	-54	34	57	65	-7	105	79
27	-17	1	-2	-123	-113	-112	-121	-125	-190
28	-4	-19	86	-97	-98	-153	35	-192	-182
29	83	1	-41	-61	-47	-25	-32	35	-22
30	36	-78	61	-24	22	19	-46	-97	-79

Table 19

Trends in surface cover with vegetation indices at 30 Big Pine Creek sample sites

Sample Site	Trends in Surface cover for each sample site (S Values)			Trends in Vegetation Indices and Tasseled Cap Transformations (S Values)					
	PV	NPV	Barren	*NDVI*	*SAVI*	$MSAVI_2$	TC_B	TC_G	TC_W
1	33	10	-20	-139	-181	-191	-159	-149	117
2	-30	95	-83	-15	-39	-41	-99	-35	-19
3	-26	22	23	21	17	11	69	-11	-97
4	-68	81	49	-71	-107	-119	21	-133	-103
5	5	-42	7	39	-23	-39	-143	-53	-35
6	62	-10	-50	9	25	29	83	51	19
7	-28	-112	67	23	23	25	17	49	5
8	6	5	-22	235	223	217	-63	191	65
9	85	-75	-9	7	5	7	-12	18	-42
10	-26	-51	98	287	333	333	-27	307	-43
11	-39	82	-70	-3	9	9	-7	33	11
12	-15	54	-5	-25	-7	5	53	-13	-89
13	-56	70	-29	329	337	339	-151	341	13
14	45	-50	25	61	45	37	7	41	9
15	-52	4	17	-25	45	51	183	45	-101
16	23	6	-10	-21	-67	-85	-211	-63	117
17	-72	83	-9	189	165	157	-116	160	108
18	12	-16	0	199	165	167	-73	161	-43
19	-47	64	-20	-115	-97	-97	67	-83	-65
20	62	-66	27	201	195	179	-33	215	85
21	-3	-14	57	237	129	129	-135	129	83
22	-25	-54	18	59	17	7	-207	21	125
23	148	-14	-59	-37	-13	-9	143	-15	-187
24	-105	52	16	-9	5	13	89	-13	-169
25	-45	50	25	163	131	131	-13	127	41
26	13	41	-54	-85	-99	-93	57	-95	-99
27	-17	1	-2	15	7	9	-145	73	155
28	-4	-19	86	149	99	97	-93	83	195
29	83	1	-41	9	-39	-37	-45	-21	-21
30	36	-78	61	-35	-55	-51	-47	-47	95

The real advantage that spectral mixture analysis has over simple spectral reflectance derived vegetation indices is the ability to discern changes in the endmembers within an individual pixel. This information is essential in determining how climate change is impacting local species assemblages. Table 20 shows the average fractional

surface cover of each of the PV types at each site for the 30 years of the study period as derived from the spectral mixture analysis of the Landsat imagery. This table shows that our study site vegetation consists primarily of shrubs with some deciduous and conifer trees. Most of the trees are located within a hundred meters of the Big Pine Creek while the shrubs are ubiquitous throughout the study area.

Table 20

Average sample site vegetative surface cover for the 30 year study period

Sample Site	Fractional Surface Cover (%)						Average *RMSE* (%)
	Trees			Sage Bush	Shrubs		
	Broad	Narrow	Needle		Needle	Broad Leaf	
1					31		0.82
2					28		0.64
3	6						1.01
4					44		0.03
5	14	23	10		14		0.52
6				9	13		0.22
7				6		5	0.47
8		33	32		2		0.02
9				7	10		0.31
10	21	30	4				0.03
11				2	10		0.76
12					4		0.66
13	19	25	3		17		0.03
14	33		28		6		0.02
15				8	24		0.54
16				6	29	12	0.52
17	38		27		11		0.02
18	30		9		23		0.05
19	20			1	26		0.03
20			19		40	15	0.02
21	30		45				0.03
22				5	24	9	0.76
23				21	40	13	0.80
24				6	38	22	0.35
25	39		29		12		0.03
26	7	7			42		0.03
27				8	9	12	1.14
28	23	3	44		16		0.02
29		35	21		21		0.27
30		11	9		23	32	0.02

Tree species identified in the study area include leaf species such as Willow, Coffeeberry, and Cottonwood, Birch, Maple and aspen, along with conifers including Yellow Pine, White Pine and California Lodgepole Pine. Three sages were identified; Big sagebrush, Black sagebrush and Low sagebrush. Numerous shrub species were identified. The shrubs were classified as needle leaf type for those with thin leaves and as broad leaf type for those with round leave. Needle leaf shrub species include Rabbitbrush, Bitterbrush, Green Ephedra, Greasewood, Tumbleweed, Sulphur flower, and Buckwheat. Leaf type shrubs are primarily Manzanita, Curlleaf Mountain-Mahogany, California Lilac, Borage and Desert Peach. Sedges were also present and classified as needle leaf for this study.

Table 21 shows how the individual endmembers have trended at each of the sample sites where the spectral analysis is consistent with compositional change. Table 22 provides a description of what the trend values are showing. In this summary, trends are defined as significant if their $|S|$ value exceeds 100, large for $50 < |S| < 100$, moderate for $20 < |S| < 50$, small for $5 < |S| < 20$, and slight for $|S| < 5$.

Table 21

Trends in vegetative composition for the 30 year study period

Sample Site	Photosynthetic Vegetation (PV) 30 Year Trends in Surface Composition					
	Trees			Sage Bush	Shrubs	
	Broad Leaf	Narrow Leaf	Needle Leaf		Needle Leaf	Broad Leaf
1					58	
2					-30	
3	-26					
4					-68	
5	3	15	-14		-12	
6				37	-19	
7				-4		-6
8		6	1			
9				23	17	
10	-112	-11	134			
11				-2	-36	
12					-15	
13	-60	98	-34		-58	
14	50		-42		29	
15				-7	-56	
16				-4	27	40
17	-95		78		-30	
18	43		13		-72	
19	96			-1	-99	
20			78		61	-140
21	-35		34			
22				-8	-7	6
23				70	14	-6
24				-20	-43	-64
25	9		10		-100	
26	-96	-21			57	
27				21	-17	-81
28	-34	1	50		-66	
29		4	70		-8	
30		-12	-53		75	8

Table 22

Endmember trend description for photosynthetic vegetation

Sample Site	Trends in Photosynthetic Vegetation (PV)
1	Large increase in greasewood; small decrease in Rabbitbrush
2	Moderate decline in Shrub
3	Moderate decline in Cottonwood
4	Large declines in Rabbitbrush
5	Small increase in Willow; small decline in Pine
6	Moderate increase in Sage; small decline in shrubs
7	Significant declines in Sage; large decline in Desert Peach
8	Small increase in Yellow Pine and Willow
9	Moderate increase in Sage; small increase in Shrubs
10	Significant increase in Pine; significant declines in Cottonwood
11	Moderate decline in shrub
12	Small decline in Shrub
13	Large increase in Willow; small declines in NL Shrubs, Pine and Cottonwood
14	Large increase in broad leaf (Birch/Cottonwood); moderate increase in shrubs
15	Large decrease in Shrub; small decline in Sage
16	Moderate increase in Bitterbrush and California Lilac; small decline in Sage
17	Large decline in Broadleaf (Birch/Cottonwood); large increase in Pine; small decline in Shrub
18	Increases in Cottonwood and Pine; decline in Bitterbrush
19	Large increases in Maple; large decline in Shrubs
20	Large increase in Pine and needle leaf shrub; significant decline in Mahogany
21	Moderate declines in Aspen/Birch; moderate increase in Pine
22	Small decline in Sage and Bitterbrush; small increase in broad leaf shrub
23	Large increase in Sage; small increase in shrub
24	Large decline in leaf shrub; moderate declines in Sage and Bitterbrush
25	Large decline in shrub; small increase in Pine, Broad Leaf
26	Large decline in Aspen; small decline in Coffeeberry; large increase in Rabbitbrush
27	Moderate increase in Sage; large decline in Mahogany
28	Moderate decline in Aspen; large increase in Pine; small decline in shrub
29	Significant increase in Lodgepole Pine; small increase in Willow
30	Large decline in Pine; small decline in Willow; large increase in needle leaf shrub

The results of our spectral mixture analysis show vegetative compositional changes at each of the thirty sites examined, with three of those sites consistent with large

compositional changes. Looking at the combined PV trends, for the two sites with statistically significant trends, 23 (S = 148) and 24 (S = -105), the results are not always consistent with the vegetative indices and Tasseled Cap transformations. At site 23, the spectral mixture analysis indicates vegetation is increasing while all three vegetative indices are declining. Likewise, the TC_B, TC_G, and TC_W scores all suggest declines in vegetative surface cover. At site 14, the spectral mixture analysis indicates declining vegetative surface cover which is in agreement with two of the vegetative indices (*SAVI* and $MSAVI_2$) and the tasseled cap transformations. However, the *NDVI* trend at this site is consistent with a small increase in vegetative surface cover. These results demonstrate the difficulty with assessing vegetative compositional change using only vegetative indices and Tasseled Cap transformations.

Table 23 summarizes the results of this analysis showing the percentage of times each indices matched the predicted red-shift theory. For example, the red-shift stretch theory of increasing vegetation was only matched at four out of ten sites using SMA, while *NDVI*, *SAVI*, $MSAVI_2$, and TC_G matched the prediction of increasing vegetation at all ten sites.

The overall results indicate tasseled cap brightness had the highest level of agreement (90%) with the red-shift prediction of vegetative change. Spectral mixture analysis generated the least overall agreement at 57%. However, it is interesting to note that SMA showed higher levels of agreement with theory in the complex cases of red-shift translation while most of the vegetative indices and tasseled cap transformation

witnessed declines in their levels of agreement. In particular, when there is a downward translation in the red-shift, the two modified vegetation indices (*SAVI* and $MSAVI_2$) performed poorly compared to theory.

Table 23

Correlation of indices to spectral response theory

Theory	SMA	*NDVI*	*SAVI*	$MSAVI_2$	TC_B	TC_G	TC_W
ALL – 30 Sites	57	80	63	60	90	70	67
Red-Shift Stretch – 10 Sites (Increasing Vegetation)	40	100	100	100	90	100	80
Red-Shift Compression – 4 Sites (Decreasing Vegetation)	50	100	100	100	75	100	75
Red-Shift Upward Translation – 8 Sites (Decreasing Vegetation w/comp change)	75	63	25	13	88	50	63
Red-Shift Downward Translation – 8 Sites (Increasing Vegetation w/comp change)	63	63	38	38	100	38	50

Percentage of times the index match the actual field data

4.2 Validation of Vegetation Indices in Trend Studies

Vegetation indices have long been used to establish the presence of vegetative surface cover and to track how vegetative surface cover changes over time. In order to determine the accuracy of vegetation indices and tasseled cap transformations in ecological trend studies, we compare how those indices and transforms compare with actual field plot data. We consider both ratio indices which analyze the large difference in the red and NIR bands characteristic of vegetation and weighted ratios which focus on physical parameters such as surface brightness, greenness and wetness.

In this analysis we look at the following indices:

Normalized Difference Vegetation Index (*NDVI*), defined as

$$NDVI = \frac{\rho_{NIR} - \rho_{RED}}{\rho_{NIR} + \rho_{RED}}, \quad (47)$$

Rouse at al., 1974), where ρ_{NIR} is the reflectance in band 4 and ρ_{RED} is the reflectance in band 3; Soil Adjusted Vegetation Index (*SAVI*), defined as

$$SAVI = (1 + L)\frac{\rho_{NIR} - \rho_{RED}}{\rho_{NIR} + \rho_{RED} + L}, \quad (48)$$

where *L* is a soil correction factor set at 0.5 (Huete, 1988); Modified Soil Adjusted Vegetation Index ($MSAVI_2$), defined as

$$MSAVI_2 = \frac{2\rho_{NIR} + 1 - \sqrt{(2\rho_{NIR} + 1)^2 - 8(\rho_{NIR} - \rho_{RED})}}{2}, \quad (49)$$

(Qi et al., 1994); and Tasseled Cap transformations for Brightness (TC_B), Greenness (TC_G), and Wetness (TC_W) which are defined as

$$TC_B = 0.2043\rho_1 + 0.4185\rho_2 + 0.5524\rho_3 + 0.5741\rho_4 + 0.3124\rho_5 + 0.2303\rho_7, \quad (50)$$

$$TC_G = -0.1603\rho_1 - 0.2819\rho_2 - 0.4934\rho_3 + 0.7940\rho_4 - 0.0002\rho_5 - 0.1446\rho_7, \quad (51)$$

$$TC_W = 0.0315\rho_1 + 0.2021\rho_2 + 0.3102\rho_3 + 0.1594\rho_4 - 0.6806\rho_5 - 0.6109\rho_7, \quad (52)$$

where $\rho_{1...7}$ is the reflectance in band 1 through band 7 respectively (Crist, 1985).

Actual field plot data was collected from 50 long term study plots throughout the Western United States including 13 plots in California's Owens Valley, (near the Big Pine Creek study area), 1 plot at the Nevada National Security Site in Nevada, 5 plots at the Desert Lab in Tucson, Arizona and 31 sites located on Mt Saint Helens in Washington. The time span of the permanent monitoring plots ranged from 12 to 28

years. At each plot, total vegetative cover and composition data were obtained. Landsat 5 TM CDR surface reflectance for every year covering the time span of the plot data.

A listing of each of the 50 plots, the change in percent vegetation cover and the spectral response and vegetative indices trends over those time periods is available at https://drive.google.com/open?id=0B-keMMag-oQ7UlBfb0NwUVB3alE&authuser=0. Descriptions of how each plot changed over the time period of the study and how well the vegetation indices and tasselled cap transformations correlate to the actual field data is available at https://drive.google.com/open?id=0B-keMMag-oQ7WEpqWm85RkZtTjg&authuser=0.

Table 24 shows the level of agreement between the vegetative indices and tasselled cap transformations with the red-shift theory prediction for vegetation. For example, for the twenty five sites demonstrating red-shift stretch, trends in *NDVI* were positive in all twenty five cases (100% agreement with theory). For those same sites, tasselled cap wetness trends were consistent with increased vegetative cover at only eight of the sites (32% agreement with theory). Overall, the vegetation indices and the tasselled cap brightness and greenness show close correlation with the predicted vegetation trends based solely on the trends in spectral response for those sites. Trends in the tasselled cap wetness index ran counter to the predicted response more than half the time.

Table 24

Correlation of indices to spectral response theory

Theory	*NDVI*	*SAVI*	*$MSAVI_2$*	*TC_B*	*TC_G*	*TC_W*
ALL – 50 Sites	84	84	80	80	84	44
Red-Shift Stretch – 25 Sites (Increasing Vegetation)	100	100	96	64	100	32
Red-Shift Compression – 3 Sites (Decreasing Vegetation)	67	100	67	67	100	100
Red-Shift Upward Translation – 7 Sites (Decreasing Vegetation w/comp change)	29	14	14	100	14	100
Red-Shift Downward Translation – 15 Sites (Increasing Vegetation w/comp change)	87	87	87	100	87	27

Percentage of times the index match the red-shift theory of vegetation trend

Table 25 shows the level of agreement between each red-shift theory and actual field data. Of the 50 plots studied, 25 demonstrated negative red trends with increasing NIR trends (Red-Shift stretch) consistent with increased vegetative surface cover. Actual transect data showed vegetative ground cover increasing in 24 of those 25 plots demonstrating Red-Shift Stretch (96% agreement with theory). Three of the plots demonstrated positive trends in the red response with declining NIR trends (Red-Shift compression) consistent with decreased vegetative surface cover. Two of the three plots did in fact show declines in surface cover (67% agreement with theory). Seven of the plots demonstrated increasing red trends with increasing NIR trends (Red-Shift upward translation). Four of these sites (57% agreement with theory) witnessed decreased vegetative surface cover while three demonstrated increases in surface cover. Fifteen plots demonstrated decreasing red trends with decreasing NIR trends (Red-Shift downward translation). Of these sites, 14 witnessed increased vegetative surface cover

(93% agreement with theory) while 1 site experienced a decline in vegetative surface cover.

Table 25

Accuracy of red-shift theory vs field data

Spectral Response Trends	Accuracy of Red-Shift Theory
All Data – 50 Sites	88
Red-Shift Stretch – 25 Sites (Increasing Vegetation)	96
Red-Shift Compression – 3 Sites (Decreasing Vegetation)	67
Red-Shift Upward Translation – 7 Sites (Decreasing Vegetation w/comp change)	57
Red-Shift Downward Translation – 15 Sites (Increasing Vegetation w/comp change)	93

Percentage of times the index match the actual field data

Table 26 details the performance of each of the vegetative indices and tasselled cap transformations versus the actual field data. Overall, the vegetative indices performed better than the tasseled cap transformation, with the $MSAVI_2$ index recording the highest level of agreement (90%) with the actual measurements of vegetative surface cover. The tasseled cap wetness index demonstrated the least correlation (36%) with field data. This finding suggests caution in using tasselled cap wetness as a measure of vegetative surface cover change, especially in regions where vegetative cover is increasing.

Composition change is evident in almost all of the surveyed plots with either the predominant species changing over the time period of the study or a significant expansion in one of the species compared to the others present in the initial survey. For those plots demonstrating red-shift upward translation, five out of the seven sites showed significant

changes in their species composition between the initial and final surveys. Likewise in the fifteen re-shift downward translation plots, thirteen of the fifteen plots witnessed significant composition change.

Table 26

Accuracy of vegetative indices and tasseled cap transformations vs field data

Spectral Response Trends	*NDVI*	*SAVI*	*$MSAVI_2$*	*TC_B*	*TC_G*	*TC_W*	AVG
All Data – 50 Sites	88	86	90	76	84	36	77
Red-Shift Stretch – 25 Sites (Increasing Vegetation)	96	96	100	68	96	28	81
Red-Shift Compression – 3 Sites (Decreasing Vegetation)	100	67	67	100	67	67	78
Red-Shift Upward Translation – 7 Sites (Decreasing Vegetation w/comp change)	57	71	57	57	57	57	60
Red-Shift Downward Translation – 15 Sites (Increasing Vegetation w/comp change)	93	80	80	93	80	33	74

Percentage of times the index match the actual field data

4.3 Meteorological Data

Ecological changes we have identified in the Big Pine Creek watershed are consistent with warming temperatures. In our previous paper, we identified statistically significant increases across the study area in both the maximum temperature (T_{MAX}) and minimum temperature (T_{MIN}). Looking at monthly trends, we found that for the maximum temperatures, the largest increases are taking place in the summer with smaller increases in the winter (Sawyer and Stephen, 2014). Precipitation and Big Pine Creek stream flow trends were also examined to determine if the moisture deficit conditions were impacting ecological responses over the study period. Here we found that although there was a slight decline in precipitation in the watershed, stream flow was slightly increasing which

is consistent with warmer temperatures increasing the melt water contribution to the stream flow from the Palisade glacier (Sawyer and Stephen, 2014).

The seasonal trends found in this analysis closely align with future climate regimes predicted by general circulation models showing milder wetter winters and hotter drier summers (Lenihan et al., 2003). Lenihan et al. (2003) show that these future climate scenarios can produce shifts in the vegetative composition. In particular, their biological distribution model simulations suggest a shift from shrubs to grasslands under these conditions (Lenihan et al., 2003). The temperature trends demonstrate that the Big Pine Creek watershed is at heightened risk from climate change and highlight the need to develop strategies to adapt to a new climate paradigm of warmer temperatures.

4.4 Confidence Levels

Multitemporal satellite imagery is impacted by several factors including changes in sensor response, sensor stability, atmospheric effects, and illumination effects (Vicente-Serrano et al., 2008). Geometric pixel registration errors are generally less than ½ pixel (Schueler and Salomonson, 1985). Radiometric uncertainty for the TM data is approximately 5% (Chander et al., 2009). The USGS surface reflectance data set has been assessed against MODIS surface reflectance data and found to be highly correlated with discrepancies between 2.2 to 3.5 percent (Feng et al., 2013).

The spectral mixture analysis performed for this study generated *RMS* errors of less than 1% on average. The average *RMSE* error values for each site are shown in table 20. However, the interpretation of what each ENVI extracted endmember represents is

somewhat subjective. Accuracy of this interpretation is dependent on the ability of the analyst to correctly match the modeled spectra to actual field collected spectra.

5.0 Summary and Conclusions

This study examined the changes in the ecosystem of the Big Pine Creek watershed as measured by trends in vegetation indices, tasseled cap transformations, and composition from spectral mixture analysis at thirty locations over a thirty year time span from 1984 through 2013. Trends in spectral response, vegetation indices and tasseled cap transformations were validated against fifty sites with known long term composition data to test the accuracy of four possible red-shift response hypotheses.

We found that red-shift stretch and red-shift downward translation trends corresponded to actual increases in vegetative cover in over 90% of the sites studied. Red-shift compression and red-shift upward translation trends were not as accurate with actual field data showing declines in only 67% and 57% of the time respectively. For the vegetative indices and tasseled cap transformations, overall agreement between the indices and actual field data was 77%. Red-shift stretch and red-shift compression demonstrated the highest level of agreement with actual field data at 81% and 78% respectively. Red-shift upward translation and red-shift downward translation trends matched actual field data only 60% and 74% of the time respectively.

In remote areas that do not have historical surface cover composition data, quantitative analysis of how each individual component affected the composite spectral signal is not possible. By performing a spectral unmixing of the sample sites, we can look

at the qualitative results of trend data to infer the impact compositional changes are having on the composite spectral response in each band. This analysis demonstrates a way to elicit a plausible explanation for the spectral responses recorded by the Landsat imager.

Comparing spectral mixture analysis trends in vegetative cover, trends in vegetation indices and trends in tasseled cap transformations at thirty sample sites in the Big Pine Creek study area, we found the tasseled cap brightness index showing the highest level of agreement with the red-shift theory (90%) while trends in vegetation cover using spectral mixture analysis showed the lowest agreement with red-shift theory of vegetation cover. It is interesting to note that the highest levels of agreement between spectral mixture analysis trends and vegetative cover predicted by red-shift theory occur with red-shift upward translation and red-shift downward translation predictions at 75% and 63% agreement respectively, while agreement levels for the vegetation indices are at their lowest for these two theories.

All of these findings suggest that identification of trends in vegetative responses to climate change must include consideration of how various indices and analytical techniques behave under various red-shift scenarios. While the vegetative indices and tasseled cap transforms perform remarkably well for simple cases of red-shift stretch and red-shift compression, when analyzing the more complex case of re-shift translation one should consider using spectral mixture analysis to increase the confidence level of the findings.

We previously hypothesized that at those sites showing red-shift translation, we would find composition change. Although our spectral unmixing shows changes in composition throughout the watershed over the last three decades, only a few sites demonstrate clear transition from one species to another. For example, at site 6 spectral unmixing identifies declining shrub population with increasing sage cover while at site 27, the spectral unmixing suggests sage is replacing Mahogany. However, composition change is also seen at sites undergoing basic red-shift stretch. For instance, at site 10, spectral unmixing identifies a definite shift from Cottonwood to Pine.

These findings suggest that a simple explanation of composition change at sites demonstrating red-shift translation is not really telling us what is taking place. Likewise, the results of this study show that simple red-shift stretch and red-shift compression are not basic indicators of increase and decrease in vegetative cover, but may in fact also be the result of compositional change. Although we can make general inferences regarding trends in vegetative indices and tasseled cap transformations, only spectral unmixing can elicit additional information about the changes taking place. Spectral response trends are influenced by several factors including changes in the amount of vegetation present and also the type. Since litter and barren surface also contribute significantly to the spectral response, changes in the percent cover of those surface components also must be considered.

Spectral responses measured by the Landsat program provide a unique resource for the ecological community to examine how sensitive areas have adapted to new

environmental parameters. Vegetative indices and tasseled cap transformations along with spectral unmixing allow us to elicit detailed information on changes taking place at the local assemblage level. Performing this type of analysis using the techniques demonstrated in this paper will allow us to validate existing theories of ecological response to climate change and to develop new hypothesis regarding the behavior of species under future climatic regimes.

References

Chander, G., Markham, B., and Helder, D.L., (2009). Summary of current radiometric calibration coefficients for Landsat MSS, TM, ETM+, and EO-1 ALI sensors. *Remote Sensing of Environment*, 113, pp. 893-903.

Chmura, D.J., Anderson, P.D., Howe, G.T., Harrington, C.A., Halofsky, J.E., Peterson, D.L., Shaw, D.C., and St. Clair, B.J., (2011). Forest responses to climate change in the northwestern United States: Ecophysiological foundations for adaptive management. *Forest Ecology and Management*, 261, pp. 1121–1142.

Crist, E.P., (1985). Short Communication: A TM Tasseled Cap Equivalent Transformation for Reflectance Factor Data. *Remote Sensing of the Environment*, 17, pp. 301-306.

Eibl, B., Bach, H., and Mauser, W., (1996). Classification of a Landsat-TM image with the spectral mixture analysis under the application of field spectroscopy, *International Archives of Photogrammetry and Remote Sensing*, 31, pp. 226 - 231.

Elmore, A.J., Mustard, J.F., and Manning, S.J., (2003). Regional patterns of plant community response to changes in water: Owens Valley, California. *Ecological Applications*, 13 (2), pp. 443-460.

Feng, M., Sexton, J.O., Huang, C., Masek, J.G., Vermote, E.F., Gao, F., Narasimhan, R., Channan, S., Wolfe, R.E., and Townshend, J.R., (2013). Global surface products from Landsat: Assessment using coincident MODIS observations, *Remote Sensing of Environment*, Vol. 134, pp. 276-293.

Gasner, M.R., Jankowski, J.E., Ciecka, A.L., Kyle, K.O., and Rabenold, K.N., (2010). Projecting the local impacts of climate change on a Central American montane avian community. *Biological Conservation*, 143, pp. 1250-1258.

Grabherr, G., Gottfried, M., and Pauli, H., (2010). Climate change impacts in Alpine environments. *Geography Compass*, 48, pp. 1133-1153.

Huete, A.R., (1988). A Soil-adjusted Vegetation Index. *Remote Sensing of the Environment*, 25, pp. 295-309.

Jackson, R.D., Pinter, P.J., Jr., Reginato, R.J., and Idso, S.B., (1986). Detection and evaluation of plant stresses for crop management decisions. *IEEE Transactions on Geoscience and Remote Sensing*, GE-24 (1), pp. 99-106.

Lenihan, J.M., Drapek, R., Bachelet, D., Kremer, and Nelson, R.P., (2003). Climate change effects on vegetation distribution, carbon, and fire in California. *Ecological Applications*, 13 (6), pp. 1667 – 1681.

Lindner, M., Maroschek, M., Netherer, S., Kremer, A., Barbati, A., Garcia-Gonzalo, J., Seidl, R., Delzon, S., Corona, P., Kolstrom, M., Lexer, M.J., and Marchetti, M., (2010). Climate change impacts, adaptive capacity, and vulnerability of European forest ecosystems. *Forest Ecology and Management*, 259, pp. 698 – 709.

Lu, D., M. Batistella, E. Moran, and P. Mausel, (2004). Application of spectral mixture analysis to Amazonian land-use and land-cover classification, *International Journal of Remote Sensing*, 10 (23), pp. 5345 - 5358.

Masek, J.G., Vermote, E.F.., Saleous, N., Wolfe, R., Hall, F.G., Huemmrich, F., Gao, F., Kutler, J., and Lim, T.K., (2006). A Landsat surface reflectance data set for North America, 1990-2000. *IEEE Geoscience and Remote Sensing Letters*, 3, pp. 68-72.

Musick, H.B. and Pelletier, R.E., (1988). Response to soil moisture spectral indexes derived from bidirectional reflectance in thematic mapper wavebands. *Remote Sensing of Environment*, 25, pp. 167-184.

Myint, S. and Okin, G., (2010). Modelling Land-Cover Types Using Multiple Endmember Spectral Mixture Analysis in a Desert City, *Arizona State University, Working Paper Number* 2010-06, pp. 1 - 30.

Opdam, P. and Wascher, D., (2004). Climate change meets habitat fragmentation: linking landscape and biogeographical scale levels in research and conservation. *Biological Conservation*, 117, pp. 285-297.

Qi, J., Chehbouni, A., Huete, A.R., Kerr, Y.H., and Sorooshian, S., (1994). A Modified Soil-adjusted Vegetation Index. *Remote Sensing of the Environment*, 48, pp. 119-126.

Rouse, J.W., Haas, R.H. Schell J.A. and Deering, D.W., (1974). Monitoring vegetation systems in the Great Plains with ERTS. *Proc. Third ERTS-1 Symposium, NASA Goddard*, NASA SP-351 pp. 309-317.

Sawyer, P., and Stephen, H., (2014). The Big Pine Creek watershed and climate change: A trend analysis of Landsat surface reflectance and PRISM datasets over the last 3 decades. *Advances in Space Research*, 54, pp. 37-48.

Schmidt, G.L., Jenkerson, C.B., Masek, J., Vermote, E., and Gao, F., (2013). Landsat ecosystem disturbance adaptive processing system (LEDAPS) algorithm description: *U.S. Geological Survey Open-File Report* 2013–1057.

Schueler, C.F., and Salomonson, V.V., (1985). Landsat Image Data Quality Studies. *Advances in Space Research*, 5 (5), pp. 1-11.

Skre, O. and Naess, M., (1999). CO_2 and winter temperature effects on white birch. *Chemosphere: Global Change Science*, 1, pp. 469-483.

Tompkins, S., Mustard, J., Pieters, C., and Forsyth, D., (1997). Optimization of Endmembers Mixture Analysis for Spectral Mixture Analysis, Remote Sensing of Environment, 59, pp. 472 - 489.

Vicente-Serrano, S.M., Perez-Cabello, F., and Lasanta, T., (2008). Assessment of radiometric correction techniques in analyzing vegetation variability and change using time series of Landsat imagery. *Remote Sensing of Environment*, 112, pp. 3916-3934.

Vittoz, P., Cherix, D., Gonseth, Y., Lubini, V., Maggini, R., Zbinden, N., and Zumbach, S., (2013). Climate change impacts on biodiversity in Switzerland: A review. *Journal for Nature Conservation*, 21, pp. 154-162.

Walther, G.R., (2010). Community and ecosystem responses to recent climate change, *Philosophical Transactions of The Royal Society B*, 365, pp. 2019-2024.

Wessman, C.A., (1992). Imaging spectrometry for remote sensing of ecosystem processes. *Advances in Space Research*, 12 (7), pp. 361-368.

Wilson, R.J., Gutierrez, D., Gutierrez, J., Martinez, D., Agudo, R., and Monserrat, V.J., (2005). Changes to the elevational limits and extent of species ranges associated with climate change. *Ecology Letters*, 8, pp. 1138-1146.

Chapter 7: Conclusions and Recommendations

The primary goal of this research was the study of recent climate driven changes in an ecosystem using remote sensing. To determine ecosystem changes, a methodology was designed using publically available remote sensing imagery and trend analysis of the changes in the imagery to elicit information regarding recent changes in vegetative surface cover. This approach exploits the observable alteration of spectral response caused by climate driven changes to physiological processes within the ecosystem. The accuracy and usefulness of vegetative indices and spectral band transforms were evaluated to validate their use in ecological studies.

Specific objectives of this research included analysis of recent climate driven changes to the study area, creation of an analytical process to find changes that have taken place from remote sensing imagery, understanding of red-shift due to vegetation compositional change, and determination of the accuracy of vegetation indices and spectral band transforms. These objectives answer important questions regarding how recent climate change has affected a fragile alpine watershed and how a similar framework can be employed to determine changes to other sensitive ecological regions.

This research is critically important to the goal of achieving a sustainable balance between the need for ecosystem resources and the capacity of the biosphere to fulfill those needs. From this study, numerous conclusions have been derived as detailed below. In addition, several areas that require additional study have been identified and are discussed.

1.0 Conclusions

This research has led to the following key findings regarding recent climate induced changes to the ecosystem and the techniques used to perform ecological evaluations.

1. The study of recent climate change impacts on the ecosystem found that surface reflectance throughout the watershed has declined in all six Landsat bands over the last three decades. At the same time, temperatures have demonstrated a statistically significant rise. The finding that surface reflectance is declining in both the visible and NIR regions highlighted a gap in the ability of vegetation indices to identify vegetative trends in these circumstances. This led to the creation of red-shift translation theory which relates vegetative composition change to instances where the visible and NIR bands are trending in the same direction.
2. The study design employed in this research included the use of numerous measures including trends in each of the six Landsat reflectance bands, trends in both ratio based vegetation indices and linear band transforms as well as trends in vegetative composition derived from spectral mixture analysis to determine climate driven changes in vegetative surface cover. This methodology avoided the pitfalls associated with reliance on individual measures. This study design provides improved confidence in the conclusions reached relating increased

vegetative growth in water rich areas along with declines in vegetation in water poor regions to the significant warming found during the study period.

3. The study of red-shift trends produced numerous findings. The hypothesis that red-shift stretch and downward translation relate to increasing vegetative cover performed remarkably well when compared to actual long-term vegetation plots. The hypothesis that red-shift compression and upward translation relate to decreasing vegetative cover were much less reliable compared to actual long-term vegetation plots. The relationship between red-shift translations and composition change require additional investigation since all the plots studied all demonstrated composition change. Thus, no conclusion can be drawn relating red-shift translations to composition change.

4. The validation study determined that vegetation indices and transforms performed reasonably well in predicting surface cover changes when compared to long term field survey data with the exception of the tasseled cap wetness transform. In general, the vegetation indices are more accurate with an average 88% agreement with actual field data. Excluding the tasseled cap wetness index, the other two tasseled cap measures for brightness and greenness demonstrated they can reasonably be relied upon as vegetative trend indicators with an average 80% agreement between them and actual field survey plots. The 36% agreement provided by the tasseled cap wetness index is in need of further examination.

5. The USGS CDR surface reflectance dataset correlates well with older dark object subtraction methods for calculating surface reflectance. The overall comparison of the two methods showed very close agreement in the surface reflectance values.
6. Ecosystem changes show distinct patterns with declining vegetation in the lower half of the watershed and vegetative increases in the upper half of the watershed. Vegetative stands in water rich areas have experienced growth while stands in dry areas experienced declines over the 30 years of the study.
7. Spectral mixture analysis identified vegetative composition change throughout the study area. This technique found widespread declines in needle leaf shrubs consistent with the conclusions from the analysis of vegetation indices in the elevational study. However, only two of the thirty sites demonstrated statistically significant transitions from one species to another.

These conclusions are briefly elaborated and discussed in the following text. The initial research question focused on the impact of increased temperatures on the spectral reflectance properties of vegetation. Elevated temperatures drive increased reaction rates and alter important physiological interactions such as decomposition that have direct effects on nutrient availability. These changes drive vegetative composition towards more drought tolerant species. Composition variations are related to the changes in the spectral reflectance characteristics of the study area.

Trends in vegetation indices alone did not identify significant climate driven changes in the ecosystem. However, by examining trends in tasseled cap transforms, the

conclusion that vegetative cover has been increasing based on strong declines in surface brightness and strong increases in wetness was made. Given the spatial limitations of the remote sensing imagery, identification of compositional changes was only possible through the use of spectral mixture analysis. These findings demonstrate the robust attributes of a study design that incorporates several different analytical measures.

Use of vegetation indices for ecological trend studies is problematic given the gap in understanding their meaning when the red and NIR bands are trending in the same direction. To address this information gap, red-shift translation postulates were developed and tested using actual field plot survey data. The red-shift translation hypotheses described here correlated with actual field survey data 93% of the time for red-shift downward translation and 57% of the time for red-shift upward translation. This compares well with the accuracy of standard red-shift stretch (96%) and red-shift compression (67%) theories of vegetative increases and declines respectively.

Overall, the vegetative indices performed better than the tasseled cap transforms, with the $MSAVI_2$ index recording the highest level of agreement (90%) with the actual measurement of vegetative surface cover. The tasseled cap wetness index demonstrated the least correlation (36%) with field data. This finding suggests caution in using tasselled cap wetness as a measure of vegetative surface cover change, especially in regions where vegetative cover is increasing. The striking difference in the accuracy of tasseled cap wetness compared to the other measures needs more in-depth investigation

The next research question focused on determining if previous studies that relied upon manual conversion of raw Landsat digital numbers to surface reflectance values varied significantly from the recently published USGS surface reflectance data. This study found substantial agreement between the two methods. Band 5 demonstrated the closest agreement between the two methods with an adjusted R^2 value of 0.9667 while the NIR band 4 showed the lowest agreement with an R^2 value of 0.8602. Mean values for surface reflectance published by the USGS were higher than those derived using the simple DOS method. The primary finding of this study was the overall close agreement between the two methods which leads to the conclusion that revisiting previous surface reflectance studies using the USGS CDR data would not significantly alter the findings or conclusions of those studies.

In the study of elevational effects, changes in the ecosystem of the Big Pine Creek watershed as measured by trends in observed surface reflectance values along a 2500 meter elevation gradient at 75 sample sites were examined. The primary findings of this study are that in densely vegetated sites adjacent to a stable water supply, vegetation is increasing coincident with increasing temperatures. In moderately vegetated sites, no consistent trends are identified with only a few of the sites demonstrating any significant positive or negative trends. Elevation dependent trends are clearly identified in sparsely vegetated sites with vegetative increases occurring in the upper half of the watershed and declines taking place in the lower half of the watershed. This finding is consistent with previous theories of warming climate driving upslope species migration patterns. At the

upper reaches of the watershed, warmer temperatures are increasing the habitable zone for these sites while at the lower reaches, increased temperatures are driving an alteration of vegetative composition towards more drought tolerant species.

The principal research question regarding the impact climate change has had on the Big Pine Creek watershed was addressed by examining thirty sites in detail including analyzing trends in three vegetation indices, the three tasseled cap transformations, and trends in surface composition as derived from spectral unmixing. The null hypotheses of no climate driven change can easily be dismissed based on all of the analysis demonstrating changes at nearly all the sample sites studied. Spectral unmixing is consistent with alternate hypothesis 2 suggesting climate change driven declines in vegetation. Spectral unmixing is used to validate the third hypothesis of climate driven composition change. At 63% of the sample sites we see both positive and negative trends in individual vegetative types consistent with composition change taking place, with eight sites demonstrating only vegetative declines and only three sites demonstrating only increasing trends. These findings support alternate hypothesis 3 suggesting composition change throughout the watershed.

These studies show that climate driven changes to the vegetation of the Big Pine Creek watershed have been taking place over the last three decades. Since predictions are for continued increases in temperatures, the trends in vegetative quantity and composition can be expected to accelerate, altering the ecosystem in ways that threaten the functioning of the interdependent systems within the watershed.

2.0 Recommendations

This research has also identified many new questions and areas of potential expansion. The following is a brief list of recommendations that could further extend and improve this research.

1. Perform additional investigation into the accuracy of the tasseled cap wetness index in order to resolve the discrepancy between its predictions and the findings of this study.
2. Since composition change was occurring at all the long-term field survey plots, additional plots with static composition need to be evaluated using a similar methodology. This will allow testing the theory that red-shift translations are a result of composition change.
3. Similarly, since few of the long-term survey plots demonstrated vegetative declines, we should perform additional comparison studies at sites experiencing vegetative declines to determine the accuracy of red-shift compression and downward translation hypothesis.
4. Examine additional study areas using the same methodology created for this research to obtain a broader picture of the impact climate change is having on a global scale.

Some of the underlying reasons for these recommendations are discussed below in the following text. In the final study, the accuracy of vegetation indices and tasseled cap transformations were validated against real field survey data. The findings from that

validation analysis demonstrated good agreement overall between the vegetation indices and the tasseled cap brightness and greenness indices with actual survey data. However the tasseled cap wetness index demonstrated little correlation to actual field data. This discrepancy in the predictive value of the tasseled cap wetness index requires further investigation.

The original hypothesis for red-shift translations included the theory that composition change causes variation in the NIR that drive the NIR response in the same direction as the visible response. However, since all the plots in this study experienced composition change, this theory could not be tested. Additional studies that examine long-term field survey plots both with and without composition change are needed to fully validate these hypotheses.

The number of field survey plots used in the validation analysis provided sufficient data to reliably conclude that red-shift stretch (twenty five plots) is an accurate predictor of vegetative growth. The other red-shift theories, downward translation (fifteen plots), compression (three plots) and downward translation (seven plots) did not provide enough data points to attach sufficient significance in their results. Additional studies that use long-term field survey plots that demonstrate spectral response patterns of compression, and upward and downward translation are needed fully validate these hypotheses.

The findings of changes in sparsely vegetated areas with increases occurring at higher elevations and declines taking place at lower elevations provides support for

existing theory on ecological response to a warming climate. The methodology created in this research provides a roadmap for additional studies of remote and inaccessible regions for the purpose of validating this and other hypothesis regarding climate change impacts on ecosystems. Additional studies will enhance our fundamental understanding of the impact environmental parameters have on physiological processes. This in turn will enable the ecological research community to determine those areas at greatest risk to further degradation, allowing for prioritization of limited resources needed to protect essential habitats.

This research program demonstrates how recent climate change has impacted a sensitive alpine ecosystem and provides a roadmap for performing the determinations needed to find changes brought about by higher temperatures on the environment. Several critical gaps were addressed regarding the use of vegetation indices for climate driven vegetation studies. An analytical methodology was produced that provides multiple indices as well as spectral mixture analysis to accurately identify vegetative changes. The gap in understanding the meaning of vegetation indices when the red and NIR are trending in the same direction was addressed by development and testing of red-shift translation hypothesis against surface vegetation plots that have accurate long-term surface cover and composition data. Also, the lack of studies validating the performance of three common vegetation indices and three tasseled cap transforms was addressed by comparing numerous long-term field survey sites with the prediction efficiency of those measures.

As final remarks, it is essential that we increase our understanding of the impact climate change has already had on the environment in order to be prepared to deal with the rapid onset of potentially severe consequences brought about by reduced ecosystem productivity. Declining resource availability coupled with the increasing natural resource demands of a growing population pose a threat to the quality of life and to the sustainability of the biosphere. If we are to mitigate the negative effects of climate change and adapt to shifting ecological resource constraints, we must first determine where those changes have already taken place and which areas will soon become vulnerable to changing environmental conditions.

Appendix A

A1 - Advances in Space Research Copyright agreement

Copyright

Describes the rights related to the publication and distribution of research. It governs how authors (as well as their employers or funders), publishers and the wider general public can use, publish and distribute articles or books.

Journal author rights

In order for Elsevier to publish and disseminate research articles, we need publishing rights. This is determined by a publishing agreement between the author and Elsevier. This agreement deals with the transfer or license of the copyright to Elsevier and authors retain significant rights to use and share their own published articles. Elsevier supports the need for authors to share, disseminate and maximize the impact of their research and these rights, in Elsevier proprietary journals* are defined below:

For subscription articles

Authors transfer copyright to the publisher as part of a journal publishing agreement, but have the right to:

- Share their article for Personal Use (http://www.elsevier.com/about/companyinformation/policies/copyright/personal- use),Internal Institutional Use (http://www.elsevier.com/about/companyinformation/policies/copyright/internal- use)andScholarlySharing (http://www.elsevier.com/about/company-information/policies/sharing) purposes, with a DOI link to the version of record on Science Direct (and with the Creative Commons CC-BY-NC- ND license (http://www.elsevier.com/about/company-information/policies/sharing/how-to- attach-a-user-license)for author manuscript versions).
- Retain patent, trademark and other intellectual property rights (including raw research data).
- Proper attribution and credit for the published work.

For open access articles

Authors sign an exclusive license agreement, where authors have copyright but

license exclusive rights in their article to the publisher**. In this case authors have the right to:

- Share their article in the same ways permitted to third parties under the relevant user license
- (together with Personal Use (http://www.elsevier.com/about/co mpany-information/policies/copyright/p ersonal-use) rights) so long as it contains a CrossMark logo (http://www.elsevier.com/about/company-information/policies/crossmark), the end user license (http://www.elsevier.com/about/companyinformation/policies/open-access-licenses), and a DOI link to the version of record on ScienceDirect.
- Retain patent, trademark and other intellectual property rights (including raw research data).
- Proper attribution and credit for the published work.

* Please note that society or third party owned journals may have different publishing agreements. Please see the journal's guide for authors for journal specific copyright information.

** This includes the right for the publisher to make and authorize commercial use, please see "Rights granted to Elsevier" for more details.

Rights granted Elsevier

For both subscription and open access articles, published in proprietary titles, Elsevier is granted the following rights:

- The exclusive right to publish and distribute an article, and to grant rights to others, including for commercial purposes.
- For open access articles, Elsevier will apply the relevant third party user license (http://www.elsevier.com/about/companyinformation/policies/open-access-licenses) where Elsevier publishes the article on its online platforms).
- The right to provide the article in all forms and media so the article can be used on the latest technology even after publication.
- The authority to enforce the rights in the article, on behalf of an author, against third parties, for example in the case of plagiarism or copyright infringement.

Protecting author rights

Copyright aims to protect the specific way the article has been written to describe an experiment and the results. Elsevier is committed to its authors to protect and defend their work and their reputation and takes allegations of infringement, plagiarism, ethic disputes and fraud very seriously.

If an author becomes aware of a possible plagiarism, fraud or infringement we recommend contacting their Elsevier publishing contact who can then liaise with our in-house legal department. Note that certain open access user licenses may permit quitebroadre-use (http://www.elsevier.com/about/company- information/policies/open-access-licenses) that might otherwise be counted as copyright infringement. For details about how to seek permission to use an article see our permissionpage (http://www.elsevier.com/about/company-information/policies/copyright/permissions).

Personal use

Authors can use their articles, in full or in part, for a wide range of scholarly, non-commercial purposes as outlined below:

- Use by an author in the author's classroom teaching (including distribution of copies, paper or electronic)
- Distribution of copies (including through e-mail) to known research colleagues for their personal use (but not for Commercial Use)
- **Inclusion in a thesis or dissertation (provided that this is not to be published commercially)**
- Use in a subsequent compilation of the author's works
- Extending the Article to book-length form
- Preparation of other derivative works (but not for Commercial Use)
- Otherwise using or re-using portions or excerpts in other works

These rights apply for all Elsevier authors who publish their article as either a subscription article or an open access article. In all cases we require that all Elsevier authors always include a full acknowledgement and, if appropriate, a link to the final published version hosted on Science Direct.

A2 - The Institute of Research Engineers and Doctors (IRED) Copyright agreement

COPYRIGHT POLICY

All published manuscripts are licensed under IRED Copyright License. Our Copyright Policy aims to guarantee that original material is published while at the same time giving significant freedom to our authors. IRED upholds a very flexible copyright policy meaning that there is no copyright transfer to the publisher and authors hold exclusive copyright to their work.

When submitting their manuscripts authors are required to accept the terms and conditions set forth in our Copyright Agreement as follows:

1. AUTHOR'S RETENTION OF RIGHTS

IRED acknowledges and agrees that the Author(s) retain(s) the copyright to the work submitted for publication, and is/are allowed:

1. to revise, reproduce, distribute, publicly perform, and publicly display the Chapter/Article
2. to republish the Work, as long as IRED is cited as the source of first publication of the Work
3. to prepare derivative works from the Chapter/Article
4. to apply all other proprietary rights to the Work (such as patents); and
5. to authorize others to make any use of the Chapter/Article.

Users are granted the right to copy, use, distribute, transmit and display the Work publicly, and to create and distribute derivative works in any medium and for any responsible purpose, as long as the Author receives credit as author, and the Book/Journal in which the Chapter/Article has been published is cited as the source of first publication of the Work.

2. PERMISSION TO USE

The author assigns to IRED all rights:

1. to publish the Work, in whole or in part, by various means such as hard copy or electronic copy formats, and in any and all forms of media, now or hereafter known; and
2. to republish, distribute, promote, publicly perform, and publicly display the Work at any time and in all IRED Publishing Group projects.

3. AUTHOR'S RESPONSIBILITIES

IRED distributes its publications throughout the world and wants to ensure that the material submitted to its publications is properly available to the readership of those publications. Authors must ensure that their Chapter/Article meets the requirements,

including provisions covering originality, authorship, author responsibilities and author misconduct. Therefore:

1. the Author(s) should only submit original work that has neither appeared elsewhere for publication, nor is under review for another refereed publication
2. the Authors(s) should determine whether disclosure of their material, content and photographs requires the prior consent of other parties and, if so, should obtain it; and
3. research carried out in collaboration with other scholars necessitates that all authors approve of submitting the Chapter/Article.

Statements and opinions expressed in the Chapter/Article are those of the Author(s) and not those of the editors or IRED. No responsibility is accepted for the accuracy of information contained in the published Chapter/Article. IRED assumes no responsibility or liability for any damage or injury to persons or property arising out of the use of any materials, instructions, methods or ideas contained inside the Chapter/Article.

4. GENERAL TERMS

By accepting the Copyright Agreement the corresponding Author:

1. warrants that he/she is the Author and has the power and authority to make and execute this assignment
2. affirms that, for jointly authored Chapters/Articles, he/she is empowered to accept this form on behalf of all authors
3. warrants that the Chapter/Article is original, has not previously been published and is not currently under consideration for publication by any other entity
4. affirms that permission will be obtained for all previously published and/or copyrighted material contained in this manuscript (to the extent that the chapter incorporates text, passages, figures, data or other material from the work of others), it is the authors' collective responsibility to obtain all copyright permissions - they can be obtained during the publishing process and need to be collected before publication; and
5. agrees to indemnify IRED against all losses, costs and expenses (including legal costs and expenses) arising from claims made by other parties due to the exceptional circumstance that the author has breached any terms, conditions and/or warranties concerning the authorship of the chapter (the whole or parts of it), the rights to publish the chapter or the infringement of any third party’s rights.

If the Author has prepared the work as part of that his/her official duties as an employee or officer of a Government agency, public institution or company and has copyrights that belong to the Government agency, public institution, or company, IRED agrees to accept their terms and conditions if they are not in conflict with IRED's Copyright Policy.

A3 - IRED Conference Acceptance Rate Letter

Acceptance Rate Letter

Ref No: - IRED/14/ABBE/E105
Dated: 18-February-2014

Subject: Letter of Acceptance and Invitation

Dear Author (Patrick Sawyer),

We are pleased to inform you that after hard review process your paper entitled **"Comparison of surface reflectance values from the USGS landsat 5 TM climate data record (CDR) with values generated using a simple dark object subtraction (DOS) method in an Alpine watershed"** with paper ID "**ABBE-14-111**" has been accepted for Oral presentation and publication in Early Bird Round of "The International Conference on Advances in Bio-Informatics, Bio-Technology and Environmental Engineering - ABBE 2014" which is going to be held at London, UK on 01-02 June, 2014. We invite you to present your full research paper in the conference, please bring *PPT* slides of your paper for presentation in the conference as there are data projectors at the venue.

Benefits of Publication:-

- Your paper will be included in the Conference Proceedings and will be published online with ISBN No and will be archived in SEEK Digital Library so that it will be universally accessed. Seek Digital Library is being accessed by thousands of Students, Researchers and Scientists over the globe. Seek Digital Library is an Open access library. You may visit the Library at www.seekdl.org.
- Each paper will be assigned Digital Object Identifier (DOI) from CROSSREF.
- Registered Papers will be published in various Issues of International Journals with ISSN Numbers.
- You will get the chance to attend the conference and to meet the researchers from the globe.

We have received more than 72 research articles for review in Early Bird Round from more than 17 countries and only 25 articles has been accepted for publication and oral

presentation with acceptance ratio of 34.72%. The Review Process has gone through Peer Review Process. The Editorial Committee focused on quality research articles to maintain the credibility of the conference.

If your research paper wins the „best paper award", it will be appreciated at the closing ceremony. With certificate in this respect for more details, please visit our website http://abbe.theired.org/. Please send us attached completed registration form along with payment Proof on or before **12 March, 2014** to confirm your participation. We do not provide any assistance relating to Visa and accommodation other than this acceptance letter for London conference. We look forward to seeing you at the conference.

With Best Regards,

Elena Alikchkina Conference Co-ordinator IRED

A4 - SciencePG Copyright agreement

Copyright
The authors' publications in SciencePG are distributed under Creative Commons Attribution (CC BY) license (http://creativecommons.org/licenses/by/4.0/). The license was developed to facilitate open access, namely, free immediate access to and unrestricted reuse of original works of all types.

Under this license, authors retain ownership of the copyright for their publications, but grant SciencePG a non-exclusive license to publish the work in paper form and allow anyone to reuse, distribute and reproduce the content as long as the original work is properly cited.

Appropriate attribution can be provided by simply citing the original work. No permission is required from the authors or the publishers. For any reuse or distribution of a work, users must also make clear the license terms under which the work was published. The standard license will be applied to the authors' publications, which ensures the publications freely and openly available in perpetuity.

Creative Commons Legal Code

Attribution 4.0 International

Creative Commons Corporation ("Creative Commons") is not a law firm and does not provide legal services or legal advice. Distribution of Creative Commons public licenses does not create a lawyer- client or other relationship. Creative Commons makes its licenses and related information available on an "as-is" basis. Creative Commons gives no warranties regarding its licenses, any material licensed under their terms and conditions, or any related information. Creative Commons disclaims all liability for damages resulting from their use to the fullest extent possible.

Using Creative Commons Public Licenses

Creative Commons public licenses provide a standard set of terms and conditions that creators and other rights holders may use to share original works of authorship and other material subject to copyright and certain other rights specified in the public license below. The following considerations are for informational purposes only, are not exhaustive, and do not form part of our licenses.

Considerations for licensors: *Our public licenses are intended for use by those authorized*

to give the public permission to use material in ways otherwise restricted by copyright and certain other rights. Our licenses are irrevocable. Licensors should read and understand the terms and conditions of the license they choose before applying it. Licensors should also secure all rights necessary before applying our licenses so that the public can reuse the material as expected.
Licensors should clearly mark any material not subject to the license. This includes other CC- licensed material, or material used under an exception or limitation to copyright. More considerations for licensors.

Considerations for the public: *By using one of our public licenses, a licensor grants the public permission to use the licensed material under specified terms and conditions. If the licensor's permission is not necessary for any reason–for example, because of any applicable exception or limitation to copyright–then that use is not regulated by the license. Our licenses grant only permissions under copyright and certain other rights that a licensor has authority to grant. Use of the licensed material may still be restricted for other reasons, including because others have copyright or other rights in the material. A licensor may make special requests, such as asking that all changes be marked or described. Although not required by our licenses, you are encouraged to respect those requests where reasonable. More considerations for the public.*

Creative Commons Attribution 4.0 International Public License

By exercising the Licensed Rights (defined below), You accept and agree to be bound by the terms and conditions of this Creative Commons Attribution 4.0 International Public License ("Public License"). To the extent this Public License may be interpreted as a contract, You are granted the Licensed Rights in consideration of Your acceptance of these terms and conditions, and the Licensor grants You such rights in consideration of benefits the Licensor receives from making the Licensed Material available under these terms and conditions.

Section 1 – Definitions.

a. **Adapted Material** means material subject to Copyright and Similar Rights that is derived from or based upon the Licensed Material and in which the Licensed Material is translated, altered, arranged, transformed, or otherwise modified in a manner requiring permission under the Copyright and Similar Rights held by the Licensor. For purposes of this Public License, where the Licensed Material is a musical work, performance, or sound recording, Adapted Material is always produced where the Licensed Material is synched in timed relation with a moving image.

b. **Adapter's License** means the license You apply to Your Copyright and Similar Rights in Your contributions to Adapted Material in accordance with the terms

and conditions of this Public License.

c. **Copyright and Similar Rights** means copyright and/or similar rights closely related to copyright including, without limitation, performance, broadcast, sound recording, and Sui Generis Database Rights, without regard to how the rights are labeled or categorized. For purposes of this Public License, the rights specified in Section 2(b)(1)-(2) are not Copyright and Similar Rights.

d. **Effective Technological Measures** means those measures that, in the absence of proper authority, may not be circumvented under laws fulfilling obligations under Article 11 of the WIPO Copyright Treaty adopted on December 20, 1996, and/or similar international agreements.

e. **Exceptions and Limitations** means fair use, fair dealing, and/or any other exception or limitation to Copyright and Similar Rights that applies to Your use of the Licensed Material.

f. **Licensed Material** means the artistic or literary work, database, or other material to which the Licensor applied this Public License.

g. **Licensed Rights** means the rights granted to You subject to the terms and conditions of this Public License, which are limited to all Copyright and Similar Rights that apply to Your use of the Licensed Material and that the Licensor has authority to license.

h. **Licensor** means the individual(s) or entity(ies) granting rights under this Public License.

i. **Share** means to provide material to the public by any means or process that requires permission under the Licensed Rights, such as reproduction, public display, public performance, distribution, dissemination, communication, or importation, and to make material available to the public including in ways that members of the public may access the material from a place and at a time individually chosen by them.

j. **Sui Generis Database Rights** means rights other than copyright resulting from Directive 96/9/EC of the European Parliament and of the Council of 11 March 1996 on the legal protection of databases, as amended and/or succeeded, as well as other essentially equivalent rights anywhere in the world.

k. **You** means the individual or entity exercising the Licensed Rights under this Public License. **Your** has a corresponding meaning.

Section 2 – Scope.

a. **License grant**

1. Subject to the terms and conditions of this Public License, the Licensor hereby grants You a worldwide, royalty-free, non-sublicensable, non-exclusive, irrevocable license to exercise the Licensed Rights in the Licensed Material to:

A. reproduce and Share the Licensed Material, in whole or in part; and
B. produce, reproduce, and Share Adapted Material.

2. Exceptions and Limitations. For the avoidance of doubt, where Exceptions and Limitations apply to Your use, this Public License does not apply, and You do not need to comply with its terms and conditions.
3. Term. The term of this Public License is specified in Section 6(a).
4. Media and formats; technical modifications allowed. The Licensor authorizes You to exercise the Licensed Rights in all media and formats whether now known or hereafter created, and to make technical modifications necessary to do so. The Licensor waives and/or agrees not to assert any right or authority to forbid You from making technical modifications necessary to exercise the Licensed Rights, including technical modifications necessary to circumvent Effective Technological Measures. For purposes of this Public License, simply making modifications authorized by this Section 2(a)(4) never produces Adapted Material.
5. Downstream recipients.
   A. Offer from the Licensor – Licensed Material. Every recipient of the Licensed Material automatically receives an offer from the Licensor to exercise the Licensed Rights under the terms and conditions of this Public License.
   B. No downstream restrictions. You may not offer or impose any additional or different terms or conditions on, or apply any Effective Technological Measures to, the Licensed Material if doing so restricts exercise of the Licensed Rights by any recipient of the Licensed Material.
6. No endorsement. Nothing in this Public License constitutes or may be construed as permission to assert or imply that You are, or that Your use of the Licensed Material is, connected with, or sponsored, endorsed, or granted official status by, the Licensor or others designated to receive attribution as provided in Section 3(a)(1)(A)(i).

b. **Other rights**.

1. Moral rights, such as the right of integrity, are not licensed under this Public License, nor are publicity, privacy, and/or other similar personality rights; however, to the extent possible, the Licensor waives and/or agrees not to assert any such rights held by the Licensor to the limited extent necessary to allow You to exercise the Licensed Rights, but not otherwise.
2. Patent and trademark rights are not licensed under this Public License.
3. To the extent possible, the Licensor waives any right to collect royalties from You for the exercise of the Licensed Rights, whether directly or through a collecting society under any voluntary or waivable statutory or

compulsory licensing scheme. In all other cases the Licensor expressly reserves any right to collect such royalties.

Section 3 – License Conditions.

Your exercise of the Licensed Rights is expressly made subject to the following conditions.

a. **Attribution**.

1. If You Share the Licensed Material (including in modified form), You must:

    A. Retain the following if it is supplied by the Licensor with the Licensed Material:
        i. identification of the creator(s) of the Licensed Material and any others designated to receive attribution, in any reasonable manner requested by the Licensor (including by pseudonym if designated);
        ii. a copyright notice;
        iii. a notice that refers to this Public License;
        iv. a notice that refers to the disclaimer of warranties;
        v. a URI or hyperlink to the Licensed Material to the extent reasonably practicable;
    B. indicate if You modified the Licensed Material and retain an indication of any previous modifications; and
    C. indicate the Licensed Material is licensed under this Public License, and include the text of, or the URI or hyperlink to, this Public License.

2. You may satisfy the conditions in Section 3(a)(1) in any reasonable manner based on the medium, means, and context in which You Share the Licensed Material. For example, it may be reasonable to satisfy the conditions by providing a URI or hyperlink to a resource that includes the required information.
3. If requested by the Licensor, You must remove any of the information required by Section 3 (a)(1)(A) to the extent reasonably practicable.
4. If You Share Adapted Material You produce, the Adapter's License You apply must not prevent recipients of the Adapted Material from complying with this Public License.

Section 4 – Sui Generis Database Rights.

Where the Licensed Rights include Sui Generis Database Rights that apply to Your use of the Licensed Material:

a. for the avoidance of doubt, Section 2(a)(1) grants You the right to extract, reuse, reproduce, and Share all or a substantial portion of the contents of the database;
b. if You include all or a substantial portion of the database contents in a database in which You have Sui Generis Database Rights, then the database in which You have Sui Generis Database Rights (but not its individual contents) is Adapted Material; and
c. You must comply with the conditions in Section 3(a) if You Share all or a substantial portion of the contents of the database.

For the avoidance of doubt, this Section 4 supplements and does not replace Your obligations under this Public License where the Licensed Rights include other Copyright and Similar Rights.

Section 5 – Disclaimer of Warranties and Limitation of Liability.

a. Unless otherwise separately undertaken by the Licensor, to the extent possible, the Licensor offers the Licensed Material as-is and as-available, and makes no representations or warranties of any kind concerning the Licensed Material, whether express, implied, statutory, or other. This includes, without limitation, warranties of title, merchantability, fitness for a particular purpose, non-infringement, absence of latent or other defects, accuracy, or the presence or absence of errors, whether or not known or discoverable. Where disclaimers of warranties are not allowed in full or in part, this disclaimer may not apply to You.
b. To the extent possible, in no event will the Licensor be liable to You on any legal theory (including, without limitation, negligence) or otherwise for any direct, special, indirect, incidental, consequential, punitive, exemplary, or other losses, costs, expenses, or damages arising out of this Public License or use of the Licensed Material, even if the Licensor has been advised of the possibility of such losses, costs, expenses, or damages. Where a limitation of liability is not allowed in full or in part, this limitation may not apply to You.
c. The disclaimer of warranties and limitation of liability provided above shall be interpreted in a manner that, to the extent possible, most closely approximates an absolute disclaimer and waiver of all liability.

Section 6 – Term and Termination.

a. This Public License applies for the term of the Copyright and Similar Rights licensed here. However, if You fail to comply with this Public License, then Your rights under this Public License terminate automatically.

b. Where Your right to use the Licensed Material has terminated under Section 6(a), it reinstates:

1. automatically as of the date the violation is cured, provided it is cured within 30 days of Your discovery of the violation; or
2. upon express reinstatement by the Licensor.

For the avoidance of doubt, this Section 6(b) does not affect any right the Licensor may have to seek remedies for Your violations of this Public License.

c. For the avoidance of doubt, the Licensor may also offer the Licensed Material under separate terms or conditions or stop distributing the Licensed Material at any time; however, doing so will not terminate this Public License.
d. Sections 1, 5, 6, 7, and 8 survive termination of this Public License.

Section 7 – Other Terms and Conditions.

a. The Licensor shall not be bound by any additional or different terms or conditions communicated by You unless expressly agreed.
b. Any arrangements, understandings, or agreements regarding the Licensed Material not stated herein are separate from and independent of the terms and conditions of this Public License.

Section 8 – Interpretation.

a. For the avoidance of doubt, this Public License does not, and shall not be interpreted to, reduce, limit, restrict, or impose conditions on any use of the Licensed Material that could lawfully be made without permission under this Public License.
b. To the extent possible, if any provision of this Public License is deemed unenforceable, it shall be automatically reformed to the minimum extent necessary to make it enforceable. If the provision cannot be reformed, it shall be severed from this Public License without affecting the enforceability of the remaining terms and conditions.
c. No term or condition of this Public License will be waived and no failure to comply consented to unless expressly agreed to by the Licensor.
d. Nothing in this Public License constitutes or may be interpreted as a limitation upon, or waiver of, any privileges and immunities that apply to the Licensor or You, including from the legal processes of any jurisdiction or authority.

References

Adams, H.D., Guardiola-Claramonte, M., Barron-Gafford, G.A., Villegas, J.C., Breshears, D.D., Zou, C.B., Troch, P.A., and Huxman, T.E., (2009). Temperature sensitivity of drought-induced tree mortality portends increased regional die-off under global-change-type drought. *PNAS*, 106 (17), pp. 7063 – 7066.

Asner, G.P., (1998). Biophysical and Biochemical Sources of Variability in Canopy Reflectance. *Remote Sensing of Environment*, 64, pp. 234-253.

Barnett, T.P., Adam, J.C., and Lettenmaier, D.P., (2005). Potential impacts of a warming climate on water availability in snow-dominated regions. *Nature, Reviews* 438 (17), pp. 303 – 309.

Belmecheri, S., Babst, F., Wahl, E.R., and Trouet, V., (2015). Multi-century evaluation of Sierra Nevada snowpack. *Nature Climate Change*, Published online 14 September 2015.

Bowerman, N.D. and Clark, D.H., (2011). Holocene glaciation of the central Sierra Nevada, California. *Quaternary Science Reviews*. 30, pp. 1067-1085.

California Pest Control Council, (2013). California forest pest conditions 2013. *California department of Forestry and Fire Protection and the USDA Forest Service*, http://www.fs.usda.gov/detail/r5/forest-grasslandhealth/?cid=fsbdev3_046704.

Chander, G. and Markham, B., (2003). Revised Landsat-5 TM radiometric calibration procedures and post calibration dynamic ranges. *IEEE Transactions on Geoscience and Remote Sensing*, 41 (11), pp. 2674-2677.

Chander, G., Markham, B., and Helder, D.L., (2009). Summary of current radiometric calibration coefficients for Landsat MSS, TM, ETM+, and EO-1 ALI sensors. *Remote Sensing of Environment*, 113, pp. 893-903.

Chavez, P.S., (1996). Image-based atmospheric corrections–revisited and improved. *Photogrammetric Engineering and Remote Sensing*, 62 (9), pp. 1025-1036.

Chavez, P.S., (1988). An Improved Dark-Object Subtraction Technique for Atmospheric Scattering Correction of Multispectral Data. *Remote Sensing of Environment*, 24, pp. 459-479.

Chmura, D.J., Anderson, P.D., Howe, G.T., Harrington, C.A., Halofsky, J.E., Peterson, D.L., Shaw, D.C., and St. Clair, B.J., (2011). Forest responses to climate change in the northwestern United States: Ecophysiological foundations for adaptive management. *Forest Ecology and Management*, 261, pp. 1121–1142.

Chung, S.Y., Ehrenfreund, P., Rummel, J.D., and Peter, N., (2010). Synergies of earth science and space exploration. *Advances in Space Research*, 45, pp. 155–168.

Crist, E.P., (1985). Short Communication: A TM Tasseled Cap Equivalent Transformation for Reflectance Factor Data. *Remote Sensing of the Environment*, 17, pp. 301-306.

Czerwinski, C.J., King, D.J., and Mitchell, S.W., (2014). Mapping forest growth and decline in a temperate mixed forest using temporal trend analysis of Landsat imagery, 1987–2010. *Remote Sensing of Environment*, 141, pp. 188-200.

Daly, C., (2006). Guidelines for assessing the suitability of spatial climate data sets. *International Journal of Climatology*, 26, pp. 707-721.

De Beurs, K.M. and Henebry, G.M., (2005). A statistical framework for the analysis of long image time series. *International Journal of Remote Sensing*, 26 (8), pp. 1551-1573.

Eibl, B., Bach, H., and Mauser, W., (1996). Classification of a Landsat-TM image with the spectral mixture analysis under the application of field spectroscopy. *International Archives of Photogrammetry and Remote Sensing*, 31, pp. 226 - 231.

Elmore, A.J., Mustard, J.F., and Manning, S.J., (2003). Regional patterns of plant community response to changes in water: Owens Valley, California. *Ecological Applications*, 13 (2), pp. 443-460.

Feng, M., Sexton, J.O., Huang, C., Masek, J.G., Vermote, E.F., Gao, F., Narasimhan, R., Channan, S., Wolfe, R.E., and Townshend, J.R., (2013). Global surface products from Landsat: Assessment using coincident MODIS observations. *Remote Sensing of Environment*, 134, pp. 276-293.

Gasner, M.R., Jankowski, J.E., Ciecka, A.L., Kyle, K.O., and Rabenold, K.N., (2010). Projecting the local impacts of climate change on a Central American montane avian community. *Biological Conservation*, 143, pp. 1250-1258.

Gond, V., De Pury, D.G., Veroustraete, F., and Cuelemans, R., (1999). Seasonal variation in leaf area index, leaf chlorophyll and water content; scaling up to estimate fAPAR and carbon balance in a multilayer, multispecies temperate forest. *Tree Physiology*, 19, pp. 673-679.

Grabherr, G., Gottfried, M., and Pauli, H., (2010). Climate change impacts in Alpine environments. *Geography Compass*, 48, pp. 1133-1153.

Green, A., Berman, M., Switzer, P., and Craig, M., (1988). A Transformation for Ordering Multispectral Data in Terms of Image Quality with Implications for Noise Removal. *IEEE Transactions on Geoscience and Remote Sensing*, 26 (1), pp. 65 - 74.

Higginbottom, T.P. and Symeonakis, E., (2014). Assessing Land Degradation and Desertification Using Vegetation Index Data: Current Frameworks and Future Directions. *Remote Sensing*, 6, pp. 9552-9575.

Hillyer, R. and Silman, M.R., (2010). Changes in species interactions across a 2.5 km elevation gradient: effects on plant migration in response to climate change. *Global Change Biology*, 16, pp. 3205-3214.

Huete, A.R., (1988). A Soil-adjusted Vegetation Index. *Remote Sensing of the Environment*, 25, pp. 295-309.

Jackson, R.D., Pinter, P.J., Jr., Reginato, R.J., and Idso, S.B., (1986). Detection and evaluation of plant stresses for crop management decisions. *IEEE Transactions on Geoscience and Remote Sensing*, GE-24 (1), pp. 99-106.

Jin, H. and Eklundh, L., (2014). A physically based vegetation index for improved monitoring of plant phenology. *Remote Sensing of the Environment*, 152, pp. 512-525.

Kaufman, Y.J., Wald, A.E., Remer, L.A., Gao, B.C., Li, R.R., and Flynn, L., (1997). The MODIS 2.1 μm channel – Correlation with visible reflectance for use in remote sensing of aerosol. *IEEE Transactions on Geoscience and Remote Sensing*, 35 (5), pp. 1286-1298.

Kelly, A.E. and Goulden, M.L, (2008). Rapid shifts in plant distribution with recent climate change. *Proceedings of the National Academy of Sciences (PNAS)*, 105(33), pp. 11823-11826.

Kondolf, G.M., (1989). Stream-groundwater interactions along streams of the Eastern Sierra Nevada California: Implications for assessing potential impacts of flow diversions. *USDA Forest Service Gen. Tech. Rep. PSW-110*, pp. 352 – 359.

Lenihan, J.M., Drapek, R., Bachelet, D., Kremer, and Nelson, R.P., (2003). Climate change effects on vegetation distribution, carbon, and fire in California. *Ecological Applications*, 13 (6), pp. 1667 – 1681.

Lindner, M., Maroschek, M., Netherer, S., Kremer, A., Barbati, A., Garcia-Gonzalo, J., Seidl, R., Delzon, S., Corona, P., Kolstrom, M., Lexer, M.J., and Marchetti, M., (2010). Climate change impacts, adaptive capacity, and vulnerability of European forest ecosystems. *Forest Ecology and Management*, 259, pp. 698 – 709.

Liu, L., Millar, C.I., Westfall, R.D., and Zebker, H.A., (2013). Surface motion of active rock glaciers in the Sierra Nevada, California, USA: inventory and a case study using InSAR. *The Cryosphere*, 7, pp. 1109 – 1119.

Lu, D., Mausel, P. Brondizio, E., and Moran, E., (2002). Assessment of atmospheric correction methods for Landsat TM data applicable to Amazon basin LBA

research, *International Journal of Remote Sensing*, Vol. 23, No. 13, pp. 2651 – 2671.

Lu, D., Batistella. M., Moran, E., and Mausel, P., (2004). Application of spectral mixture analysis to Amazonian land-use and land-cover classification. *International Journal of Remote Sensing*, 10 (23), pp. 5345 - 5358.

Macleod, R. and Congalton, R., (1998). A Quantitative Comparison of Change-Detection Algorithms for Monitoring Eelgrass from Remotely Sensed Data. *Photogrammetric Engineering & Remote Sensing*, 64 (3), pp. 207 - 216.

Masek, J.G., Vermote, E.F., Saleous, N., Wolfe, R., Hall, F.G., Huemmrich, F., Gao, F., Kutler, J., and Lim, T.K., (2006). A Landsat surface reflectance data set for North America, 1990-2000. *IEEE Geoscience and Remote Sensing Letters*, 3, pp. 68-72.

Munyati, C., (2004). Use of Principal Component Analysis (PCA) of Remote Sensing Images in Wetland Change Detection on the Kafue Flats, Zambia. *Geocarto International*, 19 (3), pp. 11 - 22.

Musick, H.B. and Pelletier, R.E., (1988). Response to soil moisture spectral indexes derived from bidirectional reflectance in thematic mapper wavebands. *Remote Sensing of Environment*, 25, pp. 167-184.

Myint, S. and Okin, G., (2010). Modelling Land-Cover Types Using Multiple Endmember Spectral Mixture Analysis in a Desert City. *Arizona State University, Working Paper Number* 2010-06, pp. 1 - 30.

Opdam, P. and Wascher, D., (2004). Climate change meets habitat fragmentation: linking landscape and biogeographical scale levels in research and conservation. *Biological Conservation*, 117, pp. 285-297.

Qi, J., Chehbouni, A., Huete, A.R., Kerr, Y.H., and Sorooshian, S., (1994). A Modified Soil-adjusted Vegetation Index. *Remote Sensing of the Environment*, 48, pp. 119-126.

Root, T.L., Price, J.T., Hall K.R., Schneider, S.H., Rosenzweig, C., and Pounds, J.A., (2003). Fingerprints of global warming on wild animals and plants, *Nature*, 421, pp. 57-60.

Rouse, J.W., Haas, R.H., Schell J.A. and Deering, D.W., (1974). Monitoring vegetation systems in the Great Plains with ERTS. Proc. Third ERTS-1 Symposium, NASA Goddard, NASA SP-351 pp. 309-317.

Salick, J., Zhendong, F., and Byg, A., (2009). Eastern Himalayan alpine plant ecology, Tibetan ethnobotany, and climate change. *Global Environmental Change*, 19, pp. 147-155.

Sawyer, P.S., and Stephen, H., (2013). Assessing ecological response of the Big Pine Creek watershed to climate change using time series analysis of Landsat surface

reflectance data over a 28-year period. *WIT Transactions on Ecology and the Environment,* 172, pp. 375-386.

Sawyer, P.S., and Stephen, H., (2014). The Big Pine Creek watershed and climate change: A trend analysis of Landsat surface reflectance and PRISM datasets over the last three decades. *Advances in Space Research*, 54, pp. 37-48.

Sawyer, P.S., and Stephen, H., (2014). Comparison of surface reflectance values from the USGS Landsat 5 TM climate data record (CDR) with values generated using a simple dark object subtraction (DOS) method in an Alpine watershed. *International Journal of Earthquake Engineering*, 1 (3), pp. 5-13.

Sawyer, P.S., and Stephen, H., (2014). Vegetative response to climate change in the Big Pine Creek watershed along a 2,500 meter elevation gradient using Landsat data. *Earth Sciences*, 3 (6), pp. 137-146.

Schmidt, G.L., Jenkerson, C.B., Masek, J., Vermote, E., and Gao, F., (2013). Landsat ecosystem disturbance adaptive processing system (LEDAPS) algorithm description. *U.S. Geological Survey Open-File Report* 2013–1057.

Schueler, C.F., and Salomonson, V.V., (1985). Landsat Image Data Quality Studies. *Advances in Space Research*, 5 (5), pp. 1-11.

Skre, O. and Naess, M., (1999). CO_2 and winter temperature effects on white birch. *Chemosphere: Global Change Science*, 1, pp. 469-483.

Steyer, G.D., Couvillion, B.R., and Barras, J.A., (2013). Monitoring Vegetation Response to Episodic Disturbance Events by Using Multitemporal Vegetation Indices. *Journal of Coastal Research*, 63, pp. 118-130.

SWReGAP, (2003). Southwest Regional Gap Analysis Project Land Cover Legend, Ecological Systems and Alliance Descriptions. *The Nature Conservancy* 1815 N. Lynn Street Arlington, Virginia 22209.

Todd, S.W. and Hoffer, R.M., (1998). Responses of spectral indices to variations in vegetation cover and soil background. *Photogrammetric Engineering & Remote Sensing*, 64 (9), pp. 915-921.

Tompkins, S., Mustard, J., Pieters, C., and Forsyth, D., (1997). Optimization of Endmembers Mixture Analysis for Spectral Mixture Analysis. *Remote Sensing of Environment*, 59, pp. 472 - 489.

Turner, W., Spector, S., Gardiner, N., Fladeland, M., Sterling, E., and Steininger, M., (2003). Remote sensing for biodiversity science and conservation. *Trends in Ecology and Evolution*, 18 (6), pp. 306–314.

United States Geological Survey, (1994). Standardized national vegetation classification system. *The Nature Conservancy* 1815 N. Lynn Street Arlington, Virginia 22209,

Prepared for the United States Department of Interior, United States Geological Survey and National Park Service.

United States Geological Survey, (2013). Landsat Climate Data Record (CDR) Surface Reflectance Version 2.0. *US Department of Interior Product Guide*, March 2013.

van Mantgem, P.J., Stephenson, N.L., Byrne, J.C., Daniels, L.D., Franklin, J.F., Fule, P.Z., Harmon, M.E., Larson, A.J., Smith, J.M., Taylor, A.H., and Veblen, T.T., (2009). Widespread Increase of Tree Mortality Rates in the Western United States. *Science*, 323, pp. 521-524.

Vicente-Serrano, S.M., Perez-Cabello, F., and Lasanta, T., (2008). Assessment of radiometric correction techniques in analyzing vegetation variability and change using time series of Landsat imagery. *Remote Sensing of Environment*, 112, pp. 3916-3934.

Vittoz, P., Cherix, D., Gonseth, Y., Lubini, V., Maggini, R., Zbinden, N., and Zumbach, S., (2013). Climate change impacts on biodiversity in Switzerland: A review. *Journal for Nature Conservation*, 21, pp. 154-162.

Vogelmann, J.E., Tolk, B., and Zhu, Z., (2009). Monitoring forest changes in the southwestern United States using multitemporal Landsat data. *Remote Sensing of Environment*, 112, pp. 1739-1748.

Walther, G-R., (2010). Community and ecosystem responses to recent climate change. *Philosophical Transactions of The Royal Society B*, 365, pp. 2019-2024.

Wessman, C.A., (1992). Imaging spectrometry for remote sensing of ecosystem processes. *Advances in Space Research*, 12 (7), pp. 361-368.

Williams, A.P., Allen, C.D., Millar, C.L., Swetnam, T.W., Michaelsen, J., Still, C.J., and Leavitt, S.W., (2010). Forest responses to increasing aridity and warmth in the southwestern United States. *PNAS*, 107 (50), pp. 21289-21294.

Williams, A.P., Allen, C.D., Macalady, A.K., Griffin, D., Woodhouse, C.A., Meko, D.M., Swetnam, T.W., Rauscher, S.A., Seager, R., Grissino-Mayer, H.D., Dean, J.S., Cook, E.R., Gangodagamage, C., Cai, M., and McDowell, N.G., (2013). Temperature as a potent driver of regional forest drought stress and tree mortality. *Nature Climate Change*, 3, pp. 292-297.

Wilson, R.J., Gutierrez, D., Gutierrez, J., Martinez, D., Agudo, R., and Monserrat, V.J., (2005). Changes to the elevational limits and extent of species ranges associated with climate change. *Ecology Letters*, 8, pp. 1138-1146.

Curriculum Vitae

Graduate College
University of Nevada, Las Vegas

Patrick Shawn Sawyer

Home Address:
7492 Grassy Field Ct
Las Vegas, Nevada 89131

Degrees:
Bachelor of Science, Chemical Engineering, 1989
California State University, Long Beach

Master of Science, Environmental Science, 2007
University of Nevada, Las Vegas

Dissertation Title:
Ecosystem response to recent climate change in Alpine Environments

Dissertation Committee:
Chairperson, Dr. Haroon Stephen, Ph.D.
Committee Member, Dr. Krystyna Stave, Ph.D.
Committee Member, Dr. Helen Neill, Ph.D.
Graduate College Representative, Dr. David Kreamer, Ph.D.

Association Memberships
American Chemical Society – Senior Member
American Institute of Chemical Engineers
Academy of Hazardous Materials Professionals

Certifications/Professional License

Engineer-in-Training (License #XE084717) – California Department of Consumer Affairs
Certified Hazardous Materials Manager (License #11757) – Institute of Hazardous Materials Managers (Since 2003)

Published Papers

1. Wannberg, V.E., Williams, G., Sawyer, P., and Venedam, R., (2010). An Experimental Field Dataset with Buoyant, Neutral, and Dense Gas Atmospheric Releases and Model Comparisons in Low–Wind Speed (Diffusion) Conditions. *J. Appl. Meteor. Climatol*., 49, pp. 1805–1817.
2. Williams, G., Sawyer, P., Venedam, R., and Wannberg, V., (2011). Comparison of Three Air Transport Models for Safety Applications under Diffusive Conditions Using Full-Scale Experimental Data: EPIcode, ALOHA, and SCIPUFF. *J. Hazard. Toxic Radioact. Waste*, 15 (1), pp. 26–36.
3. Sawyer, P.S., and Stephen, H., (2013). Assessing ecological response of the Big Pine Creek watershed to climate change using time series analysis of Landsat surface reflectance data over a 28-year period. *WIT Transactions on Ecology and the Environment*, 172, pp. 375-386.
4. Sawyer, P.S., and Stephen, H., (2014). The Big Pine Creek watershed and climate change: A trend analysis of Landsat surface reflectance and PRISM datasets over the last three decades. *Advances in Space Research*, 54, pp. 37-48.
5. Sawyer, P.S., and Stephen, H., (2014). Comparison of surface reflectance values from the USGS Landsat 5 TM climate data record (CDR) with values generated using a simple dark object subtraction (DOS) method in an Alpine watershed. *International Journal of Earthquake Engineering*, 1 (3), pp. 5-13.
6. Sawyer, P.S., and Stephen, H., (2014). Vegetative response to climate change in the Big Pine Creek watershed along a 2,500 meter elevation gradient using Landsat data. *Earth Sciences*, 3 (6), pp. 137-146.

Manuscripts in Preparation

1. Sawyer, P.S., and Stephen, H., Surface cover spectra of the Big Pine Creek watershed, 2015
2. Sawyer, P.S., and Stephen, H., Ecological response to climate change in the Big Pine Creek watershed from trend analysis of vegetation indices and spectral mixture analysis, 2015

Conference Presentations

1. Sawyer, P.S., (2007). Atmospheric Dispersion Model Validation for Low Wind Speed Conditions, American Chemical Society Western Regional Meeting – Poster Session, San Diego, CA, October 2007

2. Sawyer, P.S., and Stephen, H., (2013). Assessing ecological response of the Big Pine Creek watershed to climate change using time series analysis of Landsat surface reflectance data over a 28-year period, *Wessex Institute of Technology –WIT, River Basins Management VII*, New Forest, UK, May 2013
3. Sawyer, P.S., and Stephen, H., (2014). Comparison of surface reflectance values from the USGS Landsat 5 TM climate data record (CDR) with values generated using a simple dark object subtraction (DOS) method in an Alpine watershed. *International Conference on Advances in Bio-Informatics, Bio-Technology, and Environmental Engineering – ABBE*, Westminster University, London, UK, June 2014

Professional Experience

Principal Engineer for National Security Technologies, LLC. (NSTec), contractor for the US Department of Energy. Field Test Coordinator for experimental research activities taking place at the Nevada National Security Site (NNSS). Working at the NNSS since 1997, following several years as a Chemical Engineer for Bechtel Corporation in both Texas and California. Specific assignments and time periods are listed below:

<u>January 1990 – January 1995</u>

Chemical/Systems Engineer for Bechtel Corporation in California. Responsible for the design, procurement and construction of numerous chemical processing units at several facilities including the Unocal Santa Maria, Wilmington, and Carson refineries, the Arco El Segundo refinery and the Chevron El Segundo refinery.

<u>February 1994 – July 1997</u>

Process Engineer/Field Engineering Supervisor for the Mobil Beaumont Paraxylene facility. Responsible for the design of all the off-site and utility systems during the design stage and responsible for all on-site field engineering support for the construction of the $200 million plant in Beaumont Texas.

<u>August 1997 – June 2001</u>

Senior Chemical/Systems Engineer for the HAZMAT Spill Center at the Nevada Test Site. Responsible for the design, procurement, and construction of hazardous chemical systems. Supervise Field Technicians. Manage OSHA PSM compliance. Interact with customers from the US Government and private Industry to develop experiments utilizing the unique capabilities of the facility.

<u>June 2001 – September 2005</u>

Facility/Operations Manager for the HAZMAT Spill Center. Responsible for facility operations and work activities in support of customer testing. Developed NEPA documentation and environmental permits to allow hazardous materials testing at the NNSS. Work with customer base to design field experiment campaigns.

September 2005 – Present

Field Test Coordinator/Test Director for Test and Evaluation programs at the Nonproliferation Test and Evaluation Complex. Managed the NPTEC Operations Team. Responsible for test execution, managed field operations and work activities in support of customer testing. Coordinated all field work activities between test participants including the National Labs, the Intelligence Community, DHS, DOD and other participating government agencies. Coordinated three OCONUS missions to Europe, Central America, and Africa in support of classified government programs.